MOLTEN-BASED 3-D DIRECTWRITE FABRICATION OF MICROSTRUCTURES

A Dissertation
Presented to
The Academic Faculty Committee

By

Yining Chen

In Partial Fulfillment
Of the Requirements for the Degree
Doctor of Philosophy in the
School of Aerospace Engineering

Georgia Institute of Technology
DECEMBER 2021

MOLTEN-BASED 3-D DIRECTWRITE FABRICATION OF MICROSTRUCTURES

Approved by:

Dr. George Kardomateas, Advisor
School of Aerospace Engineering
Georgia Institute of Technology

Dr. Claudio Di Leo
School of Aerospace Engineering
Georgia Institute of Technology

Dr. Julian Rimoli
School of Aerospace Engineering
Georgia Institute of Technology

Dr. Ting Zhu
School of Mechanical Engineering
Georgia Institute of Technology

Dr. Sathyanaraya Hanagud
School of Aerospace Engineering
Georgia Institute of Technology

Date Approved: Oct 29th, 2021

ACKNOWLEDGEMENTS

I am heartily to express my deepest gratitude to my advisor, Dr. George Kardomateas, for his guidance, support, and inspiration throughout the course of my research. Special thanks to my committee members, Dr. Claudio Vinicius Di Leo, Dr. Julian Rimoli, Dr. Ting Zhu and Dr. Sathyanaraya Hanagud, their valuable feedbacks make my research work better.

During the completion of the thesis, the world is upside down due to the pandemic of COVID-19. I send my deepest condolences to people lose their beloved ones in the fighting with the virus. With science, courage and togetherness, human being will defeat the virus. Besides complex 3D microstructures, the thesis provides an efficient way to fabricate microneedle array which have potential application in vaccine and drug delivery. Wish all these novel technologies could help.

I would like to thank Dr. Mitchell Walker for his help. Without his encouragement and support, I could not finish the thesis. Really Appreciate all the members help me through the way.

I would also like to thank my colleagues, Dr. Yong Zhang, Dr. Yen-po Lin and Mr. Wei Fang and Fengze Jiang. I would like to acknowledge Dr. Yu for his helpful discussions and assistance. I would also like to thank staff members in the Institute for Electronics and Nanotechnology at Georgia Tech for their help in developing microfabrication processes. Last but not the least, I would like to thank the National Science Foundation and Georgia Tech for their support for making this research possible.

Finally, yet importantly, I want to thank my wife Lei Gu and son William Weiyan Chen, for being my strength. Thanks to my parents and my family, for their support.

TABLE OF CONTENTS

LIST OF TABLES

LIST OF FIGURES

SUMMARY

The micro fabrication is the backbone of information age. From phones people use daily to the satellite in the orbit, they all rely on the control unit, sensors that made by microfabrication techniques. With decades of rapid development, the micro fabrication technology has reached a dimension that no one can image in the past. The next state of art micro electric fabrication dimensions has reached 2nm which is 1/6000 that in 1970s. However, these fabrication techniques are mostly planar and become more and more expensive and make it only economically feasible for mass productions. Thus, it has difficulties in making 3D or very high aspect ratio structures due to it is mainly a 2D process. Meanwhile, the demand for 3D micro-structures or high aspect ratio microstructures is increasing in various fields, such as micro needles, micro antenna etc. In this dissertation, we develop a direct-write method to fabricate 3D micro-structures and high aspect ratio microstructures at low cost that can fill this gap. Our method is based on molten materials extruding from a nozzle by pressure to form microstructures on the substrates. The critical dimensions of the structures can be as small as hundred nanometer level while maintaining hundreds of aspect ratio. We explore the mechanism in the fabrication and realize precise control of the process. The bonding and mechanical strength of the fabricated structures are also strong enough to serve as senor or mold for sequential processes. It provides a unique method for micro device that has applications in biomedical and microelectronics. The process can be stacked up together to fabricate more complex or more dense structures. Very high dense and aspect ratio structure arrays are readily fabricated. Moreover, we also develop a method to fabricate microneedle arrays. These micro needles arrays can serve as mold to get polymer replica which has many applications in biomedical field, such as

medical drug/vaccine delivery, bio-signal monitoring, etc.

Chapter 1: Introduction

1.1 Background

For nearly half a century, microfabrication technology keeps pushing the boundary of human manufacturing and changes human life forward. From cellphones to the spacecraft orbiting around the earth, it is an essential technology in all the modern products. With better and better microchips and sensors, we can control our aircraft and rockets more accurate and precise. Every successful mission relies on the proper function of the devices made by microfabrication.

The most used microfabrication technology is 2D lithography-based and the biggest application of it is in microelectronics. It first cast a layer of photoresist on the substrate, usually silicon. Then it is exposed under EUV or DUV light through a patterned mask. The area that exposed under the light would have some chemical changes in the photoresist. After developing, the pattern is transferred onto the it. With the remained photoresist serve as a protective layer, the pattern is replicated onto the substrate after etching.

Figure 1 the process of the lithography-based microfabrication

Nowadays the interest in microfabrication is far more beyond microelectronics.

More and more 3D functional structures with micro- or nano- features have become active in research [1] [2] [3]. These 3D microstructures have many applications such as biomedical devices [4] [5], microelectromechanical systems [6], photonics and optoelectronics [7], and energy storage [8] [9]. Among all these applications, the micro 3D structures with high aspect ratio draw specially attention because they are not only difficult to fabricate but also the ideal geometry to serve as medicine/vaccinate [10] or bio signal collection [11] media. Moreover, these 3D microstructures should also be fabricated in array forms and bond strongly on the substrate so that they can serve as useful devices.

However, most microfabrication technology is 2D based and their ability to fabricate 3D structures are usually limited. LIGA (a German acronym for a process involving lithography, electroforming, and molding) and 3D-printing is two most common ways to fabricate high aspect-ratio microstructures. They have successfully fabricated various device but still have limitations due to their intrinsic mechanisms.

1.2 Review of High-Aspect Ratio 3D Micro Fabrication Method

1.2.1 LIGA technology

Planar based microfabrication is the standard procedures to make IC circuits. These technologies also extend to fabrication MEMS (microelectromechanical systems) components. It had achieved great commercial success such as accelerometers, pressure sensors, optical switches, lab-on-chip, and gyroscope etc. All the these facilitate our daily life and increase the efficiency of our research. First it needs to make patterns on the mask. Then by exposing UV light to a substrate coated by photoresist through the mask and

development, the designed patterns are transferred to the surface of target material. Finally, the unwanted parts on the substrate are etched way by either chemical wet etching, or physical dry etching. These steps complete one cycle of the fabrication process. Since it is 2D intrinsically and the thickness each cycle can build up is limited, to fabricate high aspect ratio structures, they need a lot of cycles which make it inefficient and unfeasible.

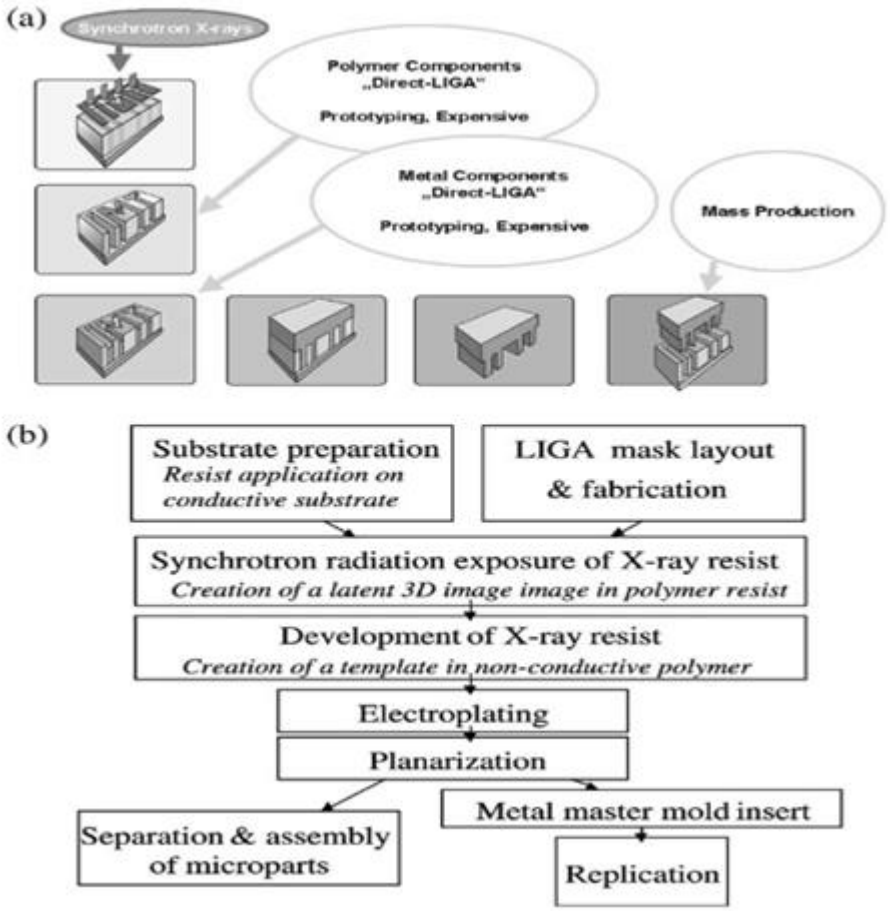

Figure 2 Illustration of the basic LIGA process steps. (a)The six panels stand for lithography, polymer components after development, electroplating and overplating the polymer template, a metal mold, and replication. (b) Basic LIGA process sequence. From [12]

To overcome the drawbacks of planar based microfabrication in the high aspect ratio microstructures fabrication, the LIGA process has been developed for decades. Figure

2 is the illustration of the basic LIGA process steps and sequence. Like the traditional method, it also needs masks. Then it uses synchrotron x-ray to expose special photoresist (usually PMMA, Su-8 etc. [13] [14]) which can be several millimeters in height to transfer the patterns on the mask to the resist layer. After the exposure, selective dissolute of the resist layer in a chemical developer and result a polymeric relief replica of the mask pattern. Depending on the material and parts of the final product, electroforming and/or different molding techniques (injection molding, embossing, casting, compression molding) can be used for further steps of microreplication [12].

However, the high energy X-ray synchrotron equipment and mask making process is usually expensive and limits applications which are cost sensitive. Besides, its ability to make complex 3-D microstructures is limited as the patterns are defined by X-ray and the variation in the out-of-plane dimension is limited. Two categories of methods are used to solve this problem: one is sequential planar formation of individual levels to form 3D structures [15] and the other is varying the absorbed dose [16] [17] [18] [19].The first method needs accurate re-planarization process and precise mask-alignment procedure between each level which adds up the cost of the whole fabrication. The second method is achieved by tilting/rotation of the mask/substrate during the exposure process, and it adds complexity to the systems.

1.2.2 3-D Printing Fabrication

To have greater ability to fabricate structures in out-of-plane dimension, the 3-D method has no theoretical limits in geometry and height and has become a hot research area in decades [20] [21] [22]. It is an additive manufacturing that continuously deposits

material at the targeted location to produce the desired 3D structures. As it does not need lithography process, its cost is usually much less than conventional planar fabrication method and LIGA. It also has more design flexibility and rapid prototyping ability, which makes it popular.

Two examples of these methods are silver nanoparticle-inked based micro 3D printing [23] and solvent-cast direct-write (SC-DW) 3D printing [24]. The first used synthesized silver nanoparticle inks to print flexible, stretchable, and spanning silver microelectrodes and the latter used solvent ink with dissolvable thermoplastic polymers such as PLA to manufacture 3D high aspect ratio microstructures. Both methods realize 3D micro fabrication and generate structures that are hard to make by planar lithography methods. However, due to their ink properties, they would have volume shrinkage when part of the ink is gone. The volume loss can be up to 30 % which limits their application in precise structure fabrication.

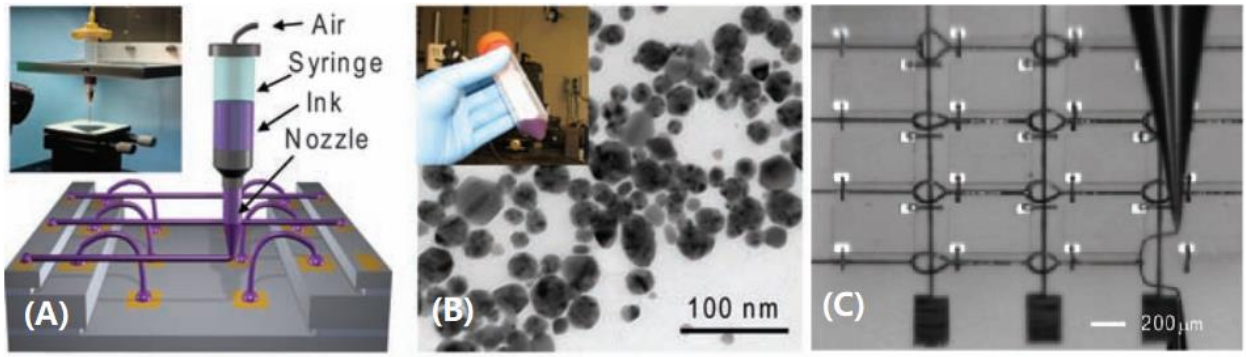

Figure 3 (A) Schematic diagram illustrating omnidirectional printing and optical image of apparatus used (inset). (B) Transmission electron microscopy image of the synthesized silver nanoparticles and optical image of the concentrated ink (inset). (C) Optical image acquired during patterning of silver interconnects on a gallium arsenide–based, 4-by-4 LED chip array. From [23]

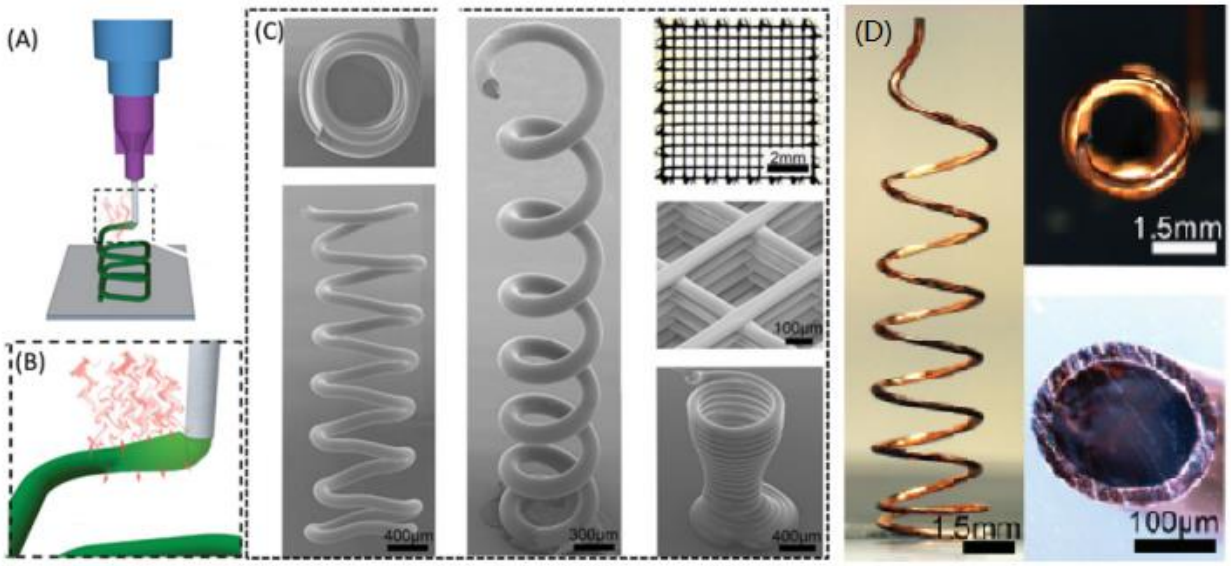

Figure 4 illustration of solvent-cast direct-write (SC-DW) 3D printing (A) Deposition of the polymer solution through a micronozzle. (B) Rapid solvent evaporation post extrusion. (C) Microstructures manufactured by SC-DW (D) Optical side, top and cross-sectional view images of the copper coated 3D variable pitch spiral antenna. From [24]

In general, 3D Printing Fabrication can be categorized to several methods according to the methods it uses. It includes Fused deposition modeling [25], Powder bed fusion [26] (SLS, SLM, 3DP), inkjet printing and contour crafting [21] [27], stereolithography [28], direct energy deposition [29] and laminated object manufacturing [30]. However, not all these methods are suitable for high aspect ratio microscale fabrication. Table 1 is a comparison of all these methods [31]. Fused deposition modeling usually uses filaments of thermoplastic polymer that has weak mechanical properties. Powder bed fusion usually produces rough surface because of the porosity formed during the sintering/melting process of the powder [32]. Inject printing has coarse resolutions and stereolithography is relatively slow and expansive. The direct energy deposition is used for large component with low complexity and laminated objective needs post-processing [31].

Table 1 A summary of materials, application, benefits and drawbacks of the main methods of additive manufacturing. From[31]

Methods	Materials	Applications	Benefits	Drawbacks	Resolution range (μm)
Fused deposition modelling	Continues filaments of thermoplastic polymers Continuous fibre-reinforced polymers	Rapid prototyping Toys advanced composite parts	Low cost High speed Simplicity	Weak mechanical properties Limited materials (only thermoplastics) Layer-by-layer finish	50-200 μm [13]
Powder bed fusion (SLS, SLM, 3DP)	Compacted fine powders Metals, alloys and limited polymers (SLS or SLM) ceramic and polymers (3DP)	Biomedical Electronics Aerospace Lightweight structures (lattices) Heat exchangers	Fine resolution High quality	Slow printing Expensive High porosity in the binder method (3DP)	80-250 μm [13]
Inkjet printing and contour crafting	A concentrated dispersion of particles in a liquid (ink or paste) Ceramic, concrete and soil	Biomedical Large structures Buildings	Ability to print large structures Quick printing	Maintaining workability Coarse resolution Lack of adhesion between layers Layer-by-layer finish	Inkjet: 5–200 μm Contour crafting: 25–40 mm [32]
Stereolithography	A resin with photo-active monomers Hybrid polymer-ceramics	Biomedical Prototyping	Fine resolution High quality	Very limited materials Slow printing Expensive	10 μm [13]
Direct energy deposition	Metals and alloys in the form of powder or wire Ceramics and polymers	Aerospace Retrofitting Repair Cladding Biomedical	Reduced manufacturing time and cost Excellent mechanical properties Controlled microstructure Accurate composition control Excellent for repair and retrofitting	Low accuracy Low surface quality Need for a dense support structure Limitation in printing complex shapes with fine details	250 μm [23]
Laminated object manufacturing	Polymer composites Ceramics Paper Metal-filled tapes Metal rolls	Paper manufacturing Foundry industries Electronics Smart structures	Reduced tooling and manufacturing time A vast range of materials Low cost Excellent for manufacturing of larger structures	Inferior surface quality and dimensional accuracy Limitation in manufacturing of complex shapes	Depends on the thickness of the laminates

Several methods are used to extend the 3D-printing to microfabrication. Figure 5 shows the classification of 3D micro Additive Manufacturing.

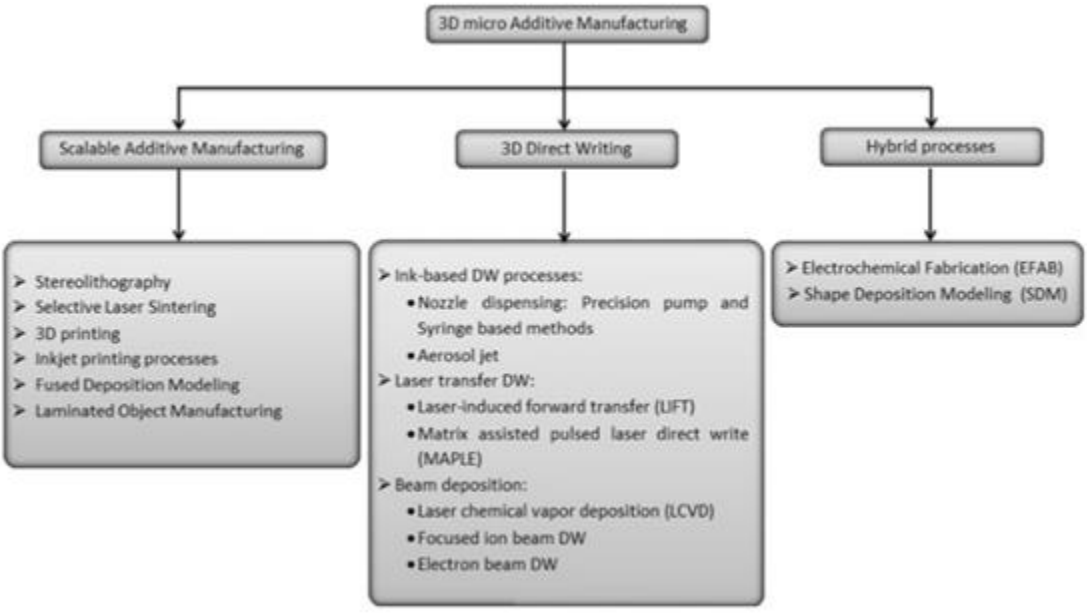

Figure 5 the classification of 3D micro-AM process from [33].

These techniques usually use thermoplastic polymer materials such as acrylonitrile

butadiene styrene (ABS), polylatic acid (PLA), polyami(PA) and polycarbonate(PC) as well as thermosetting polymer material like epoxy resin [34]. However, most 3D printing products lack the mechanical strength to serve as functional components. Several groups have explored ways to strengthen the polymers by composite polymers which have matrix and reinforcements [35]. The reinforcement materials added to the composite improves the mechanical properties of the polymers but still not strong enough to compete with components made with traditional material such as alumina, silica and they also create porous structures due to the weak bonding between the matrix and reinforcement. Besides the weakness of the mechanical strength, the surface of the polymer-based 3D writing or printing is very rough and needs post-process treatment.

Glass is a material that has been used by humans for thousands of years. It has clear optical transparency, rigid mechanical strength, smoothness on the surface, great chemical, and thermal resistance along with electrical insulating properties [36] [37] [38]. It is a good material to solve the problems mentioned above.

To take advantage of the favorable material property of glass, glass-based 3D printing has been proposed by some groups. Frederik at el introduced a glass-based fabrication method by stereolithography [3]. They first mixed ultraviolet curable monomer with SiO2 to make nanocomposite. Then used stereolithography to make polymerized composite. Finally, they sintered at 1300 ºC to make fused silica glass. Although this method can make very complex structures with high strength, it involves multiple steps. John Klein at el presented an extrusion printer for optically transparent glass [39]. It heats up the glass to 1000 ℃ and extrudes the material by weight and uses lay by lay method to build up optical structures. Its resolution is in mm scale and has not been extended in

micro/nano scale yet.

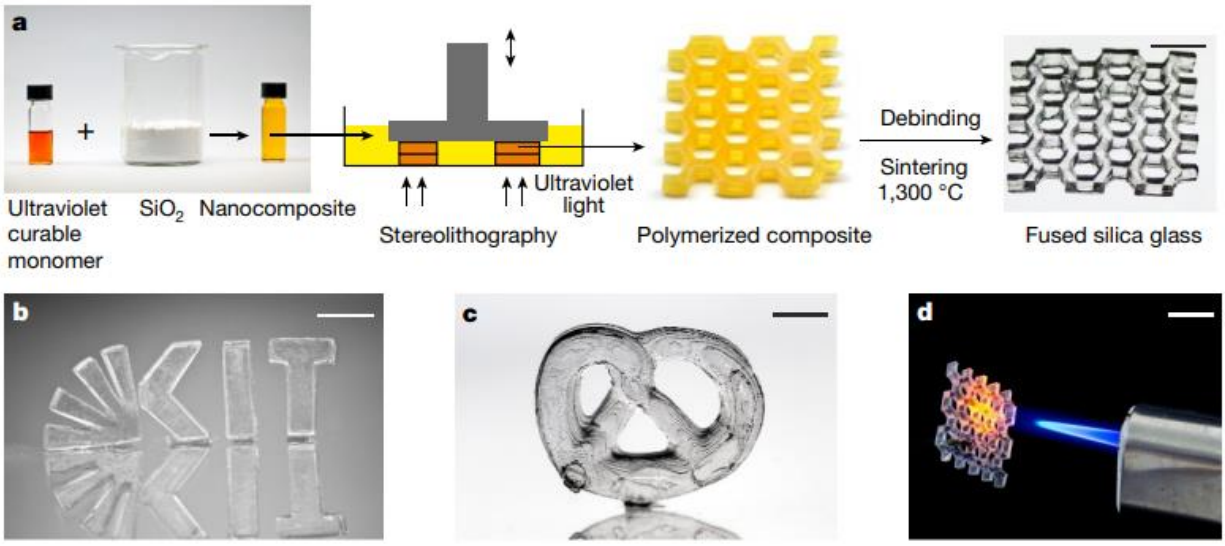

Figure 6 3D printing of fused silicon glass a, Ultraviolet-curable monomer mixed with amorphous silica nanopowder is structured in a stereolithography system. The resulting polymerized composite is turned into fused silica glass through thermal debinding and sintering (scale bar, 7mm). b, c, Examples of printed and sintered glass structures: Karlsruhe Institute of Technology logo (b; scale bar, 5mm) and pretzel (c; scale bar, 5mm). d, Demonstration of the high thermal resistance of printed fused silica glass (scale bar, 1 cm). The flame had a temperature of about 800 °C.From [3]

Figure 7 (A) Evolution of the printing process from its early stages (B) through the introduction of a nozzle (C) to the current setup with an annealing chamber. From [39]

1.3 Objective and Outline

To make the 3D micro fabrication process be more efficient and useful in applications, such as sensors, molding masters, the novel microfabrication needs to combine the following breakthroughs.

- First, the fabrication process should be flexible and should have no geometry limitations.

- Second, the mechanical properties of the fabricated structures should be higher than the polymer so they can be directly used as molding or functional structures.
- Third there should be strong bonding on the substrates, so we do not need extra assembly process to make a device from it.

The objective of the research is to develop a direct-write method to efficiently fabricate high-aspect-ratio or complex microscale 3D glass structures bonded on a substrate surface for the purpose of making surface-engineered devices, such as a mold with high mechanical quality, nanometer surface smoothness and sub-micrometer resolution for manufacturing high quality microneedles.

In this dissertation, Chapter 2 describes the molten based direct write fabrication method and the system setup of it. Chapter 3 covers the material property related to the process, the driving force of the growth and the evolution between different structures. Chapter 4 shows several critical growth stages including base formation, uniform segment growth and termination and tip modification. Chapter 5 describes the arrays fabrication process followed by Chapter 6 showing the mold from the arrays that are made. Finally, Chapter 7 is a summary of the whole research.

Chapter 2: Molten Based Direct-Write Fabrication

2.1 Introduction

2.1.1 Molten Based Direct-Write Fabrication

To take advantage of the direct-write based 3D fabrication and overcome the drawbacks of the conventional system, Molten Based Direct-Write Fabrication System is designed and built-up in our lab to produce high aspect-ratio micro and micro/sub-micro 3D structures that can be used in a wide variety of applications.

The following shows the schematically setup of the molten based direct-write fabrication.

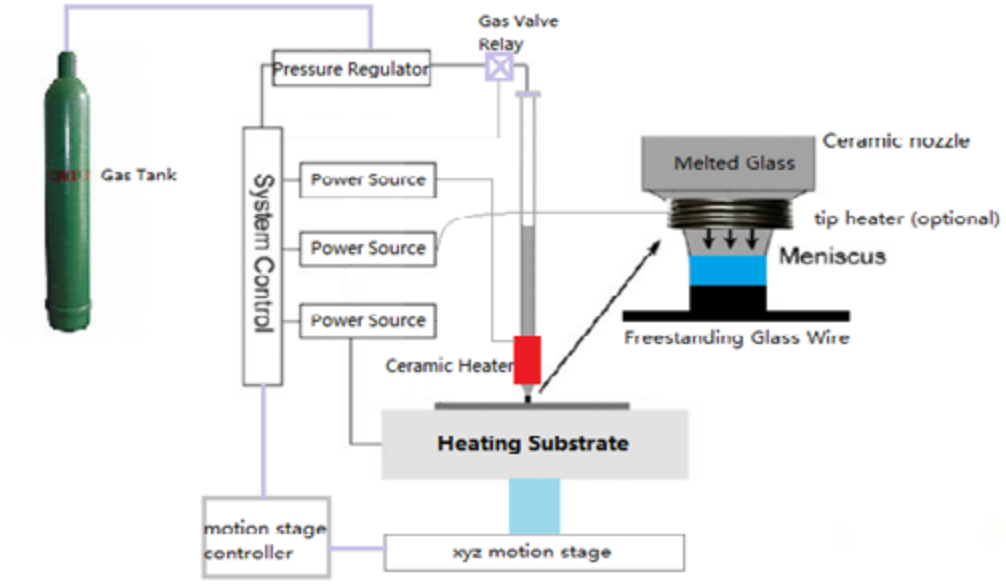

Figure 8 the schematic diagram of the Molten-Glass Based Micro Fabrication System

The working principle is based on the 3D direct writing. Molten glass based micro fabrication uses an assembly of ceramic tube with micro opening nozzle that is filled with molten glass. Two-stage heating systems is used to keep the glass in molten status and its viscosity in the operational range. A regulated pressure system is used to control the on/off and fabrication rate of the process. XYZ motion stage controls the growth path of the melted glass.

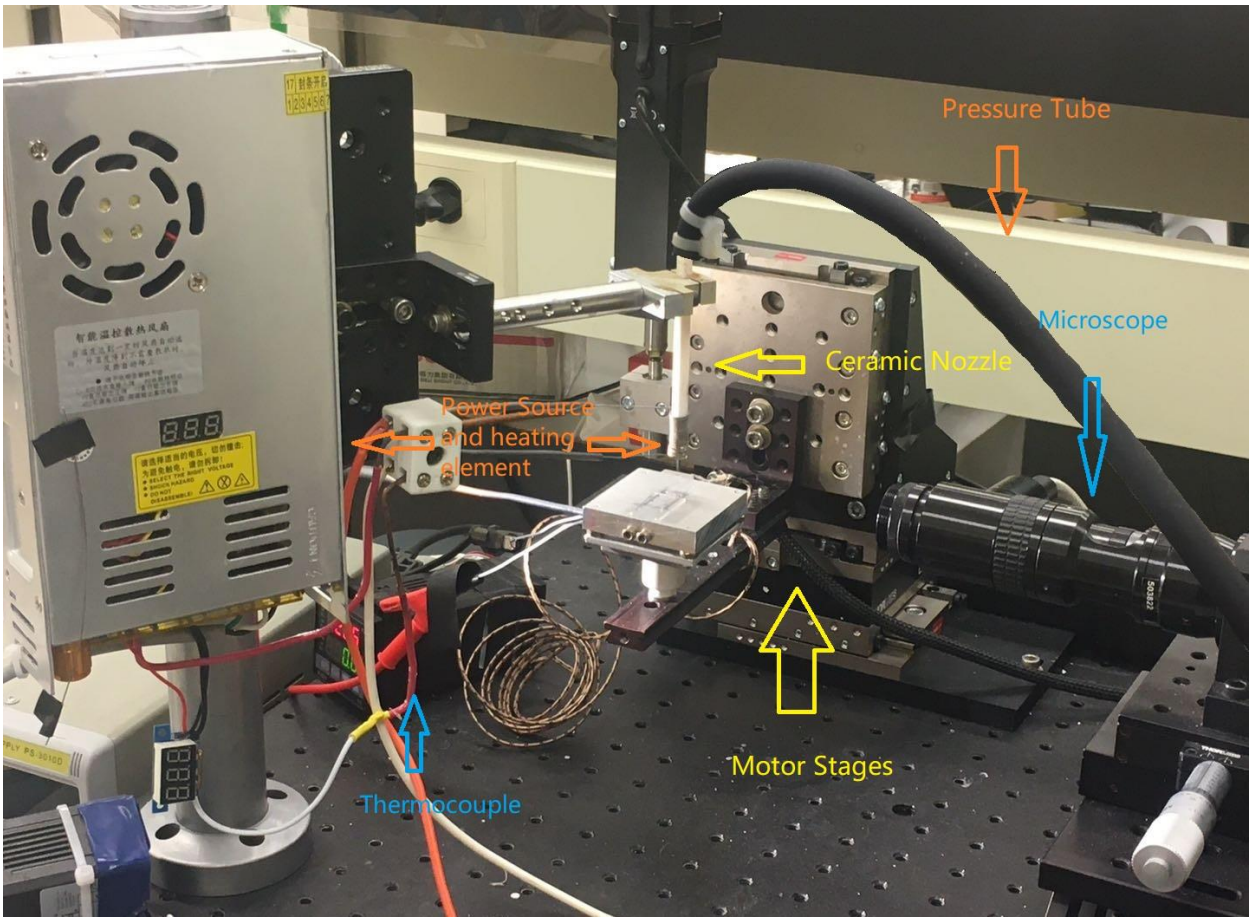

Figure 9 Parts of the hardware components of the system setup

The figure above shows parts of the hardware components of the system setup. The ceramic nozzle is mounted on the frame. It has Kanthal® A-1 heating wire wrapping

around which can provide temperature up to 1400 °C to maintain the glass in the ceramic nozzle in melted status. A heating power is connected to the heating wires. Motors stages are mounted on the platform to control the XYZ motion of a heated substrate. The temperature of the substrate is monitored by K type thermocouple. One end of the pressure tube is connected to the back of the ceramic nozzle while the other end is connected to a pressure regulator. A microscope connected to a CCD camera is used to observe the growth process. The control box of the motors, gas tank, second stage of heating etc. are not shown in the figure.

The fabrication procedures are as follows. Before the start of fabrication, the glass is heated above the melting temperature and stand still for half an hour to remove the bubble formed during the melting process of the glass powder. Then the substrate is approaching the nozzle and once they are engaged the pressure is on. Meniscus is formed between a nozzle and a substrate. The meniscus stability governs the fabrication process and determines the features of structures. With cooling process during the moving of the XYZ motor, 3 D structures can be fabricated in the designed way. All the process should be precisely controlled by a program. The rate of the movement of the substrate is synchronized with the rate of the flow rate of the molten glass to realize high-speed manufacturing. With high-speed 3D movement, 3D structures were fabricated with complex shapes at up to mm/s rate.

It has freedom to make real 3D structures. Based on wetting between the molten glass and substrate, the fabricated structures can be strongly bonded onto the substrate. It makes them easier to convert to another device or be used as a mold. The surface smoothness is also perfect.

2.1.2 Parameters involved in the Fabrication process

Unlike conventional direct-write method based on ink [40], the molten based process involves the phase transformation from liquid to solid. The temperature which is a dynamic balance between heating and cooling play a critical role in the process. It determines some critical property of the material, especially viscosity which further influence the stability of the fabrication process. The back pressure, which is the driving force to extrude the material out determines the ultimate grow speed. The motion speed needs to be synchronized with the glass flow rate during uniform growth. It must match with the rate of the material exiting speed from the nozzle in the stable condition. During the termination process, the motion speed become an active parameter that can determine important aspect of the structures such as the length of the end part, tip sharpness for the micro needles, the sharp of wire end.

2.2 Molten-Based Direct Fabrication System

2.2.1 System Overview

The Molten-Based Direct Fabrication is fully automated by Programed Control System. The system consists of four subsystems, Motion stages, a nozzle assembly incorporating a ceramic nozzle (MICRO_SWISS) having inner opening diameter as small as 40 um, Temperature control unit for the nozzle assembly capable of reaching 1400 ºC for melting glass powder, Pressure control unit for regulating the back pressure needed to drive and control the flow of the molten glass through the ceramic nozzle, and visualization systems. All the subsystems are connected to a computer and controlled by programs

written in LabVIEW. Besides them, there is also a heating system for the substrate to form good bonding in the fabrication process.

2.2.2 Motion Stage Control System

The Motion Stage system includes 3 motorized stages (Model LNR50, THORLABS) for X, Y, Z motion. All these stages connected to their controller (BSC 203, THORLABS) and the controller is connected to the computer.

LNR50 has a travel range of 50 mm with resolution of 10 um. The long travel range ensures the working space can be 50 mm × 50 mm × 50 mm which is large enough for most micro fabrication requirement. The maximum speed of the motor is 50 mm/sec with less than 10 μm accuracy. BSC 203 is three channel stepper motor Controller that can provide precise control of three axis motors simultaneously to form the desired growth path in the fabrication process.

The motion stages are placed on BM-8 Bench Top Vibration Isolation Platform which provides a vibration isolation to the system. It is adjusted according to the payload of the motors, camera, mounting stages.

2.2.3 Temperature Control System

The temperature is controlled by adjusting the power delivered by Power Source (Model 1687B, BK PRECISION). The programmable power source is connected to computer and can deliver up to 360 W. The power source heats up a Resistance Wire (20/32 AWG, Kanthal A1) that is wrapped around a nozzle assembly incorporating a ceramic

nozzle (P/N 41690 MICRO_SWISS) having inner opening diameter as small as 40μm. If a ceramic coating were pasted around the resistance wire as thermal isolator, the temperature can be up to 1200 ºC. A k type thermal couple is used to monitor the temperature. Feedback control is also realized by a control box (Model SYL-2342 Auber) according to the reading from the thermal couple.

There is also another power source (Model PS-3010D, YiHUA DC power source) to heat up the substrate. It can also go up to 320 W. Its task is to heat up the substrate reaching around 300 ºC to create good wetting condition for bonding purpose.

2.2.4 Pressure Regulation System

The pressure regulation system is the main driving force for the extrusion of the molten material and have five parts, a pressure instrument, electronic relay, magnetic gas valve , a DAQ and gas tank. The gas tank is connected to the pressure instrument (WPI PV830 Pneumatic Pico Pump) and then the magnetic gas valve. There is a magnetic gas valve to control the on/off the gas supply to the backside of the ceramic nozzle assembly. The magnetic gas valve is attached to an electronic relay and the relay is computer-controlled by a DAQ (HYTECK IUSBDAQ). The whole system is computer-program controlled and can provide precise timely regulation for the pressure. The computer sends a signal to the DAQ when the pressure needs to be on/off and the DAQ provides control of the electronic relay. When the relay is off, the magnetic gas valve is closed, and pressure is off. When the relay is on, the magnetic gas value is open, and pressure is applied from the back of the ceramic nozzle.

2.2.5 LabView Programed UI interface

All the control of the above system is integrated in a LabView program developed in our lab. It provides synchronized control over heating, pressure, motion of the system. It can adjust the heating power as well as the on/off the pressure at specific time in the growth process. It controls the motor to move according to pre-designed path based on the spatial coordinates with desired acceleration and speed which provide a wide range of adjustable parameters. In the follow is the User Interface of the LabView program.

Figure 10 the User Interface of the LabView Program developed in our lab

The yellow box in the left top segment is an automatic tiling adjusting function to prevent crush of the nozzle onto the substrate. It would calculate the tilting status of the glass substrates and provide compensation for the tilting during the moving of the motors.

The blue segment below is to control the heating power from the Model 1687B, BK PRECISION to adjust the temperature of the nozzle. The purple box in the right is to control the on/off the magnetic gas valve. The segment in the red box is used to control the acceleration, speed, and spatial coordinates of the motors. Three instrument interfaces between the blue and red box provide in situ information of the motors during fabrication.

2.3 Conclusion

In this chapter, the concept of Molten Based Direct-Write Fabrication is introduced. The system setup is explained in detail, it has three main subsystems, the motion stage control system, temperature control system and pressure regulation system. The system is placed on a vibration isolation platform to damp the interference from the environment. Parts of the hardware is illustrated. All these subsystems are computer controlled by lab developed LabView Program and can provide accurate control of motion, heating, pressure to realize complex task during the fabrication process. The user interface of the lab developed LabView control program is also illustrated.

CHAPTER 3: Molten Glass Properties and the Molten Based Direct-Write Fabrication Process

3.1 Introduction

Unlike other fabrication process, the molten based direct-write method involves surface tension, phase transformation, fluid flow. The material property and theory behind the fabrication process will be explained in this chapter. In this chapter, First, we will explore the unique physical characteristics of the material we encountered in the process. Then we dip into the stable condition of our fabrication. The stable condition of the growth is essential for the growth of wires, which is the basic unit in all other more complex structures. After that, we talk about the needle growth, which is an unstable growth condition but have potential applications in many areas such as micro/nano biomedical engineering. Finally, a COMSOL model that can capture the uniform wire growth and needle formation process qualitatively is build.

3.2 The Property of Material

3.2.1 The Temperature effect on the viscosity

In the molten state of the glass, viscosity is a critical parameter that governs many aspects of the process, such as fabrication speed, meniscus stability etc. The viscosity is a material property that relates the viscous stress to the rate of change of a deformation. It relates to the shear stress with the following equations.

$$\tau = \mu \frac{\partial v}{\partial x} \qquad 1$$

that μ is the viscosity of the fluid, τ is the shear stress and $\frac{\partial v}{\partial x}$ is the gradient of the velocity.

The unit of viscosity is $Pa \cdot s$.

However, the range of the glass viscosity varies several orders of magnitude during the fabrication process. The following table shows the definition of fixpoints and description for glass.

Table 2 Glass Viscosity Fixpoints & Viscosity

Glass Viscosity Fixpoints & Viscosity Units

$\log_{10}$(viscosity in ...) Pa·s	Poise	Description
1	2	Melting Point (glass melt homogenization and fining)
3	4	Working Point (pressing, blowing, gob forming)
4	5	Flow Point
6.6	7.6	Littleton Softening Point (Glass deformes under its own weight. Standard procedures ASTM C338, ISO 7884-3)
8-10	9-11	Dilatometric Softing Point Td, depending on load
10.5	11.5	Deformation Point
11-12.3	12-13.3	Glass Transition Temperature Tg
12	13	Annealing Point (Stress is relieved within a few minutes.
13.5	14.5	Strain Point (Stress is relieved within several hours.)

Viscosity Units:
10 Poise = 10 P = 1 Pa·s
log(viscosity in Poise) = log(viscosity in Pa·s) + 1

http://glassproperties.com/viscosity/Glass-Viscosity-Fixpoints.htm

Several points in the table above can help to understand the property of glass. Annealing point is where the glass can relieve its internal stress. The glass transition temperature is temperature that begin glass transition. At this temperature, glass transits from a rigid hard state to a viscous state. The softening point is where the glass deforms under its own weight. The working point is where most industrial glass factory focuses on. It has great formability and can make into various shapes with pressure, blowing, etc. The

melting point is where the glass melts homogenized. For the glass powder that is used in our experiments, glass transition temperature and soften temperature are provided by the manufacturer to help us understand the properties of the glass we used.

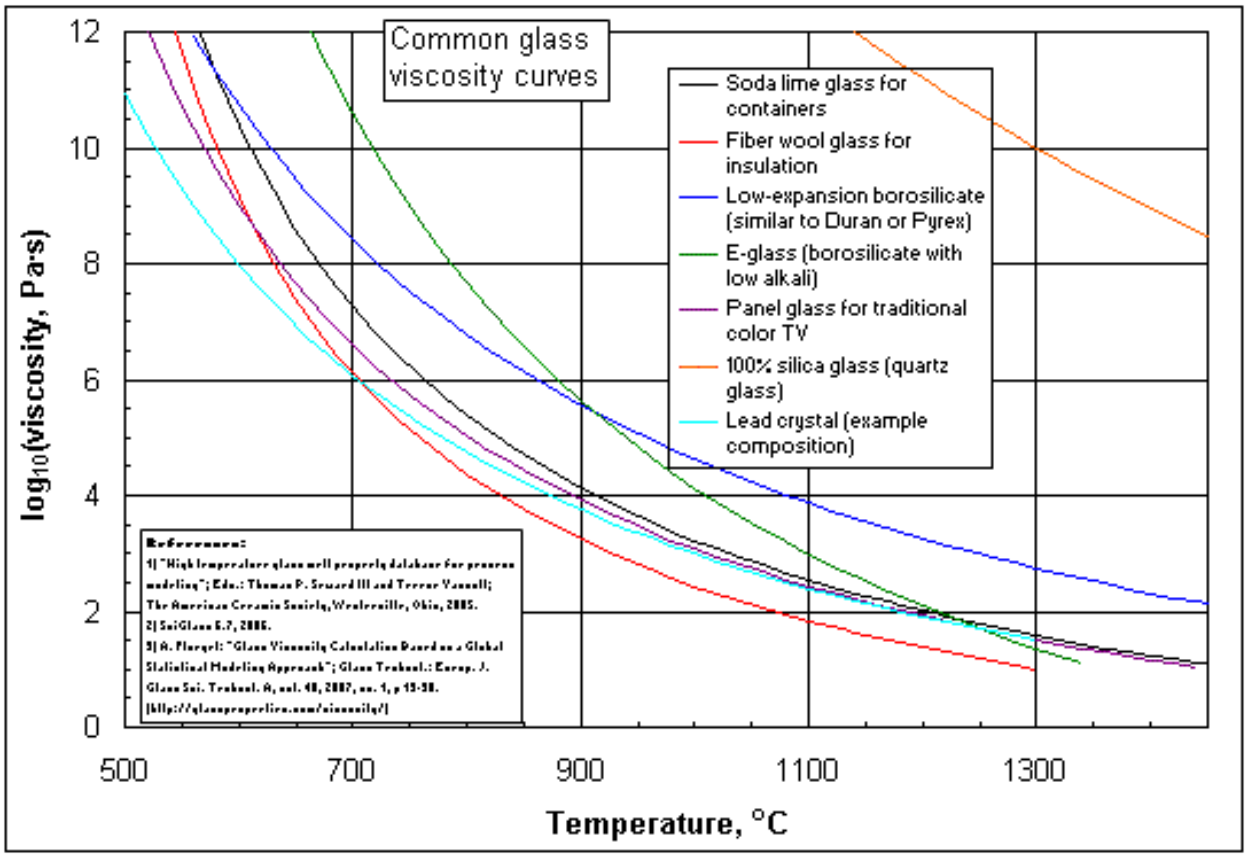

Figure 11 Common Glass viscosity curves from [41]

From the figure above, we can see that within a hundred-degree Celsius, the viscosity can change nearly 2 orders of magnitude, which makes the molten based fabrication more challenging than the polymer-based micro fabrication.

By experiment, two equations are commonly used to describe the relationship between the viscosity of the glass and the temperature. First is the Vogel-Fulcher-Tammann equation and it is as follows:

$$\mu(T,x) = \mu_0(x)exp(-\frac{A(x)}{T-T_0(x)}) \qquad 2$$

Where T is temperature, x is composition of the glass, $\mu_0(x)$ and $A(x)$ are empirical parameters depending on the composition of glass, $T_0(x)$ is also a fitting parameter which is usually below transition temperature. The equation is also called Williams-Landel-Ferry equation in the polymer community. The other is Arrhenius equation and it is as follows:

$$\mu(T,x) = \mu_0(x)exp(-\frac{\Delta E_a}{k_B T}) \qquad 3$$

that ΔE_a is the activation energy, which is temperature dependent, k_B is the Boltzmann constant and is $1.38 \times 10^{-23}\, J \cdot K^{-1}$ in SI base unit. Compared to Vogel-Fulcher-Tammann equation, this equation fits covalent glass better. Both equations show the exponential dependence of the viscosity on temperature.

In our research, I use the following three kinds of glass and their corresponding properties are listed in the table. T_g is the transition temperature, Ts is the soften temperature and ρ is the density of glass.

Table 3 critical temperature of the glass powder used in the research

	Soda lime glass	Borosilicate glass	Lead glass	B-Bi-Zn glass
T_g (ºC)	573 ºC	560 ºC	451 ºC	325 ºC
T_s (ºC)	700 ºC	820 ºC	600 ºC	390 ºC
ρ (g/cm^3)	2.52	2.23	2.52	7.3

B-Bi-Zn glass (from Winngle company) is a kind of 3-phase system glass powder. It has Low-Melting Temperature and low thermal coefficient. It is usually used as sealing glass

in the electrical industry. It is more environmentally friendly than the lead glass which is commonly used as seal glass before. Our setup can reach 1200 ºC and can use different glass to finish the fabrication.

In the motion of liquid in a channel, viscosity plays an important role to determine the flow speed. For example, in the laminar flow, by fluid mechanics, the flow resistance of a circular channel is

$$R = 128\mu\frac{L}{\pi D^4} \qquad 4$$

R is the flow resistance, μ is the viscosity, L is the pipe length and D is the diameter of the channel. From the figure 11, the viscosity of the glass depends on the temperature. Thus, the fabrication rate which is determined by the flow rate of the molten glass also rely on the temperature. In the stable fabrication conditions, the fabrication rate should be synchronized with the flow rate of the glass in the channel or the shape of the structure would change.

Besides the growth rate, the viscosity also affects the surface finish of the microstructure. As shown in the figure below, high viscosity causes roughness and variation in the structures. To get smooth surface finish as in (c), the exiting glass flow should have viscosity around 10-1000 $Pa \cdot s$.

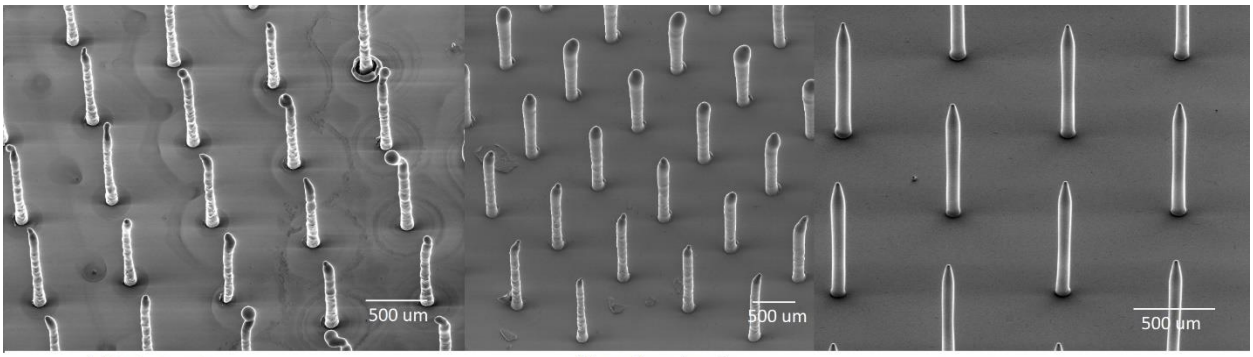

Figure 12 Different Surface Finish under Different viscosity

3.2.2 The Mechanical Strength

Most 3D micro fabrication uses polymers or ink which has a mechanical range of hundreds of M Pa [42] [43]. PEEK which is a strong polymer typically used for 3-D printing can reach elastic modulus of 2-4 GPa [44]. For comparison, the glass, which usually has Young's Modulus more than 20 GPa, is much stiffer than polymers. However, its strength may depreciate due to defects of the fabrication process. Bubbling and surface flaws are two most common reasons to reduce the mechanical strength of the glass structures. To verify our process does not have such issues, we compare the Young's Modulus of the material and wire structures fabricated by our process. The most used glass system in our experiment is B-Bi-Zn glass. The Young's Modulus of both bulk glass and fabricated structures are measured.

The Young's Modulus of bulk (B-Bi-Zn glass) glass is measured by a nano indenter (HYSITRON TriboIndenter ® Nanomechanical Test Instrument) and following is the result. It shows the Young's Modulus of the bulk glass system is 25.1 GPa, much stronger than that of polymer materials.

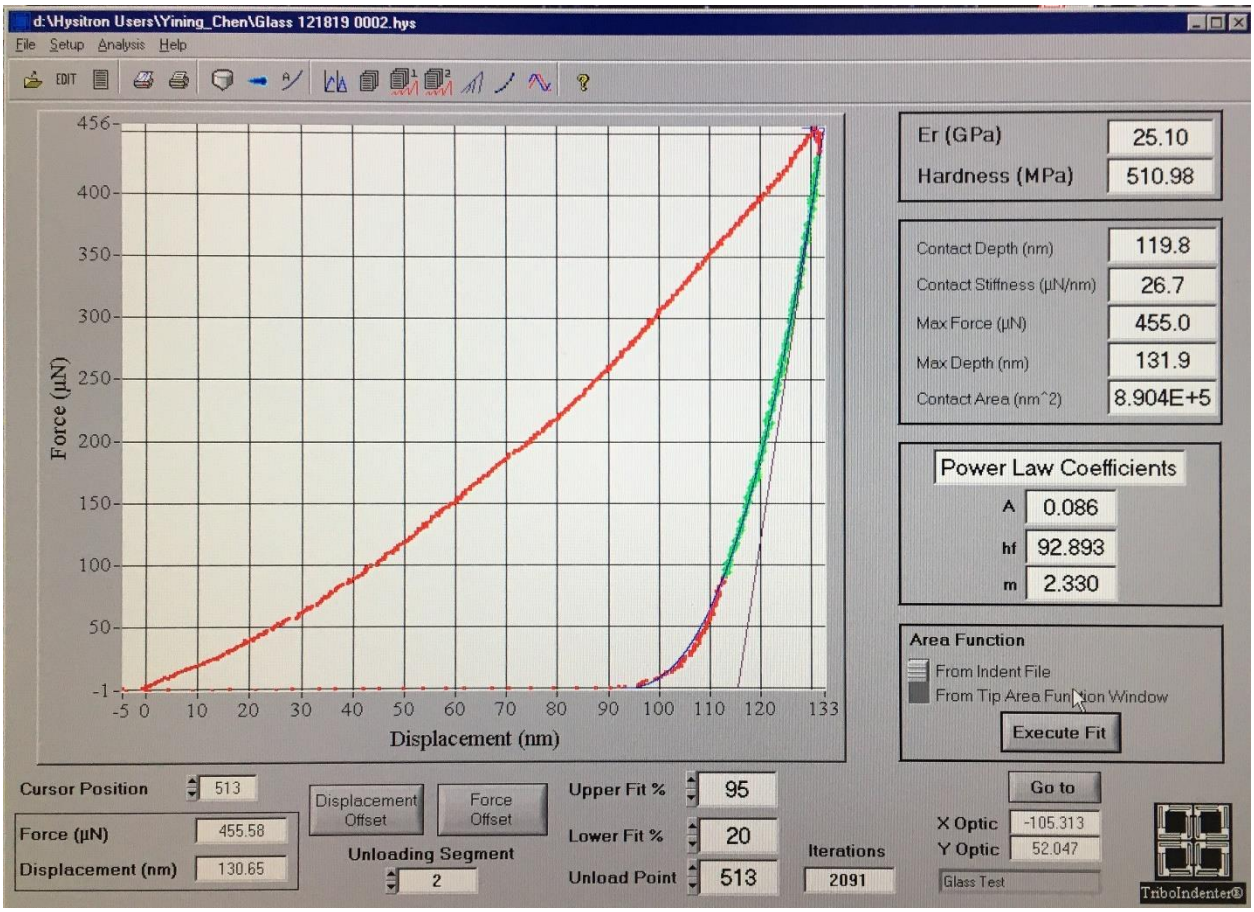

Figure 13 Nano Indenter Result for Bulk B-Bi-Zn Glass

To measure the mechanical strength, we fabricated a 70 μm diameter wires with 430 μm length and did bending test to get the Young's Modulus of the material. In the following is the displacement of tip deflection VS force. The applied force is on the tip of the cantilever. The equation of bending of a cantilever beam is

$$\delta = \frac{FL^3}{3EI} \qquad 5$$

where I is the area moment of inertia. For a circular cross section, it is $I = \frac{\pi d^4}{64}$. So we can calculate the Young's modulus as 25.56 GPa.

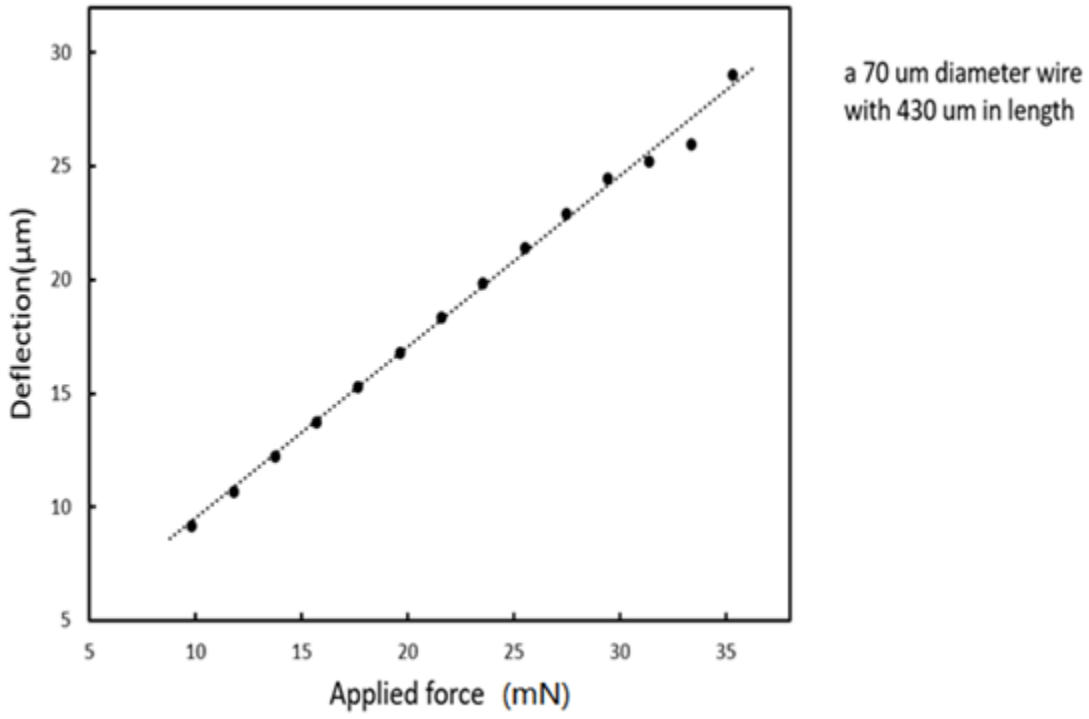

Figure 14 Deflection VS Applied force for 70 um diameter 430 um length micro wire

Compare the Young's Modulus with bulk glass material. It shows that the Young's Modulus of the fabricated structures and bulk glass matches well. It indicates that the process preserves the strong mechanical property of the glass and no significant defects such as bubbles are introduced in the micro/submicron structures in the fabrication process.

In summary, the fabricated structures and bulk material has similar Young's Modulus, and the process does not depreciate the mechanical strength. The strong mechanical strength of the structures gives advantage over other 3D microstructures, especially polymers.

3.2.3 The Wetting of the molten glass on different substrate and bonding strength

Besides the mechanical strength of the micro/nano structure itself, its bonding strength with the substrate is also important. Only with strong bonding with substrates, the fabricated structures can serve as templates of molding or functional structures in devices.

The bonding strength is related to the wetting properties of the glass on the substrate during the fabrication process [45]. Strong chemical bonding between glass and metal can be formed when contact angles is 25° and less under appropriate conditions [46]. In this bonding, glass and metal interchange or sharing electrons and leads to good adherence. The bonding strength between glass and glass substrate is determined by the contact angles which is governed by the wetting property of the molten glass.

We use Low-Melting T B-Bi-Zn system glass powder (from Winngle company) as the growth material and borosilicate glass as the substrate. The required temperature for good bonding on the substrate is 300 $^\circ C$. To get qualitive understanding of the bonding strength, it is compared to the flexures stress of the growth glass material. First four-point bending test is conducted on 550 μm length wire with 50 μm in length, the flexure stress is 320 MPa. Then when conducting the pulling test of a micro wire in room temperature, it always breaks in the middle of the wire which shows the bonding strength is larger than the flexure stress of the glass. It shows with proper temperature conditions during the fabrication process, we can get bonding strength larger than the flexure stress of the material which, will satisfy most application requirements.

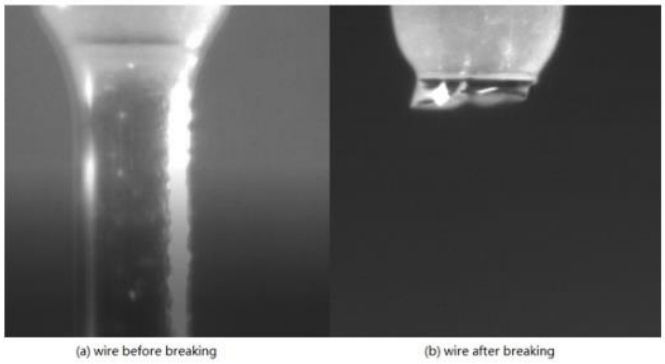

Figure 15 the breaking front in the pulling test.

From the figure above. We can see the clear breaking front in the wire. The bonding between the wire and the substrate is intact. It proves the bonding can be stronger than the wire itself. Thus, the structures fabricated by this method doesn't need a assemble process to mount it on the substrate.

Different substrate material and glass composition needs different substrate temperature to ensure good bonding strength. The substrate we mostly use in the experiment is borosilicate glass. For the low-melting 3-phase B-Bi-Zn system glass it need 300˚C to form good bonding on borosilicate substrate. We also try to bond this kind of glass powder on different substrates as well. By conducting pulling test, the bonding temperature is the temperature of the substrate when the bond is stronger than the wire itself. At the contact point of meniscus and substrate, the temperature is higher because the nozzle and meniscus provide additional heating on the spot. The results are show as follows:

Table 4 bonding temperature of different substrates of the low-melting 3-phase B-Bi-Zn system glass

Substrate material	The bonding temperature
Borosilicate glass	300˚C
Aluminum substrate	377˚C
Borosilicate coated with Ni	300˚C
Borosilicate coated with Cu	250 ˚C

Note: The nozzle temperature is kept the same in all cases and the glass is fully melted in the nozzle.

Rest the nozzle on the substrate seems helps the bonding process. As with same heat powering (nozzle and substrate), we can also increase the bonding strength by letting nozzle and substrate stand still and wait for 1 or 2 seconds before pulling up since it would increase the temperature at the contact. But the bonding strength without the waiting is already strong enough for many applications [47].

3.3 The Driving Force of the Fabrication Process

3.3.1 The Growth Rate and Pressure

As a stable glass wire forming process is essentially an extrusion process with the natural cooling process solidifying the molten glass upon exiting the nozzle opening, the growth rate of glass wire is simply governed by the flow mechanics of the molten glass through the nozzle, i.e., the wire growth rate $v \propto Q$, where Q is the volume flow rate of the

molten glass through the nozzle. Q is, in turn, proportional to $\Delta P/R$, where ΔP is the pressure difference between two end of the nozzle and R is the flow resistance determined by the viscosity of the molten glass μ, the nozzle diameter D and the channel length L. The fluid resistance can be defined as $R_F = \frac{\Delta p}{Q_v}$ which is determined by geometry of the nozzle, the inside finish of the channel and fluid properties.

To check whether the flow is laminar or turbulent, we need to estimate the Reynolds number. Based on the range of glass density, flow speed, channel diameter and viscosity, the Re is

$$Re = \frac{\rho \times v \times d}{\eta} \approx 7.4 \times 10^{-8} \ll 1, \textit{ thus, the flow is laminar.} \qquad 6$$

In a laminar flow regime, the flow resistance through a tube channel is described by

$$R = 128\mu L/(\pi D^4). \qquad 7$$

$$\Delta p = p_{gauge} + \rho g h \qquad 8$$

Rearranging the fluid resistance equation, we can get

$$Q_v = \frac{\Delta p}{R_F} = \frac{p_{gauge} + \rho g h}{R_F} = \frac{p_{gauge}}{R_F} + \frac{\rho g h}{R_F} \qquad 9$$

The geometry of the micro nozzle used is demonstrated as follows. It has a big ceramic tube with OD 2.5 mm and ID 1.58 mm to serve as a reservoir of the molten glass material. A ceramic micro nozzle (micro-swiss P/N 41690-0013-335) is glued on to one end of the big tube by ceramic glue (OMEGABOND “600”, OMEGA Engineering, INC) . The ceramic micro nozzle has two parts, one is a 3 mm tapered section changing OD from 1.8 mm to 0.8 mm and a straight tip with 45 μm opening and 500 μm length.

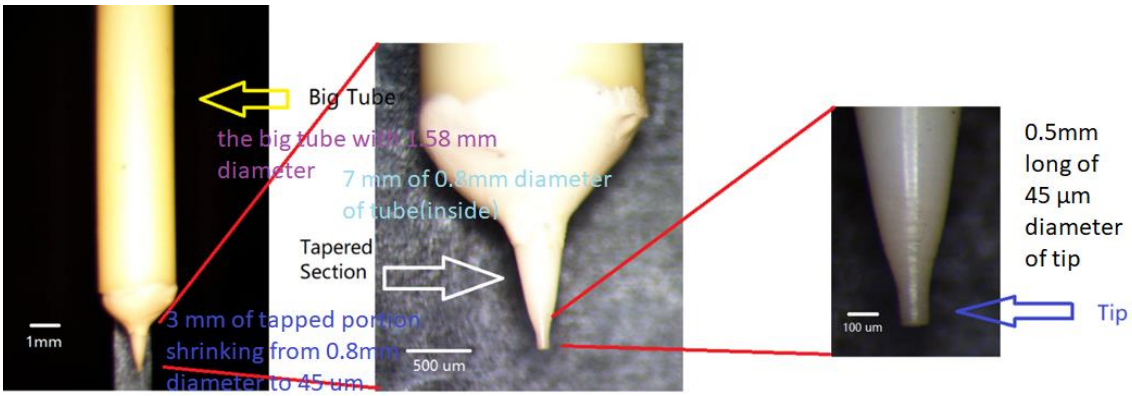

Figure 16 Different section of ceramic nozzle

We tabulate each section and by series principle to get the total fluid resistance of the assembly. The consist of the nozzle: 0.5mm of 45 µm diameter of tip, 3 mm of tapped portion shrinking from 0.8mm diameter to 45 um and 7 mm of 0.8mm diameter of tube, and the big tube with 1.58 mm diameter.

The resistance of new tube:

The tip: $R = 128\mu\frac{L}{\pi D^4} = 128 \times 10 \times \frac{0.5\times10^{-3}}{\pi(45\times10^{-6})^4} = 4.96798 \times 10^{16}\ \frac{Pa}{m^3/s}$

The taped portion: $R=6.907884883665216 \times 10^{15}\ \frac{Pa}{m^3/s}$

The third portion: $R=7.957747154594767 \times 10^{12}\ \frac{Pa}{m^3/s}$

The total R is $5.66 \times 10^{16}\ \frac{Pa}{m^3/s}$

Table 5 flow resistance of different sections of the nozzle

Portion	R in $\frac{Pa}{m^3/s}$	Percentage (%)
Tip	4.97E16	87.77
Taped section	6.9E15	12.21
Third Portion	6.96E12	0.014
Big Tube per cm	1.89E10	0.001

From the calculation above, the resistance is dominated by the uniform tip section. So, we

can use it to estimate the growth rate of the fabrication process. When we knock off the very tip of nozzle, the flow rate increases about 5~6 times which proves the correctness of our analysis of the geometry of the nozzle assembly.

To verify the relationship between pressure and growth rate from the equation above, experiment is conducted with the pressure increasing from 1.5 psi to 10 psi. The growth rate falls into the range of the estimate and shows the linear dependent on pressures as expected from above.

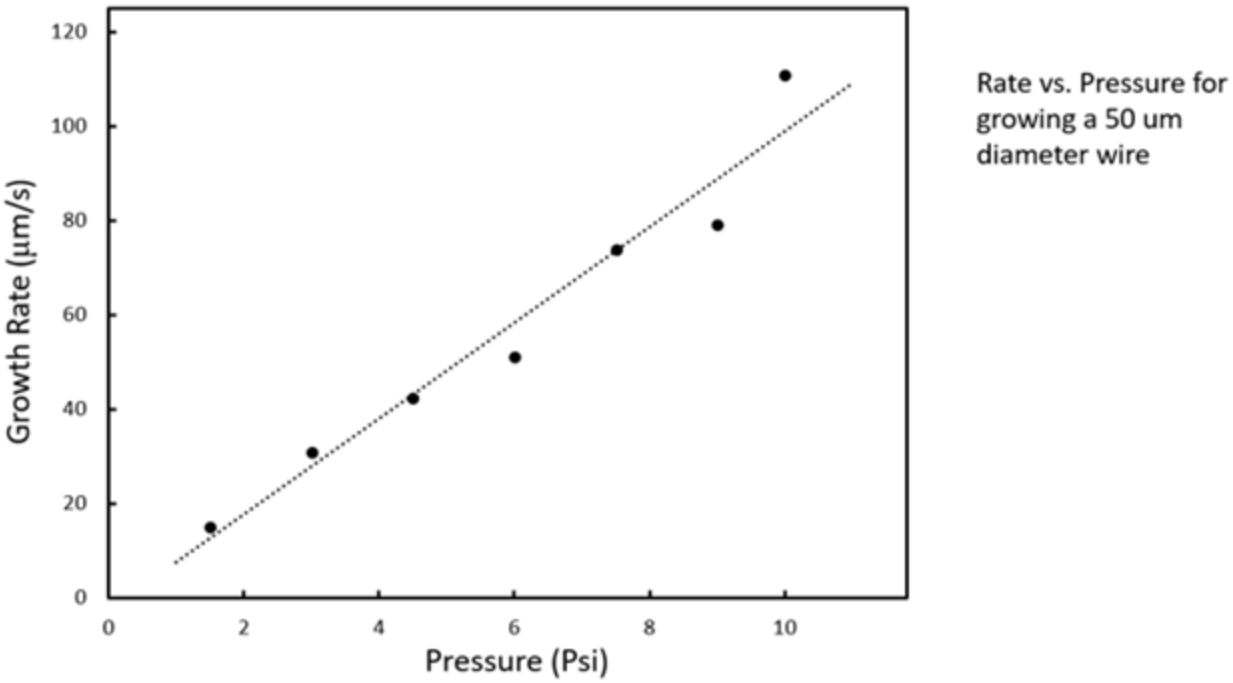

Figure 17 Rate VS Pressure for growing a 50um diameter wire

The figure shows the linear dependence between the growth rate of glass wire and the applied back pressure.

Since micro nozzles (MICRO_SWISS)) are made of machinable ceramic, we can

machine it to change its opening and wall thickness. In this way, we can change the diameter of the fabricated structures. Moreover, we can also change the moving speed of the motor to change the diameters which would be shown in later chapter. The following pictures show the change of the nozzle opening and its side wall by machining.

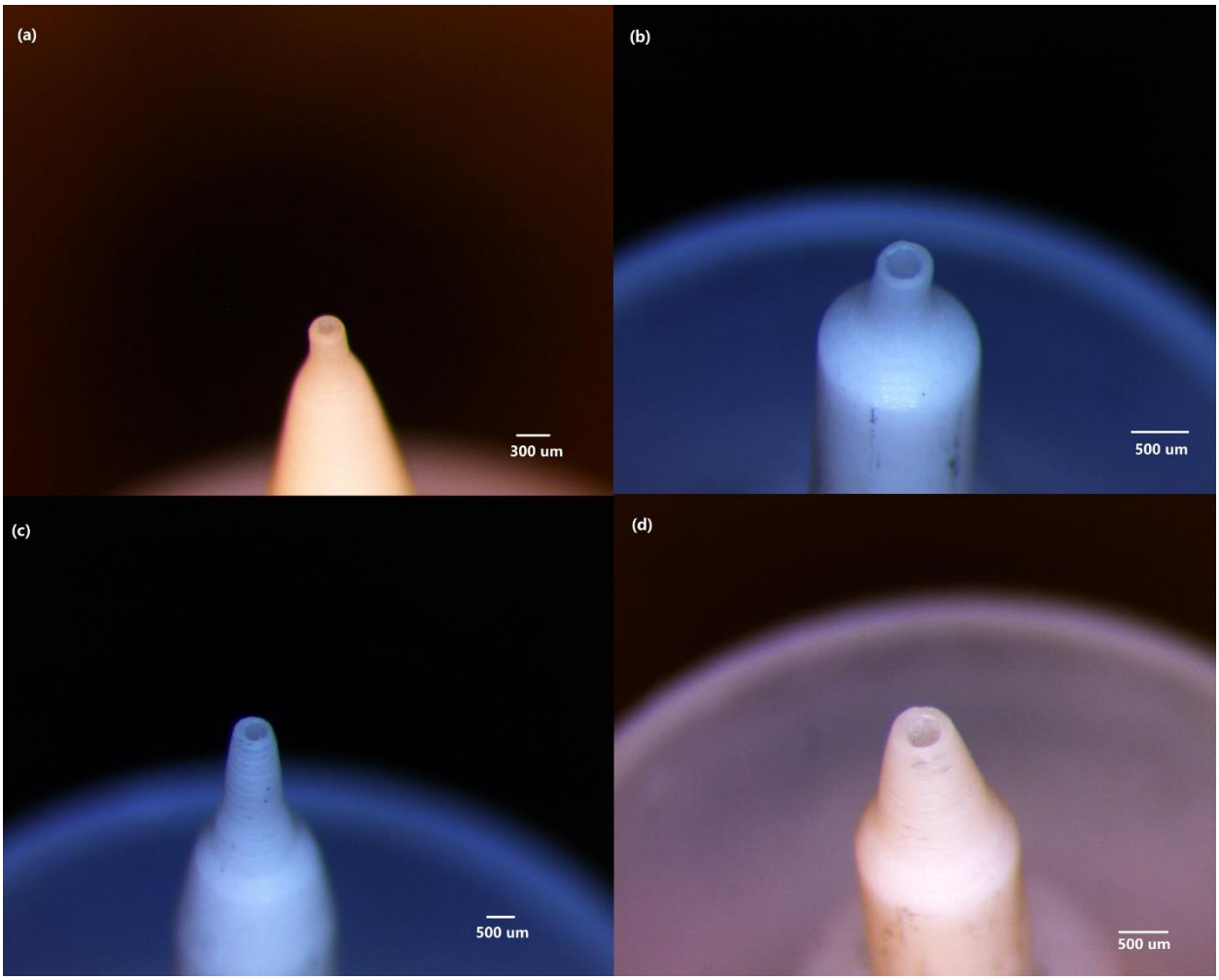

Figure 18 different nozzle openings and side wall thickness made by machining

Figure 18 (a) is nozzle with 200 μm opening in diameter and 50 μm side wall thickness. (b) is nozzle with 350 μm opening in diameter and 75 μm side wall thickness. (c) is nozzle with 400 μm opening in diameter. (d) is nozzle with 400 μm opening in diameter and 75 μm side wall thickness. The changing of the nozzle opening does not

change the inside structures of the nozzle, the analysis of the flow resistance should be still valid.

3.3.2 The Effect of Surface Tension and Gravity

Unlike macro-scale glass fabrication such as the group in media lab from MIT [39], micro-scale fabrication introduces more force, such as surface tension, that needs to be paid attention to. In their case the surface tension is negligible, and the gravity is the driving force of the growth. In our fabrication, the surface tension cannot be negligible and determine several important aspects of the growth.

Like the viscosity, the surface tension of the molten glass depends on temperature. W.B. Pietenpol used the bulb method to measure the surface tension of various composition of glass [48]. The following figures shown the surface tension of various molten glass dependence of temperature.

TABLE I. *Composition of glasses investigated.*

	No. 3 Soda-Potash-Lead	No. 4 Potash-Lead	No. 6 Potash-Lead	No. 7 Boro-Silicate	No. 8 Soda-Lime-Zinc	No. 10 Boro-Silicate
SiO_2	62.5	57.5	63.0	81.0	67.0	(Flint?)
PbO	21.0	28.6	22.0	—	—	Alkali-free
Fe_2O_3	0.2	0.2	—	—	—	
Al_2O_3	0.8	1.4	1.0	2.0	2.5	Composition undetermined
CaO	0.5	0.4	—	—	7.0	
MgO	0.5	0.4	—	—	—	
K_2O	6.0	8.0	6.0	—	—	
Na_2O	9.0	4.2	8.0	4.25	14.0	
B_2O_3	—	—	—	12.5	2.0	
ZnO	—	—	—	—	7.0	
Density g/cc	3.34	3.50	3.21	2.28	2.66	2.82

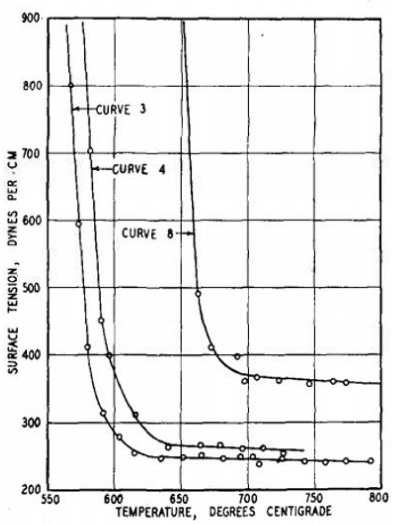

FIG. 3. Variation of surface tension with temperature for the glasses listed in Table I.

Figure 19 the surface tension dependence on the temperature of various composition of glass from [48].

The method started from 200 ℃ above the annealing temperature and the viscosities of different glass are stabilized within 100 ℃ after a quick drop. This property is shared by all the glass material we used in our experiment. For the class of 3-phase B-Bi-Zn low melting temperature glass powder, S.-B. Shim et al measures their surface tension [49]. Its surface tension does not change a lot after the temperature reaches the melting temperature. The surface tension of soda lime [50], borosilicate glass [51] and lead glass [52] have similar characteristics when the glass is in molten status.

When the surface of liquid is curved, there would be a pressure difference caused by the surface tension between the inside and outside of the surface which is called Laplace pressure. This pressure is negligible in macro scale because the principal radii of curvature are large. In the micro scale, the principal radii of curvature are small, it cannot be negligible and play an important role in the fabrication process. Using the 3-phase B-Bi-Zn glass as an example. By taking the typically value of the surface tension and molten height in our experiment, we can compare the Laplace pressure caused by the surface tension and the gravity of the molten glass. Use the 3-phase B-Bi-Zn glass as an example. We use the lower bound of surface tension of the 3-phase B-Bi-Zn glass powder which is $0.15\ \frac{N}{m}$.

The Maximum Laplace pressure is $P = \frac{4\gamma}{d} = \frac{0.6}{50\times10^{-6}} = 12000\ Pa = 1.74\ psi$

γ is the surface tension of the molten glass and d is the opening diameter of the nozzle.

The typical the overall height of the glass is 4 cm. Use this value to calculate the driving force by gravity and the result is

$$P = \rho gh = 7400 \times 9.8 \times 0.04 = 2900Pa = 0.421Psi \qquad 10$$

ρ is the density of the molten glass, g is the acceleration of gravity and h is the height of the molten glass.

From the calculation above, we can see the Laplace pressure caused by the surface tension is larger than the pressure caused by the gravity. So, the molten glass would keep itself on the nozzle when it is in molten status. Back pressure is needed to push the glass out to form microstructures. For the soda lime, borosilicate glass and lead glass, their surface tension are larger, and their density is smaller. So, their Laplace pressure can also hold the molten glass as the 3-phase B-Bi-Zn glass powder case.

Figure 20 Heated nozzle without/with back pressure

Figure above shows the heated nozzle with and without back pressure. From the figure we can see, the molten glass is kept inside the nozzle when no back pressure is present. When a little back pressure is present, the molten glass formed a bump at the front of the nozzle opening. It is a self-regulated process to counter the applied pressure by the surface tension. Only when the back pressure is larger than the surface tension, the glass could be pushed out to start the fabrication process.

The surface tension change is not significant when temperature goes up if the glass is already in molten status. It can counteract the gravity force on all the operation condition of our experiment.

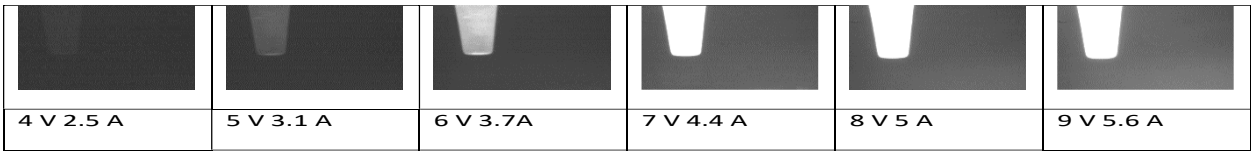

Figure 21 Nozzle Heating under different powers without back pressure

Figure 21 shows the nozzle filled with glass powder under different nozzle heating power (which is tip heater in figure 8). The brightness indicates the increasing temperature of the nozzle. For all the heating conditions, the molten glass is kept inside nozzle. It demonstrates the Laplace pressure is larger than the gravity of the molten glass in all the range of the heating power.

3.3.3 Other Considerations: the corrosion of the metal by the molten glass

Another important effect that the surface tension can cause is called the Marangoni effect [53]. It is important in deposition of DNA/RNA microarrays [54] [55], manufacture of electronic and optical materials [56] [57]. It is mass flow caused by the difference of the surface tension gradient. Evaporation usually is the reason that causes the gradient, but in our research, the gradient is caused by the thermal gradient of the molten glass at different spots of nozzle. Besides that, the wetting property of molten glass also depends on the temperature. With higher temperature, the molten glass wet better on the same surface. The difference in the wettability of glass on the ceramic surface leads it to move onto the higher temperature side. It also provides a driving force for the molten glass to climb onto to the upper side of the nozzle as the temperature in the upper section of the nozzle is higher. These two effects need specially attention in the molten glass based micro 3D process and the combination of them can introduce instability into the process.

The upper section of the nozzle has higher temperature than the lower section because the heating source was placed above the nozzle opening. Once the glass molten was climbed onto the wall the nozzle, it would move upward since the wettability between glass and ceramic surface is better when temperature is higher. The surface tension, on the other hand, could be either increase or decrease with temperature increases. It depends on the composition of glass and temperature range [48] [49] [58]. Once the radius of the molten glass shrinks, the Laplace pressure due to surface tension is increased. It breaks the balance of pressures, and the higher pressure would squeeze the molten glass into the lower pressure region. This effect leads the radius to shrink even more and increases the pressure imbalance and gradually contribute to the break of the meniscus. The combination of these two results the gradual covering of the outside wall of the ceramic nozzle with molten glass in certain conditions.

In the figure below shows the combination of these two effects on the growth of the wires. Under certain temperature, pressure and pulling speed conditions, the molten glass prefers to climb onto the side wall of the nozzle instead of forming wires. (a)(b)(c)(d)(e) show the growth status at different time after beginning of one fabrication. In this case, it cannot maintain uniform wire growth and the molten glass would be accumulated on the tip of the nozzle.

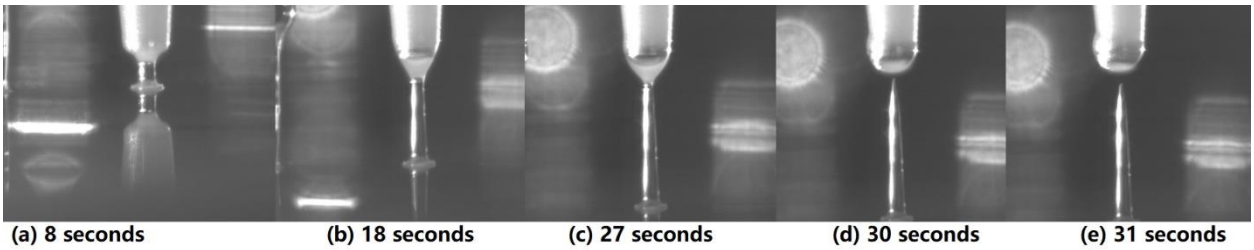

Figure 22 The effect of the surface tension on the growth of the wire

In figure 22 (a) is the wire after 8 seconds when the growth begins, (b) is 18 seconds, (c) is 27 seconds, (d) is 30 seconds and (e) is 31 seconds respectively. In the case above, the glass meniscus breaks up and the molten glass flow to the side wall of the nozzle.

The competition between these two effects and the deposition on the wire determines the stability of the wire grow process. These two effects usually result on instability of the uniform growth. Finding ways to suppress them would be desirable in the fabrication of uniform micro wires/rods.

We tried different materials to suppress the tendency of the molten glass to climb onto the side of the nozzle. The wetting property of glass on metal is different from that on oxides [59]. If the molten glass is less preferred to wet with the side wall of the nozzle, this effect can be reduced so the stability of the growth process should increase. Although the metal nozzle with tens of micrometer opening can also be made many methods such as micro-electro-discharge machining [60] or Through-Mask Electrochemical Micromachining [61], they need to different setup of the systems to prevent gas leaking and binding with molten glass reservoir. To make use of the current setup, coating is an alternative way to get nozzle with metal surface. Sputter is used to coat the ceramic nozzle to get metal surface. The sputter process is finished in the IEN facility of Georgia Institute of Technology by Unifilm Sputter.

However, many metals such as Chromium can be corroded by glass melts under oxidation reactions [62]. It would also form some oxidated products that may block micrometer nozzle opening with around 100 μm diameter. Moreover, when glass is in molten status, it is a good solvent for metals [63]. Even metals which is inertia to oxidation such Au can dissolve as ions in glass melts. We made an 200 nm-Au coating nozzle which

has a 100 nm Cr seed layer to form good bonding between ceramic and Au by sputtering and the coating would disappear after using for a while. Thus, our research would focus on the molten glass on the ceramic surface. During the experiment of uniform micro-wire growth, the pulling speed should be carefully adjusted according to the temperature and back pressure so the surface tension and wettability would not affect the stability and the meniscus of molten glass can keep its shape.

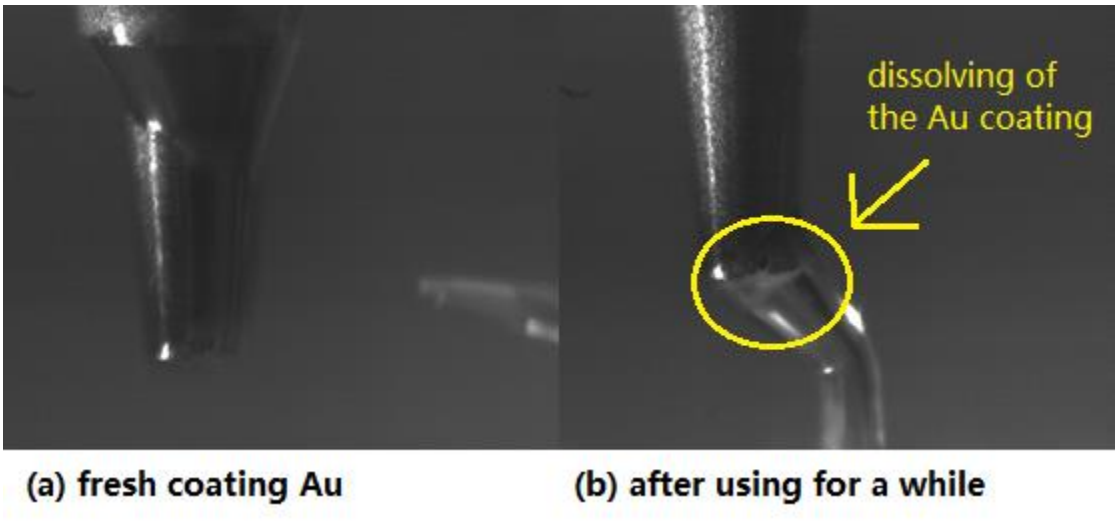

Figure 23 shows the corrosion effect of the molten glass on the metal

The figure 23 (a) on the left is the ceramic nozzle fresh sputter coated with a layer of 200 nm Au by Unifilm Sputterer in the cleanroom at IEN facility in Georgia Institute of Technology, the figure 23 (b) is the ceramic nozzle after fabricating several arrays of the structures.

3.4 The Evolution of Growth

3.4.1 The Stable Growth for Continuous Uniform Wire/rod

To realize stable growth, one necessary condition is the glass pushed out of the nozzle should be equal to the glass consumed in the wire/rod growth. If this condition is violated, the shape of the meniscus would change and thus the growth cannot be stable. The molten glass would be stretched and reduce its diameter when the pulling speed increases. As the pulling speed increases further, the pushed-out glass cannot match up with the growth front of the structures so the meniscus would eventually break to stop the fabrication. Experiments with different pulling speed under same conditions are conducts and the results are shown below.

It shown the evolution of the structures with increasing motor speed. For the results below, in the setup of figure 8, the ceramic heater is kept at 1.8A 20.4V to molten the reservoir of the glass, tip heater is kept at 1.2V 1.2A to control the viscosity of the exiting glass melts and Substrate heater is powered at 3.3A 13.8V to form good bonding. The experiment is conducted in room temperature. The back pressure is 6 psi.

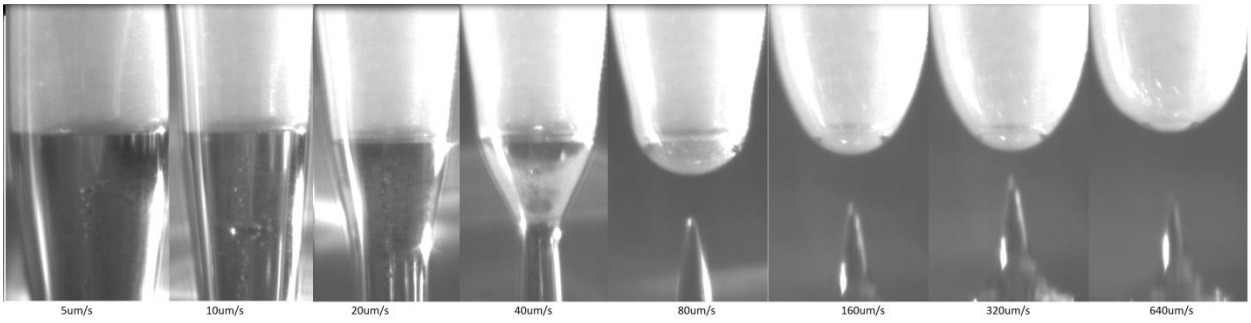

Figure 24 the evolution of structures with increasing pulling speed

When the pulling speed further increase, the meniscus of the melt glass can no longer reach equilibrium and break up happens. The break-up will form the needle naturally. The needles shape and tip sharpness are related to the pulling speed. Section 3.5 will explain the relationship between the needle and the pulling speed.

Before the needle forming happens, the meniscus can adjust its diameter to keep up with the flow rate of molten glass out of the nozzle. v_1 is the flow out speed of the melted glass which is determined by the geometry of the ceramic assembly, viscosity (temperature) and driving force (back pressure). r_1 is the nozzle opening and ρ_1 is the density at the exit of the ceramic nozzle. v_2 is the stable wire growth speed which is equal to the moving speed of our motors in stable growth condition. r_2 is the diameter of the uniform micro-wires/rod and ρ_2 is of the micro-wires/rod.

The mass of melting glass coming out of nozzle opening would be equal to the mass increase of the micro-wire rod. Thus,

$$\rho_1 \pi r_1^2 v_1 = \rho_2 \pi r_2^2 v_2 \qquad 11$$

After arranging the equation above and cancel out π, it becomes

$$\frac{v_1}{v_2} = \frac{\rho_2 r_2^2}{\rho_1 r_1^2} \qquad 12$$

Neglecting the density change due to the temperature difference and solidification process, we can further simplify the relationship between diameter and velocity. It becomes

$$\frac{v_1}{v_2} = \frac{r_2^2}{r_1^2} \qquad 13$$

Experiments are conducted to check whether the equation above are valid. In the following table is the comparison of the measured diameter VS estimation based on the estimate equation.

Table 6 Comparison of the estimate diameter and measured diameter.

Pulling Speed (in mm/s)	0.01	0.011	0.012	0.013	0.014	0.015	0.016	0.017	0.018	0.019	0.02
Est. dia(μm)	-	57.2	54.8	52.6	50.7	49.0	47.4	46.0	44.7	43.5	42.4
Act. Dia(μm)	60	58	56	52	51	49	47	46	45	44	42

The actual diameter is very close to the estimate diameter which means the process follows equation 13 above. The density change due to temperature and solidification can be neglected. The volume rate at exit of the ceramic nozzle is almost kept the constant under different pulling speed which means the back pressure is main driving force of the molten glass flow. It provides a way to control the diameter of the micro-wire/rod during the growth.

In the stable region, the growth of the wires is quite consistent. In the figure are B-Bi-Zn glass wire array. They were grown at $20\ \mu m/s$ with 6 psi pressure and the ceramic Heater kept at 1.8A 20.4V tip Heater kept at 1.2V 1.2 A. The estimation of the molten glass exiting the nozzle is around 700 ºC. The temperature of the substrate is kept at 300 ºC. The diameter of the wire are constant which indicates stable growth condition during the fabrication.

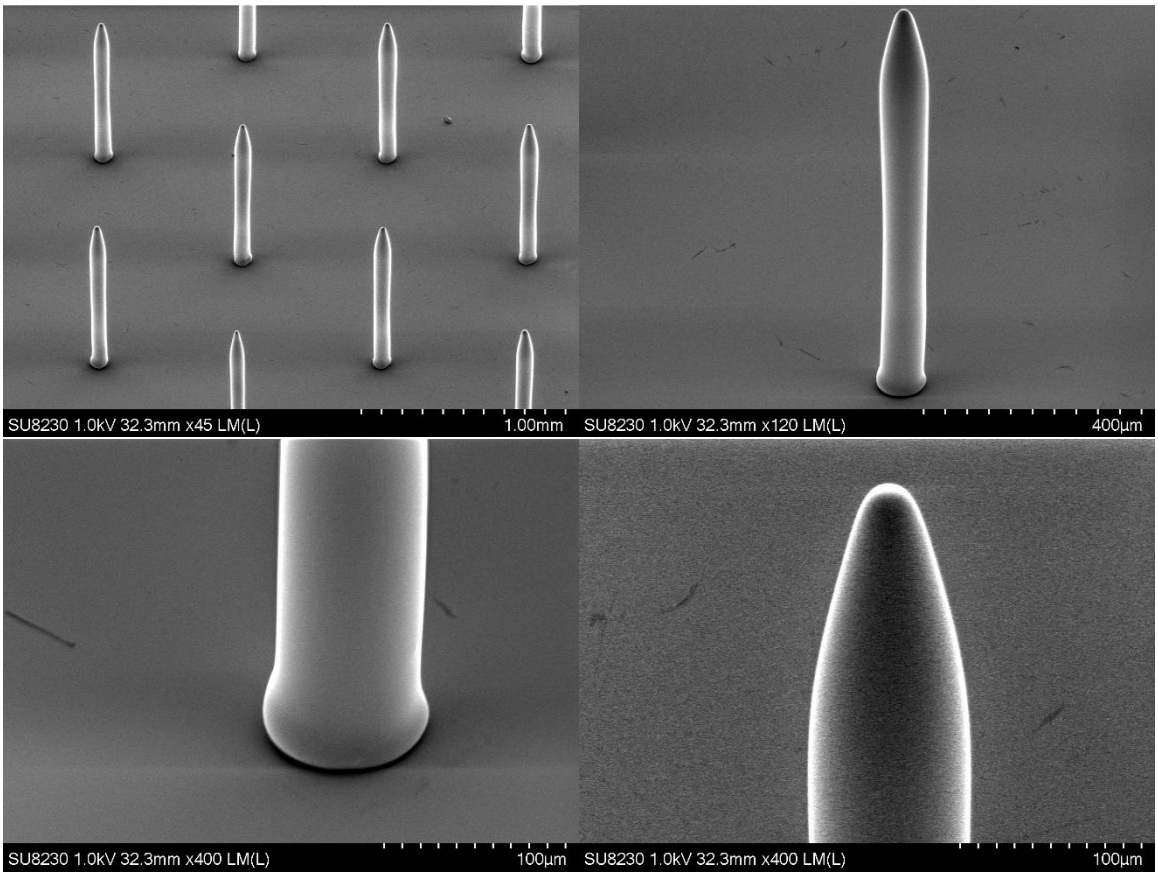

Figure 25 Array of uniform wires with tapered tip

3.4.2 Diameter Tuning

From the diameter estimation and experiment results, pulling speed can change the shape and size of the fabricated structures. Within the stable wire formation range, we can achieve different diameters of the wires. As the speed of the motor increases, the meniscus between the nozzle and substrate is stretched. The higher the speed of the motion, the smaller the diameter. It is a way to control the diameter of wires. Within the stable wire formation range, we can achieve different diameters of the wires. Experiments are conducted to show this relationship with tip heater at various heating power. The tip heater determines the temperature at the exit of the nozzle. The ceramic heater is kept constant to melt the reservoir of glass.

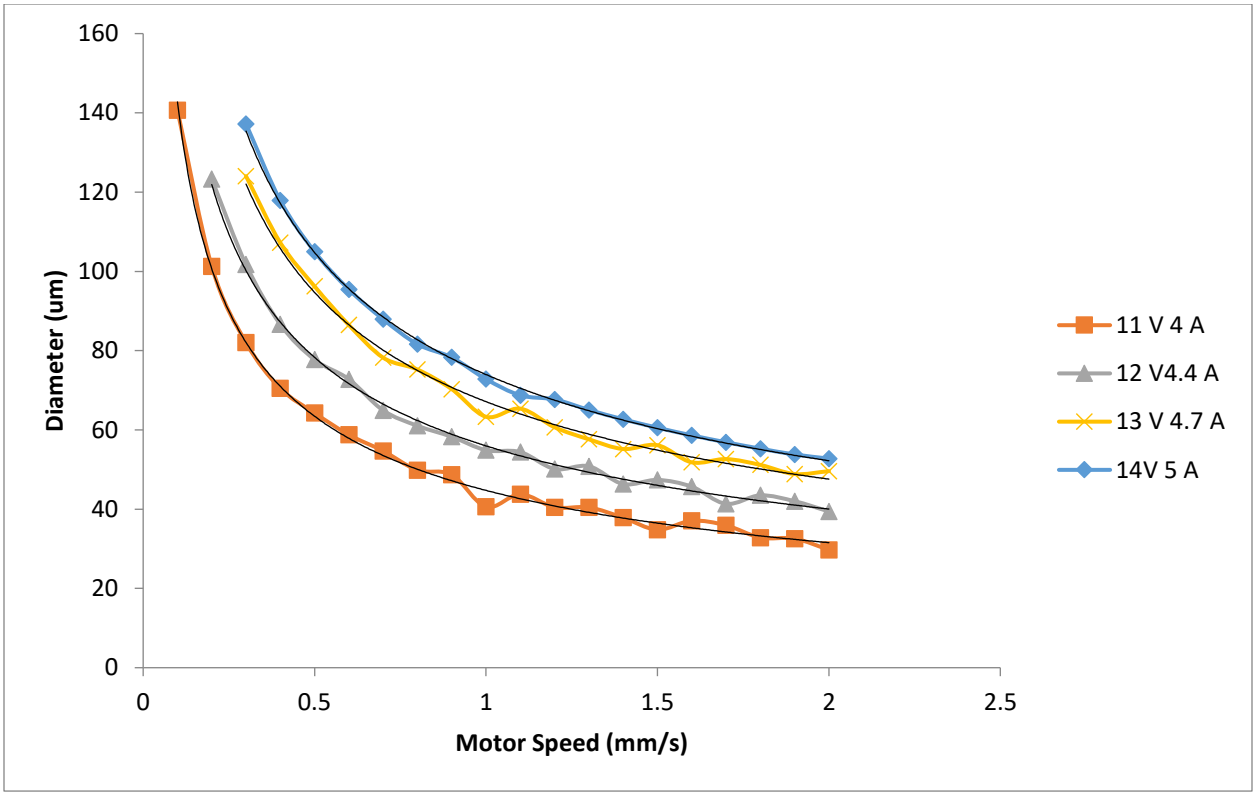

Figure 26 The Diameter under various pulling speed with different heating power

In the graph above shows the diameter change with different power of heating source under same driving pressure (3 Psi back pressure). The source power is related to temperature of the melt glass. The higher the power, the higher the temperature and the lower the viscosity. All the curve starts with the diameter of the nozzle and decreases as the motor speed increase. The higher the power, the larger the diameter of the grown wire as the flow rate is larger due to the low viscosity.

This relationship is established when the pushing-out speed of the molten glass matches the growth rate of the solid wires under the stretched meniscus. There are complex meniscus stability problems here. If the speed of the motor increases further, the pushed-out glass can never match up the growth front, so the meniscus breaks down and the fabrication process goes out of the stable region.

Thus, both the temperature profile which is affected by the heating power and pulling speed can change the size of the uniform micro wires/rod. With same diameter, high temperature is used in high-speed fabrication as the volume rate of the molten glass out of the nozzle is higher due to the lower viscosity in the stable growth region. The highest fabrication speed can be several mm/s.

3.5 Needle Growth

When the pushed-out glass cannot catch up with the moving speed, the meniscus breaks and forms needles under the cooling process. The shape of needles is determined by the pulling speed at constant pressure and temperature conditions.

The break-up process provides an alternative way to fabricate needles with sharp tip. Common way to get sharp tip is by etching process which is an extra step after the structures is fabricated [64]. The tilting angle of tip is also limited by the lattice structure of the material such as silicon. In our fabrication, it can be integrated as a single step. In the following is an experiment showing how the needle shape can be controlled during the process. The needles under different pulling speed are distinguished in height and tip sharpness. Under proper conditions, very sharp needles can be formed in a single step. The following demonstrates the evolution of the needle formation.

The experiment are set with ceramic heater at 2.0 A 18.5 V and tip heat at 1.8A 2.5V. The reading of the thermocouple near the ceramic nozzle tip is 509˚ C. the glass substrate is heated to 300˚ C to get good bonding. There is no pressure applied.

Figure 27 shows the needles fabricated with the condition above with motor speed

shown in table 7. The experiments can be repeated with the same result. The height and tip sharpness of the needles in each experiment are similar among the experiments with the same motor speed. It shows the fabrications of the needles are consistent and pave the way to make uniform arrays of needles with tunable heights and tip sharpness.

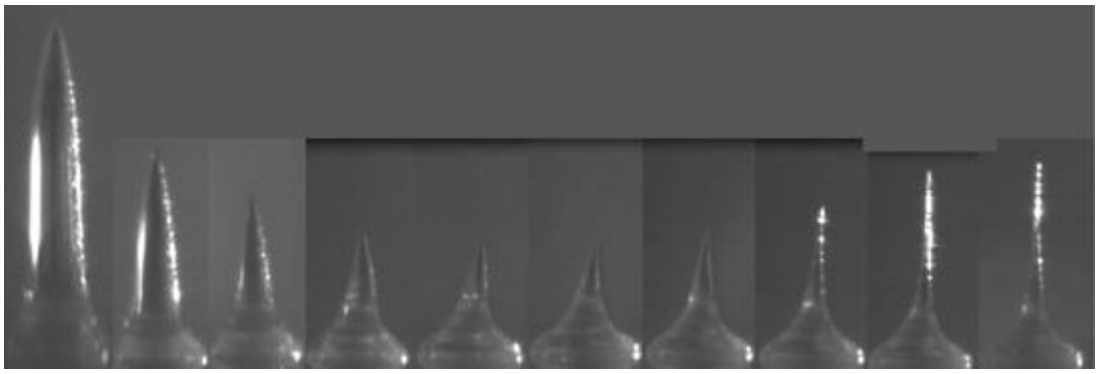

Figure 27 The evolution of needles with increasing pulling speed

Figure 28 shows the SEM images of the needles in Fig 27 with tilting angle at 45˚.

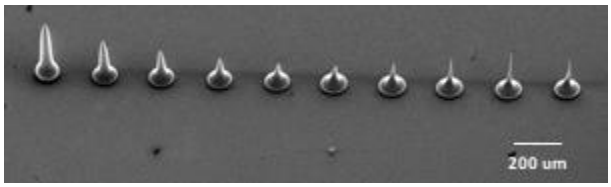

Figure 28 SEM image of needle array in Fig 27

Table 7 The height and tip size of needles with different pulling speed

Char.(μm)\Velocity(mm\s)	0.01	0.02	0.04	0.08	0.16	0.32	0.64	1.28	2.56	5.12
Height (μm)	300	200	160	140	120	110	130	180	250	220
Tip Size (μm)	10*	4.2	3.75	2.5	2.0	1.625	1.25	1.0	0.85	0.38

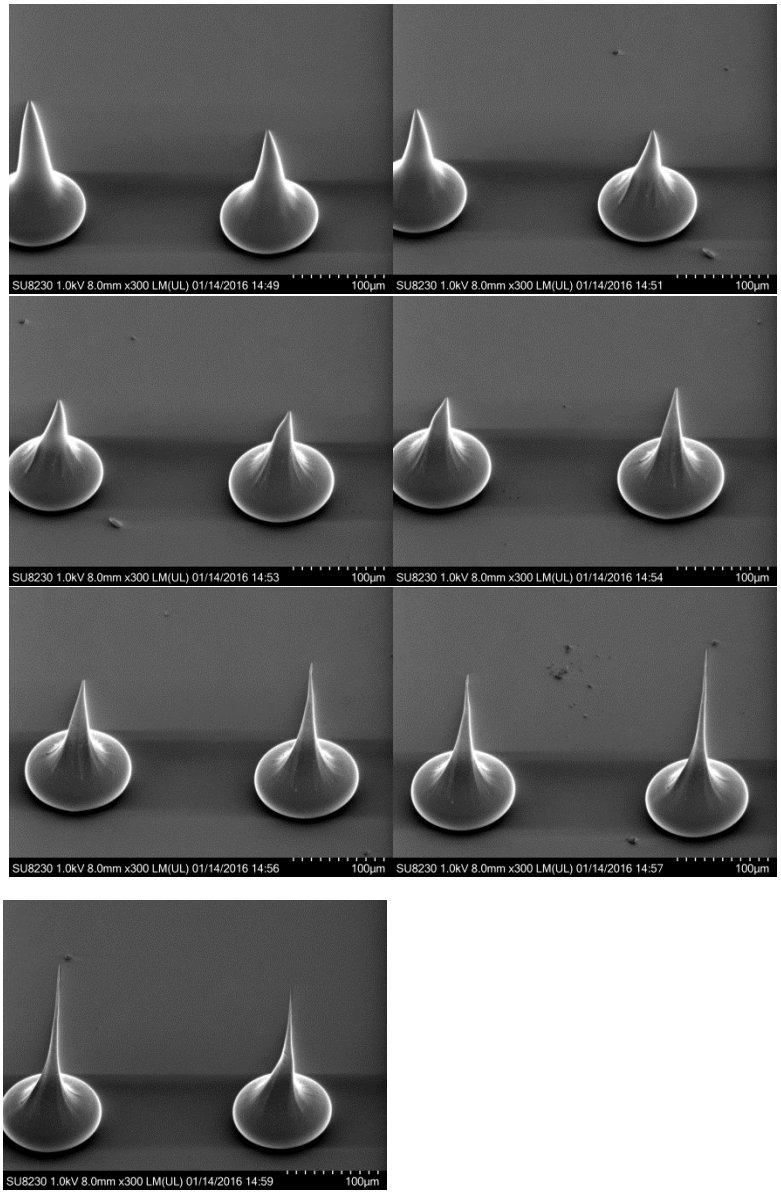

Figure 29 Closer look of the needles in Fig 28

Figure 29 is a closer look of the needles in Figure 28. In each SEM image, there are two consecutive needles in Figure 28. The order of the needles in Figure 29 is the same as that of figure 28 From left to right.

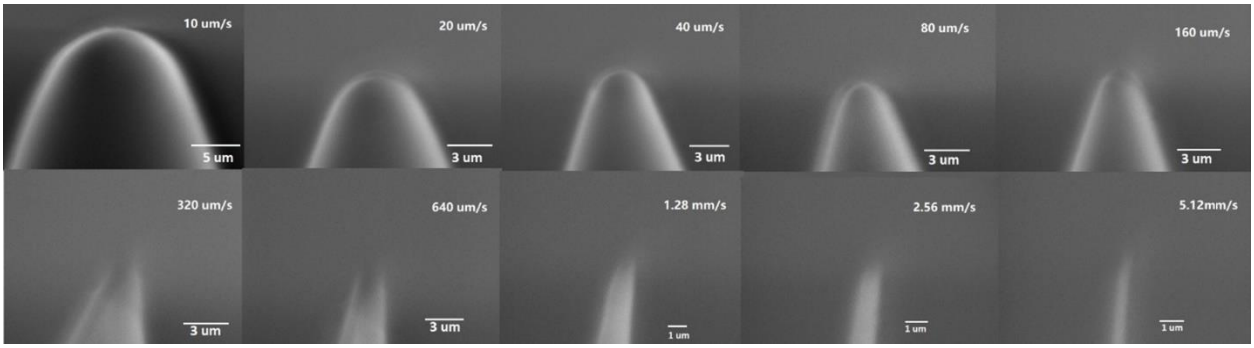

Figure 30 The tip of needles in Fig 28

Figure 30 shows the tip diameter of the needles. With the increasing of the pulling speed, its sharpness increased. The diameter of the tip of needles decreased from 5 μm to about 300 nm.

The height of the needle decreases with the pulling speed first and then increases. In the experiment above, the needle with smallest height is grown at 32 $\mu m/s$. Surface tension can cause the formation of the needle shape. As the meniscus stretches, the surface tension tends to decrease the surface area of the growth front. Thus, the radius of growth front shrinks and needle shape structures are form under rapid cooling of the glass melts.

In the low speed, the surface tension is the more dominant factor in the breakout of meniscus. There is enough time for the melt glass from the nozzle to be pushed out to the growth front. However, to make the surface energy lowest, the glass melts need to change its shape and the wire/rod shape cannot be maintained. The redistribution of the glass melts leads to form the needle-shaped structures.

In the high-speed case, there is not enough time for the melt glass to be pushed out which is another factor to break the grow process. The material used in forming the needle is less than the low-speed case. The needle is formed by the viscous force between different

layers of the melt glass that can withstand the shear force caused by the pulling process. As the pulling speed increases, the needles taper faster. The faster the pulling speed is, the less new melt glass can go down to supply the consumed volume. The meniscus must use less melt glass to cover the same distance. Thus, the needle is more tapered.

For the pulling speed in the middle of the range, the surface tension break and lack of material break have comparable effects on the forming of the needle shape. It makes the needle formation process can either break by the surface tension or the lack of material, which made it most unstable in that region. When one of the factors dominates, the growth mechanism is simple and more stable. So, from the figure above we can see the needles are more stable at the low or high pulling speed cases. It can also be shown by the symmetry of the formed needle tip. The tips at formed at the slower or faster pulling speed is more symmetric than the needle tip in the middle range. The middle speed also produces needles with the shortest height.

In summary, by intentionally terminating the glass wire growth at high pulling speed exceeding the speed for stable wire growth, sharp-needled glass structure can be readily fabricated. Such a needle array would be difficult or costly to fabricate by conventional methods such as etching [65], lithography [66] [67], electric discharge machining [68]. The height and other geometrical parameters of the needles can be easily tuned by adjusting the growth conditions in the system. The needle array fabricated by this method have ultra-smooth surface and is also strong enough to serve as mold for biocompatible polymer material for the medical application.

3.6 Governing Equations and COMSOL Model of the Process

The stability region provides a guideline to determine the pulling speed during uniform wire growth. The molten glass-based fabrication has some similarity with the glass fiber drawing process. They both extruding the molten glass from a nozzle. The difference is that the glass fiber drawing process uses winding, and our fabrication is moving the substrate.

Scientists had put a lot of effect to build up model to find the stability of molten fluid. J.R.A. Pearson et al put equations for the stability analysis of molten threadline in 1969 [69]. Later, Pearson et al analyzed the stability of non-isothermal fiber spinning [70] [71]. By solving the eigenproblems of the linearized small disturbance equation on the governing equation for constant viscosity, the predicated critical draw ratio (ratio of the average fiber speed at the winder to that at the nozzle) is approximately 20.21 [72]. When the drawing ratio is above the critical draw ratio, the process becomes instable. In practice, the ratio can easily pass the predicted critical value. Fisher and Denn developed a theory of isothermal melt spinning and draw resonance in 1976 [73]. Gyanesh K. Gupta et al developed a non-isothermal model of glass fiber drawing stability [74]. A stability analysis specific to our process is desired if possible.

The general governing equations for fluid mechanics are conservation of mass, conservation of momentum and conservation of energy.

$$\frac{D\rho}{Dt} + \rho\nabla \cdot \vec{V} = 0 \ (conservation\ of\ mass) \qquad 14$$

$$\begin{cases} \rho f_x - \frac{\partial P}{\partial x} + \mu\left(\frac{\partial^2 u}{\partial x^2} + \frac{\partial^2 u}{\partial y^2} + \frac{\partial^2 u}{\partial z^2}\right) = \rho\left(\frac{\partial u}{\partial t} + u\frac{\partial u}{\partial x} + v\frac{\partial u}{\partial y} + w\frac{\partial u}{\partial z}\right) \\ \rho f_y - \frac{\partial P}{\partial y} + \mu\left(\frac{\partial^2 v}{\partial x^2} + \frac{\partial^2 v}{\partial y^2} + \frac{\partial^2 v}{\partial z^2}\right) = \rho\left(\frac{\partial v}{\partial t} + u\frac{\partial v}{\partial x} + v\frac{\partial v}{\partial y} + w\frac{\partial v}{\partial z}\right) \\ \rho f_z - \frac{\partial P}{\partial z} + \mu\left(\frac{\partial^2 w}{\partial x^2} + \frac{\partial^2 w}{\partial y^2} + \frac{\partial^2 w}{\partial z^2}\right) = \rho\left(\frac{\partial w}{\partial t} + u\frac{\partial w}{\partial x} + v\frac{\partial w}{\partial y} + w\frac{\partial w}{\partial z}\right) \end{cases} \quad 15$$

$(conservation\ of\ momentum, also\ called\ navier\ stokes\ equations)$

f_x, f_y, f_z are x, y, z components of the body force such as gravity, electrical or magnetic force acting on the fluid.

$$\rho\left(\frac{\partial h}{\partial t} + \nabla \cdot (hV)\right) = -\frac{\partial p}{\partial t} + \nabla \cdot (k\nabla V) + \Phi\ (conservation\ of\ energy) \quad 16$$

Where h is enthalpy, k is thermal conductivity and Φ is heat dissipation term.

To be clear for the equations, $\frac{D}{Dt}$ is the substantial derivative which includes the local derivative and convective derivative. The local derivate is time rate of change and the convective derivative is the due to the movement of the fluid element. In formula form, it is as follow

$$\frac{D}{Dt} = \frac{\partial}{\partial t} + (\vec{V} \cdot \nabla) = \frac{\partial}{\partial t} + \mu\frac{\partial}{\partial x} + v\frac{\partial}{\partial y} + w\frac{\partial}{\partial z} \quad 17$$

∇ is the vector operator defined as $\nabla = \vec{\imath}\frac{\partial}{\partial x} + \vec{\jmath}\frac{\partial}{\partial y} + \vec{k}\frac{\partial}{\partial z}$,and $\vec{V}$ is the velocity vector and (μ, v, w) are three components of $\vec{V}$. Mathematically it is equivalent to total derivative.

The force normal to the surface is balanced by the surface tension. Thus, the boundary condition for a steady growth is

$$\sigma_{ij}\hat{n} + 2\alpha H\hat{n} = 0 \quad 18$$

Where α is the surface tension and σ_{ij} is the stress tensor and H is the mean curvature of the surface.

In the steady-state case, the flow doesn't depend on the change of time, thus the conservation of mass and conservation of momentum equation can be simplified as

$$\frac{\partial(\rho u)}{\partial x}+\frac{\partial(\rho v)}{\partial y}+\frac{\partial(\rho w)}{\partial z}=0\ (conservation\ of\ mass) \qquad 19$$

$$\begin{cases} \rho g_x-\frac{\partial P}{\partial x}+\mu\left(\frac{\partial^2 u}{\partial x^2}+\frac{\partial^2 u}{\partial y^2}+\frac{\partial^2 u}{\partial z^2}\right)=\rho\left(u\frac{\partial u}{\partial x}+v\frac{\partial u}{\partial y}+w\frac{\partial u}{\partial z}\right) \\ \rho g_y-\frac{\partial P}{\partial y}+\mu\left(\frac{\partial^2 v}{\partial x^2}+\frac{\partial^2 v}{\partial y^2}+\frac{\partial^2 v}{\partial z^2}\right)=\rho\left(u\frac{\partial v}{\partial x}+v\frac{\partial v}{\partial y}+w\frac{\partial v}{\partial z}\right) \\ \rho g_z-\frac{\partial P}{\partial z}+\mu\left(\frac{\partial^2 w}{\partial x^2}+\frac{\partial^2 w}{\partial y^2}+\frac{\partial^2 w}{\partial z^2}\right)=\rho\left(u\frac{\partial w}{\partial x}+v\frac{\partial w}{\partial y}+w\frac{\partial w}{\partial z}\right) \end{cases} (conservation\ of\ momentum)$$

20

In our cases, the effect of the gravity is trivial. Thus, the gravity term can be neglected. Sone researchers such as R. Pitchumani et al applied the sets of equation to optical drawing process [75] [76]. From their work, the conversation for mass, momentum, and energy without gravity term in polar coordinates are as follows.

$$\frac{\partial(\rho u)}{\partial z}+\frac{1}{r}\frac{\partial(\rho r v)}{\partial r}=0\ (conservation\ of\ mass) \qquad 21$$

$$\begin{cases} \frac{\partial(\rho u^2)}{\partial z}+\frac{1}{r}\frac{\partial(\rho r u v)}{\partial r}=-\frac{\partial p}{\partial z}+2\frac{\partial}{\partial z}(\mu\frac{\partial u}{\partial z})+\frac{1}{r}\frac{\partial}{\partial r}[r\mu(\frac{\partial u}{\partial r}+\frac{\partial v}{\partial z})] \\ \frac{\partial(\rho u v)}{\partial z}+\frac{1}{r}\frac{\partial(\rho r v^2)}{\partial r}=-\frac{\partial p}{\partial r}+\frac{\partial}{\partial z}(\mu(\frac{\partial u}{\partial r}+\frac{\partial v}{\partial z}))+\frac{2}{r}\frac{\partial}{\partial r}(r\mu\frac{\partial v}{\partial r})-\frac{2\mu\cdot v}{r^2} \end{cases} (conservation\ of\ \text{momentum})$$

$$\frac{\partial\left(\rho c_p u T\right)}{\partial z}+\frac{1}{r}\frac{\partial\left(r\rho c_p v T\right)}{\partial r}$$

$$=\frac{\partial}{\partial r}\left(k\frac{\partial T}{\partial z}\right)+\frac{1}{r}\frac{\partial}{\partial r}\left(rk\frac{\partial T}{\partial r}\right)+\mu 2\left[\left(\frac{\partial u}{\partial r}\right)^2+\left(\frac{u}{r}\right)^2+\left(\frac{\partial v}{\partial z}\right)^2\right]+\left(\frac{\partial u}{\partial z}+\frac{\partial v}{\partial r}\right)^2$$

$$(conservation\ of\ energy) \qquad 22$$

Based on these governing equations and the boundary conditions, the fabrication process was simulated with finite element analysis by Two-Phase Laminar Flow model in COMSOL (version 5.5).

Due to the symmetry of the geometry, 2D Axisymmetric model is used. The COMSOL model is as follows.

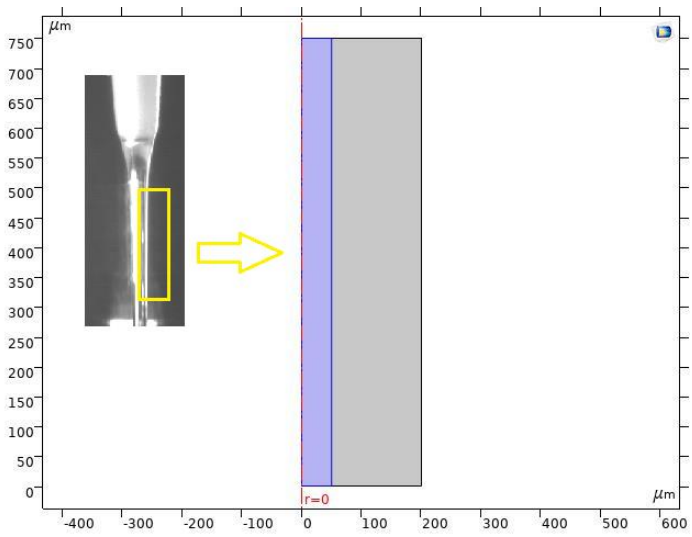

Figure 31 Axisymmetric model of the glass flow from COMSOL

It is symmetric about the red axis. The highlighted part in purple is the glass flow out of the nozzle and the gray part is the air. In this model, the interface is represented by a boundary which has zero thickness. The inertial reference frame is used since molten glass is moving at constant speed in stable condition.

At the top of the glass flow, the molten glass is pushed out by the applied back pressure. Thus, a pressure proportional to it is enforced as the boundary condition at the top end. At the bottom of the glass flow, the glass flow is moving together with solidified glass wire which has the same speed of the substrate. Thus, a velocity equal to the moving speed of the substrate is enforced as the boundary condition at the bottom end of the glass flow.

Since the surface tension and viscosity both are function of temperature and the temperature varies with z axis, we define surface tension and viscosity of the glass flow varies along the z axis. Since it is difficult to get precision measurement of these two parameters in such a small scale, we use models discussed in section 3.2.1 and 3.3.2 are used. The COMSOL model only provide qualitative simulation of the fabrication process. To get more precise quantitative simulation of the process, a way to measure these two parameters are needed which is beyond the scope of this research. From Seung-Bo at el [49], a linear equation was used in the COSMOL model to simulate the surface tension change depends on temperature.

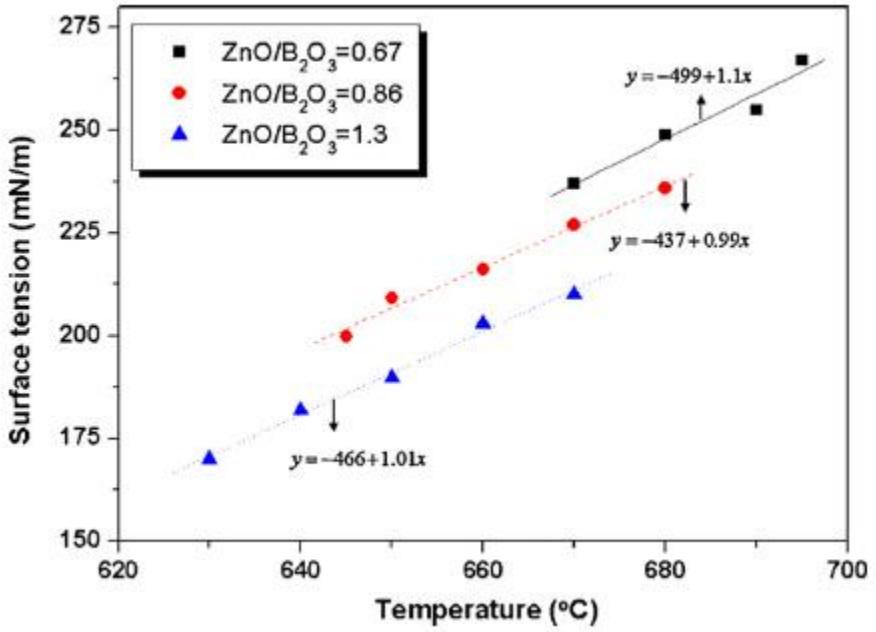

Figure 32 surface tensions of the $Bi_2O_3 - B_2O_3 - ZnO$ glass frits on alumina substrate from [49]

When the fabrication process is in stable region, the shape of the glass flow would keep constant and don't change with time. However, when it is not in stable region, the

shape of the glass flow would change with time and finally breaks and form needle shaped structures in the molten glass column.

For the COMSOL model, we have following assumptions to simplify the simulation process:

1. The viscosity of the molten glass is strictly followed the curve in section 3.2.1 and follows an exponential function with temperature and the change is instantaneous.
2. The surface tension of the molten glass is strictly followed the curve in section 3.3.2 and the change is instantaneous.
3. The temperature depends on the z coordinates of molten glass flow and does not depend on time.

The first two assumptions help simplify the properties change of the molten glass and the third assumption is only valid when the molten glass is in stable region. However, a model with these three assumptions is good enough to get a qualitive simulation of the process.

The parameters used in the model is based on B-Bi-Zn glass whose density is 7.3 g/cm^3, the viscosity is set to be 10 $Pa \cdot s$ when the glass is in molten status and 10^6 $Pa \cdot s$ when glass is in soft temperature. The surface tension is 0.275 $\frac{N}{m}$ when the glass is fully molten and decrease with temperature.

This model could capture both the needle forming process and uniform wire fabrication qualitatively. Under combination of different pressure and pulling speed as boundary conditions, the model would show the two following evolution of the process.

One was maintaining the shape which meant uniform diameter wire was fabricated in the condition. The other was broken in the upper portion of the molten glass and finally formed wires.

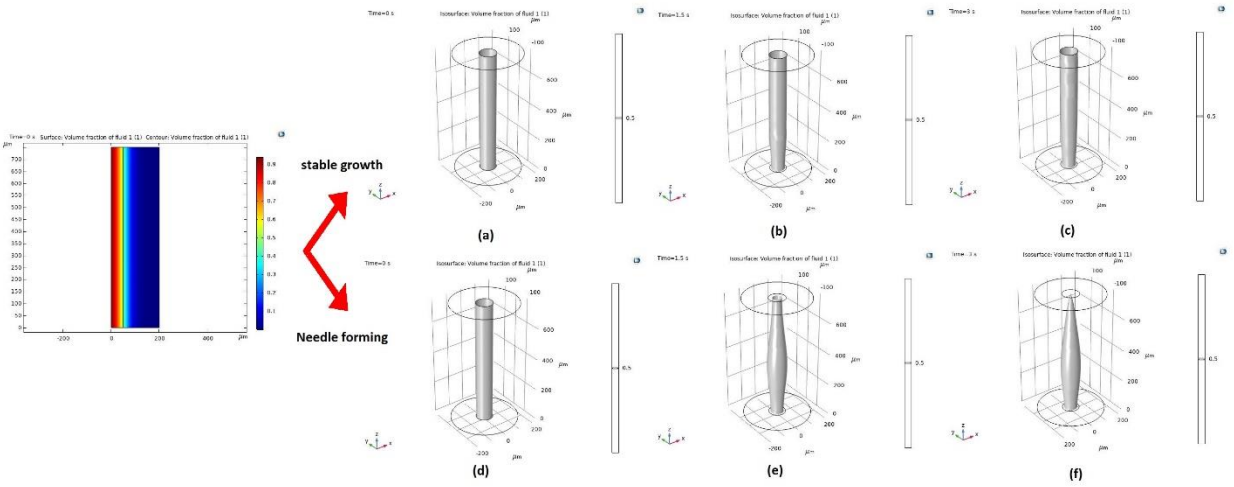

Figure 33 Two different simulation results from the COMSOL model.

The figure above demonstrates the change of the shape of the molten glass column from the COMSOL model. (a)(b)(c) are the shape of the molten glass at 0s, 1.5s and 3s when the growth is stable and (d) (e)(f) are the corresponding shape at the same time when needle was formed.

The simulation results are the solution of the equations 19, 20 with a changing viscosity and surface tension under different coordinates by level set method. The uniform diameter wire growth was results from balance of pressure, viscosity, surface tension and pulling speed. The needle forming broke the balance and the increasing viscosity from bottom to top played an important role in the process.

The model could only be used to understand qualitatively of the process. It is not a quantitative model which would reveal the exact relationship between the pressure,

pulling speed and so on. In the experiment, the temperature profile would change once the shape of the molten glass changes. The model simplified the computation by assumption 3. Besides these assumptions which reduce its accuracy, the temperature profile used in the model was also not accurate. In the experiment, measurement of temperature distribution profile at the microscale was not feasible with our setup. The temperature distribution profile in the model were based on experience.

3.7 Conclusion

In this chapter, the unique properties of glass that is related to the fabrication process is shown. The viscosity of the molten glass has a strong dependence on the temperature. The mechanical strength of the glass is greater than most polymer materials in other 3D printing systems and the fabrication process maintains the mechanical strength of the glass. Surface tension is important in the microscale in our fabrication, it prevents the molten glass from dropping out of the nozzle under effect of gravity. But together with wettability, it could also cause the molten glass to climb onto the sidewall of the nozzle which could affect the meniscus stability during uniform wire growth. Back pressure is needed to provide the driving force of pushing the molten glass out. It determined the glass volume rate. The evolution of growth is demonstrated. The method could grow uniform wires/rod and the diameter of them could be tuned by changing the pulling speed. When pulling speed is beyond the range of uniform growth, needles with different heights and tip sharped can be formed by a single step. These needles are also bonded on substrate which can be used as mold for further research and applications. The governing equations are showed and the COMSOL model are demonstrated. The uniform growth and needle

formation process could be simulated qualitatively by the model. More precise modeling needs better measurement of temperature and viscosity profile which is beyond the scope of this research.

Chapter 4 Fabrication of High-Aspect Ratio and More Complex Microstructures

In Chapter 3, the material properties and the molten glass-based fabrication process are analyzed and demonstrated. Wires with different diameter and various shape needles with strong mechanical properties can be fabricated in proper combinations of temperature, back pressure and pulling speed. The wires/needles form the basic building block of more complex structures. In practice, structures with high-aspect ratios, or modified base/tops are more useful and difficult to fabricate. In this chapter, how these micro-structures could be fabricated by our method would be discussed. All these requirements need control of the fabrication process to be stable and precise. More complex structures would also be included in this chapter.

4.1 Ultra-High-Aspect Ratio Wire

Ultra-High-Aspect ratio micro-structures have a wide application in electrical and biomedical field. They can be used as micro antenna to filter microwave signals [77], sensors to detect flow viscosity and directions [78] [79] as well as microelectrodes to detect neural signals [80]. However, they are also difficult to fabricate. Conventional lithography methods need so many layers of mask/patterns, which makes the cost unacceptable, and recent polymer or ink-based methods are limited by the intrinsic material properties. Molten Glass-Based Fabrication can easily achieve very high aspect ratios with low cost.

A simple mechanical stability analysis indicates that for a freestanding glass wire having an elastic modulus of 25 GPa and a diameter of 40 μm, the wire can reach 129 cm in height before it is bucking by its own weight. For comparison, for the robust polymer

typically used for 3-D printing (PEEK), which has young's modulus of 3.6 GPa, a similar wire would begin to bend over at a height of 67 cm and typical 3D printing material such as PLA cam only reaches 58.6 cm with an elastic modulus of 2 GPa.

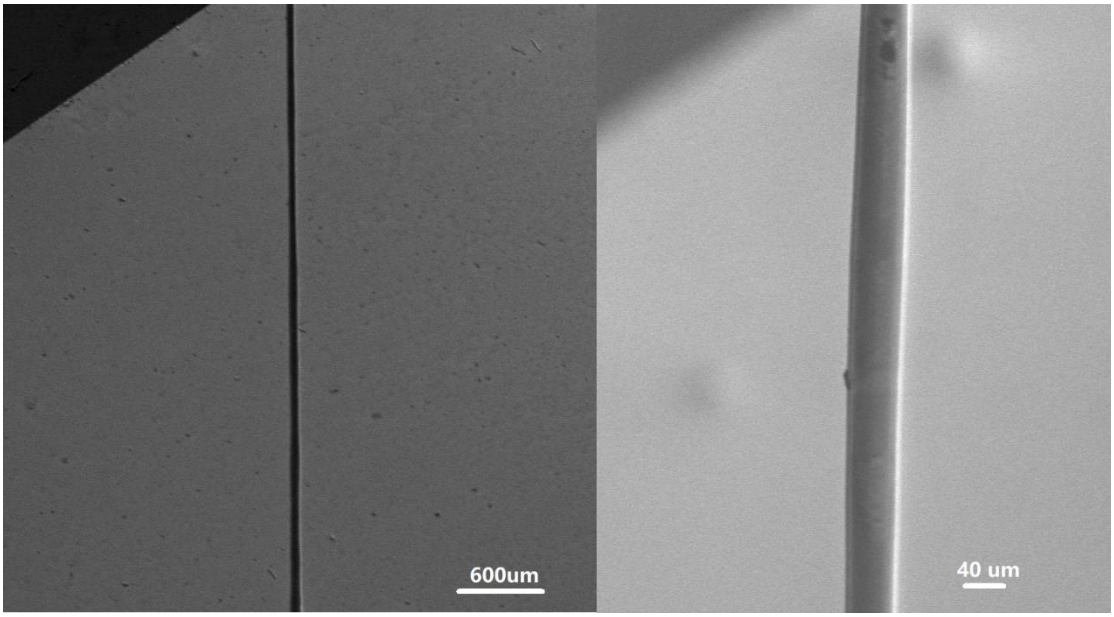

Figure 34 Ultra High Aspect Ratio Wires

The challenge in fabrication of uniform ultra-high aspect ratio wire is to keep the condition stable over the length of the growth. Before the molten glass meniscus forms, we heat up the substrate to form strong bonding between the micro-structures and the substrate. But the heated substrate will cause temperature difference in the near substrate region and far substrate region. The variation in temperature will cause the variation of the diameter of the wires due to the viscosity change by the temperature as shown in figure 35. This phenomenon is negligible when the height of the structures is not high since the temperature variation is small within hundreds of micrometers. However, to make several centimeter long wires, we need to take this effect into considerations.

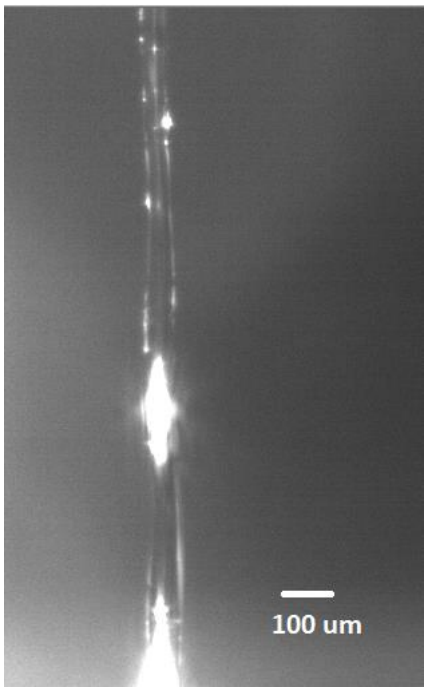

Figure 35 diameter change far away from heated substrate

In our experiment, we have two methods to solve this. One is adjusting the heating power according to the distance from the heated substrate to make the temperature variation as small as possible. It needs careful calibration of the heating power according to the distance between the nozzle and substrates. During the wire growth, the heating power is adjusted by the program as the function of the moving distance to make the temperature of the molten glass stable during the whole process. The second method is to fabricate a bonding post on the substrate first with the heated substrate. Then turn off the heat power to cooling to room temperature. Take advantage of the re-joining properties of glass during molting and fabricate the whole structures without heated substrate. The structure in the figure 34 is fabricated by the second method.

4.2 The Control of Base formation

After the meniscus is formed between the nozzle and substrate, the fabrication process begins. From the user manual of BSC203 Benchtop Stepper Motor Controller (THORLAB), the motion of the motor can be controlled by the following graph (Figure 36) on the left below. It has an acceleration stage to reach the desired speed and keeps moving with the desired speed before deaccelerating to zero. Both the acceleration and maximum speed of the motors can be controlled. Combined with flow status of the molten glass, it provides the tools to modify the base/end of the fabrication process.

The base formation starts together with the acceleration stage of the motor. In stable growth case, the maximum speed of motor and the velocity of the glass flow should be equally. However, it is not necessary in the starting case. The acceleration of melt glass and motor can be different. The acceleration of the melt glass out of nozzle is determined by the pressure, temperature, interaction with the substrate. By controlling the acceleration rate of the motor, the shape of the base can be modified. When the motor accelerates faster than the glass, it will form necked bases. As the different narrows, the necking section will be shortened. When it matches each other, the base can be same size as the diameter of uniform section. However, as the meniscus is confined around the edge of the ceramic nozzle by the surface tension, the size of the base cannot be significantly larger than the diameter of the nozzle opening.

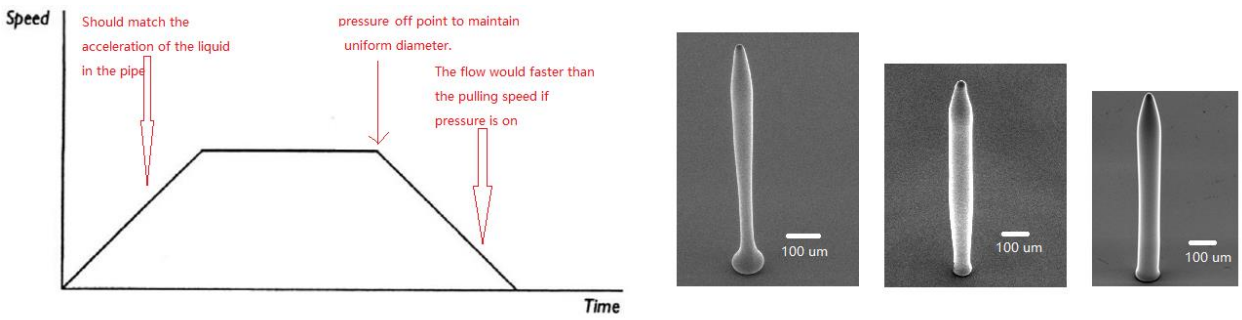

Figure 36 Modification of wire shape with different stage of motor motion

Figure 36 shows different stages of the motor used in the system. These wires on the right shows three different scenarios. First the acceleration is less than the push-out process of the molten glass. So, the base is larger than its diameter. Second it is faster than the push-out process, producing a base smaller than its diameter and a neck during the transition. Third it matches with the molten glass. Thus, base and diameter are kept constant.

4.3 The Termination of Growth and Top Modification

Like the base formation process, deacceleration of motor could also be used to realize different end of the wire. Besides that, more powerful way to modify the growth top is utilizing the molting property of the glass under different distance from heating source (the ceramic nozzle end).

Since it is a melting/solidification process, the surface tension will redistribute melt glass to a perfect smooth curve. Taking advantage of the remelting properties of glass, we can modify the end of the structures by holding the nozzle above. By carefully controlling the distance between the heated nozzle tip and wire and the holding time,

various shape of top can be fabricated. Changing the parameters such as distance between nozzle and wire top, holding time above it, we can modify the finish of the micro-structure.

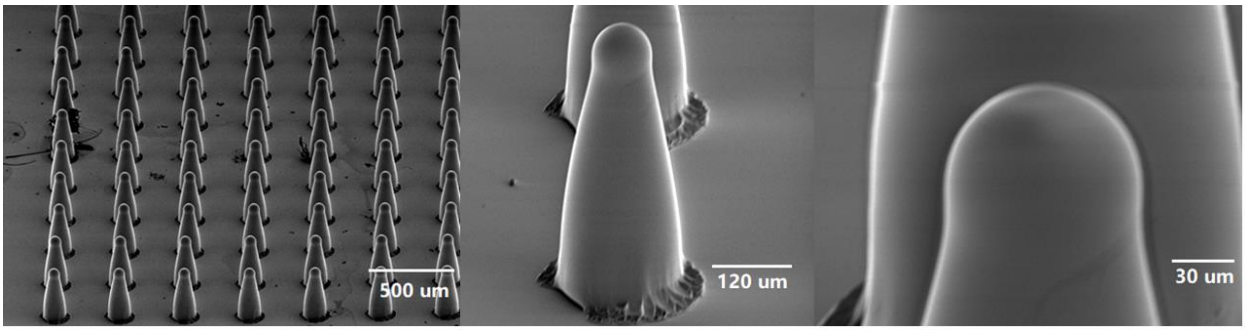

Figure 37 Round Head Needle Array

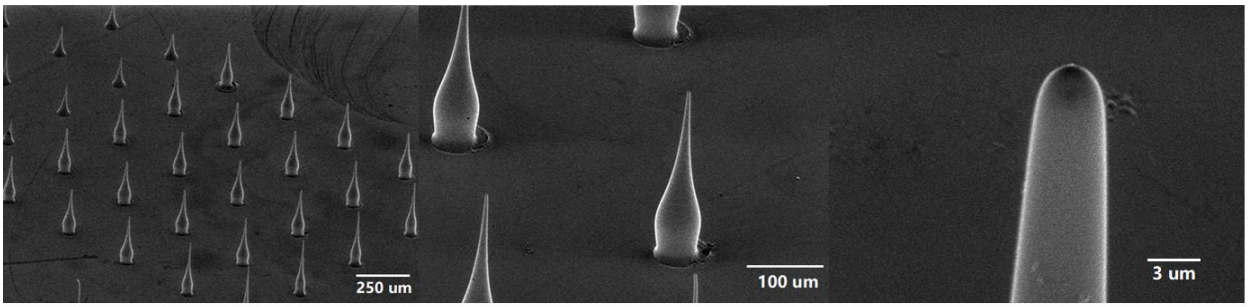

Figure 38 3um tip Needle Array with a straight base

Figure 37 shows an array with round end on the top and Figure 38 shows an array with sharp tip on the top end. During the fabrication of structures in Figure 37, a waiting process controlled by the program in implemented after each needle is fabricated. The heated nozzle would stand still on the top of the structures for 3 seconds after the melted glass breaks away from it. The heating from the nozzle remelts the top section of the structures and it forms ball shape by surface tension to minimize the surface energy.

When the position of the nozzle during the waiting is off the symmetric line of the structures, tilted structures can be fabricated. Figure 39 shows an array of structures tilting toward one direction by letting the heated nozzle waiting on the same relative position after each growth. By this method, devices with directional mechanical properties can be made.

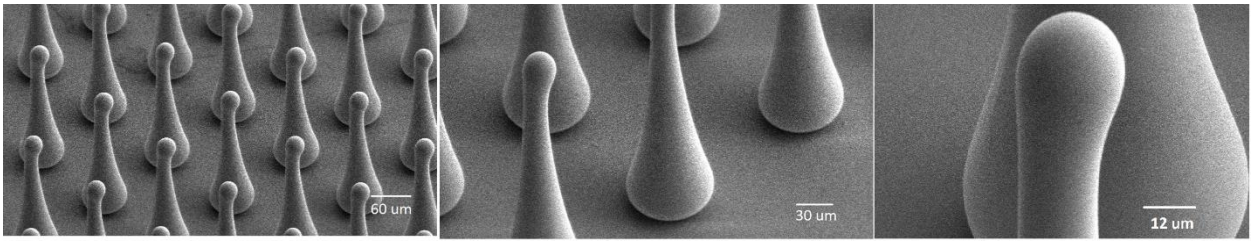

Figure 39 shows the tilted end arrays

By adding a slow backward motion after fabrication of the wire array, more the top part of the wires can be melted, and bigger ball can be formed on the end. Due to the surface tension of the molten glass, the surfaces of the array are very smooth. The figure below shows a wire with ball bigger than its diameter is fabricated by the backward methods. The diameter of the wires is about 60 μm and the ball has a diameter of 180 μm.

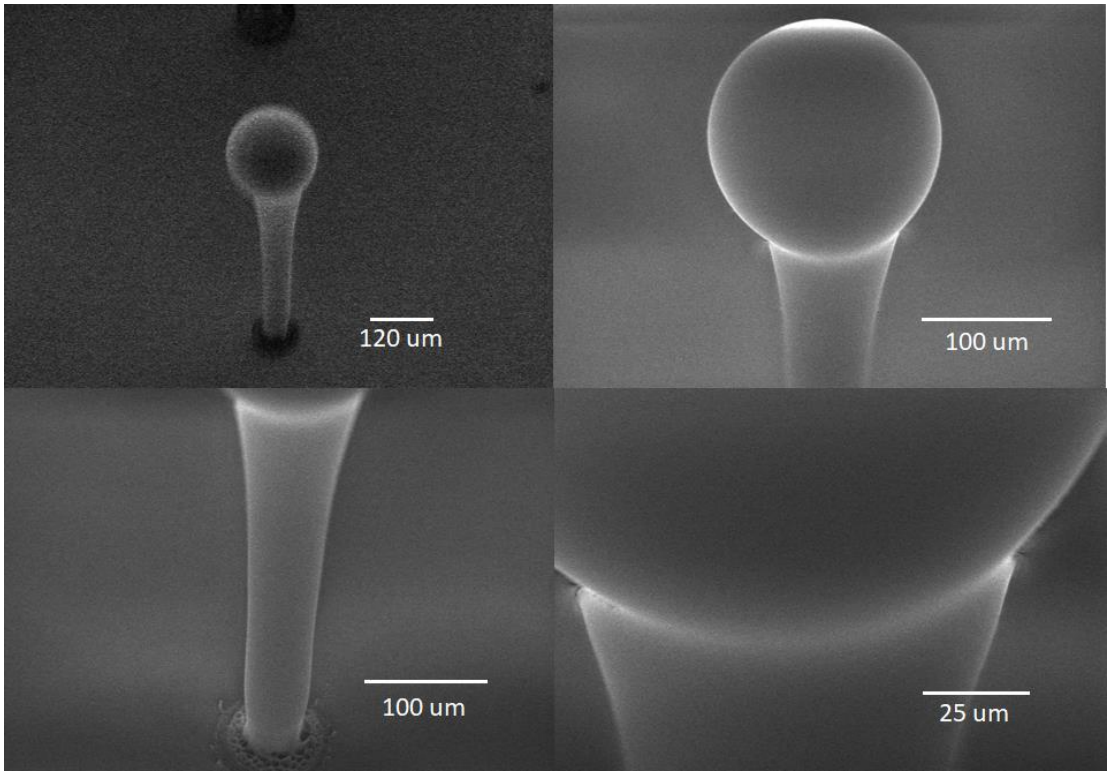

Figure 40 Wire with Round Ball top

With careful control of the parameters, various sizes of the ball on top can be realized. Figure 41 shows an array of wires with different size of the ball on top by changing the waiting time of the nozzle after each fabrication of the wires. With the waiting time implemented by the software, repeated precise control of the shape of the arrays are realized.

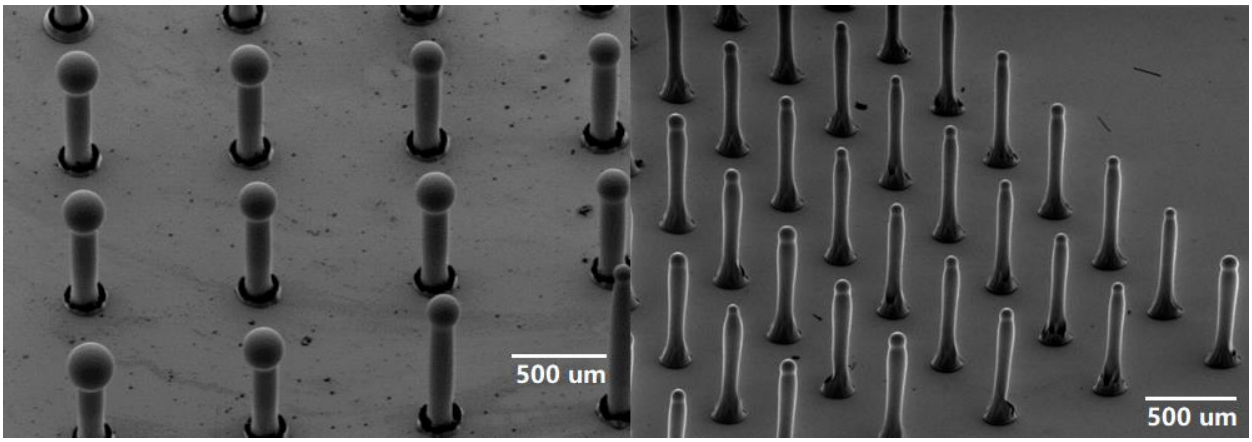

Figure 41 Wires with different size of the top ball with controlling of distance after meniscus breaks and waiting time. Left with waiting 15 seconds above the wires and right with waiting 3 seconds above the wires with distance 100 um.

Besides utilizing the waiting time after each fabrication of the structures, pulling speed can also modified the end of the structures. The relationship between shape at end and pulling speed has already discussed in section 3.5. With various pulling speed under different viscosity, tip with a few hundred nanometer tip sharpness can be made. As surface tension will minimize the surface area during the melted/meniscus state and the fast cooling maintains the shape when it transits from molten state to solid state, the process can form microneedles with ultra-smooth surface. Varying the pulling speed and the viscosity of the melted glass, we can fabricate different shape of microneedles. Later, we can use the fabricated microneedle arrays as mold to make PDMS replica of the Micron Needle Arrays.

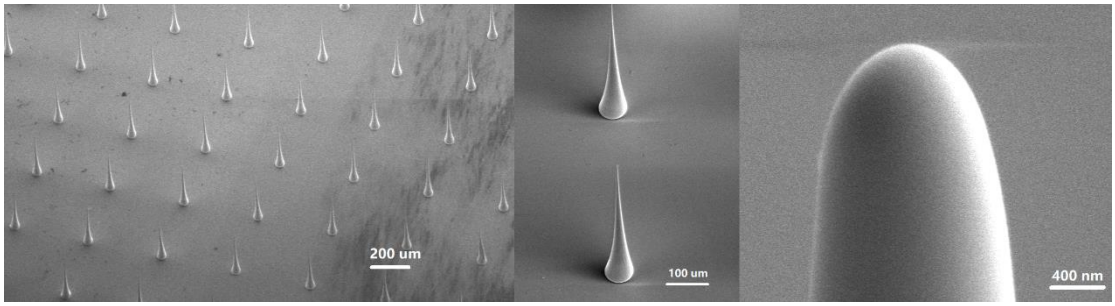

Figure 42 Needle Array with 400 nm tip

Figure 42 shows a part of array of sharp needles with an each spacing of 500 µm. The height of the fabricated needles is about 300 µm. The zoomed-in image in the middle and right of Figure.42 shows the tapered needle geometry with a typical tip radius 400 nm. By intentionally terminating the glass wire growth at high pulling speed exceeding the speed for stable wire growth, sharp-needled glass structure can be readily fabricated. Such a needle array would be difficult or costly to fabricate with the all the other available methods. The height and other geometrical parameters of the needles can be readily adjusted by adjusting the growth conditions in the system. The needle array fabricated by this method is also strong enough to serve as mold for biocompatible polymer material for the medical application.

4.4 Curved and Flexible Structures

The molten glass-based fabrication also has very flexible growth directions due to the fast solidification of the melt glass. In the micro/nano scale, the big the surface area to volume ratio provides a fast- cooling condition. Shortly after the melt glass is pushed out from nozzle, it become solid which can support itself. The follow figure shows different

growth angles by combinations of x and y motor speed. For example, 45˚ is realized by setting the rate of x and y speeds to 1:1.

The experiment is conduct with ceramic heater powered at 11.4 V 3.1A and growth rate at 0.5 mm/s.

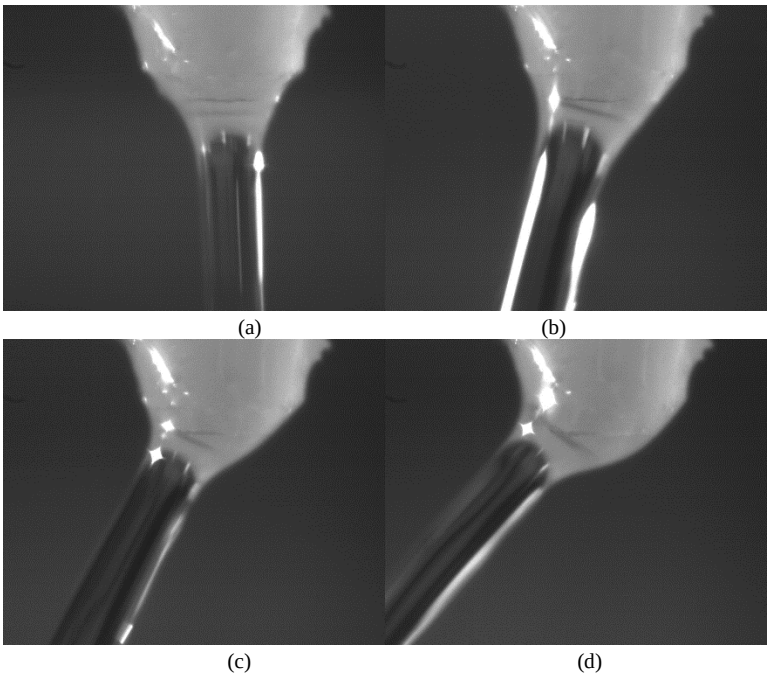

Figure 43 Wire growth with different angles

In the figure above, (a) is set with 0˚ degree tilting and the measured angle is 0˚, (b) is set with x and y speed to realize 15˚ tilting and the measured angle is 15˚, (c) is set with x and y speed to realize 30˚ tilting and the measured angle is 29.28˚, (d) is set with x and y speed to realize 45˚ tilting and the measured angle is 42˚. With the directional growth of the molten glass, the curved and flexible structures are made possible by our setup. Figure 44 shows some fabricated truly 3D microstructures.

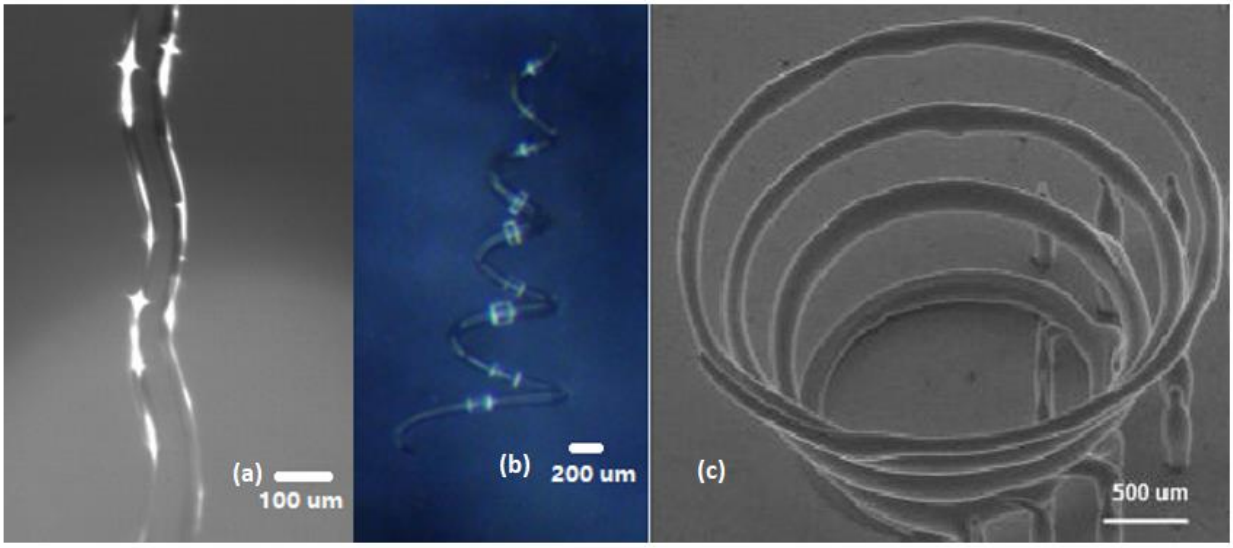

Figure 44 (a) is periodic curved wires. (b) is a helix with decreasing radius from 500 um in radius in bottom to 100 um in radius on top. (c) is a helix mounting on the substrate

These microstructures show the flexibility of the fabrication direction during growth process.

4.5 More Extensions: Surface Pattern drawing, Layer by Layer Structures and Micro Lens

By design the moving path of the motor, the same setup can also be used to complete some extension tasks. The first is surface pattern drawing. When the distance between the nozzle tip and the substrate is kept constant during the x-y planar moving, thin layer of the glass can be draw on the surface. It demonstrates potential patterning application. The line width is around 100 μm.

Before drawing begins, the surface variation profile of the substrate is provided to program. So that during the moving in the x-y plane, the program would adjust the z motor to keep the distance between the nozzle tip and substrate constant automatically.

Then, the designed patterns are input in the program to set the moving path of the x-y motor. The line with is around the outer diameter of the ceramic nozzle. With proper combination of the back pressure and drawing speed, the patterns can be laid at mm/s level. The relationship between the pressure and drawing speed is similar to that in Figure 26.

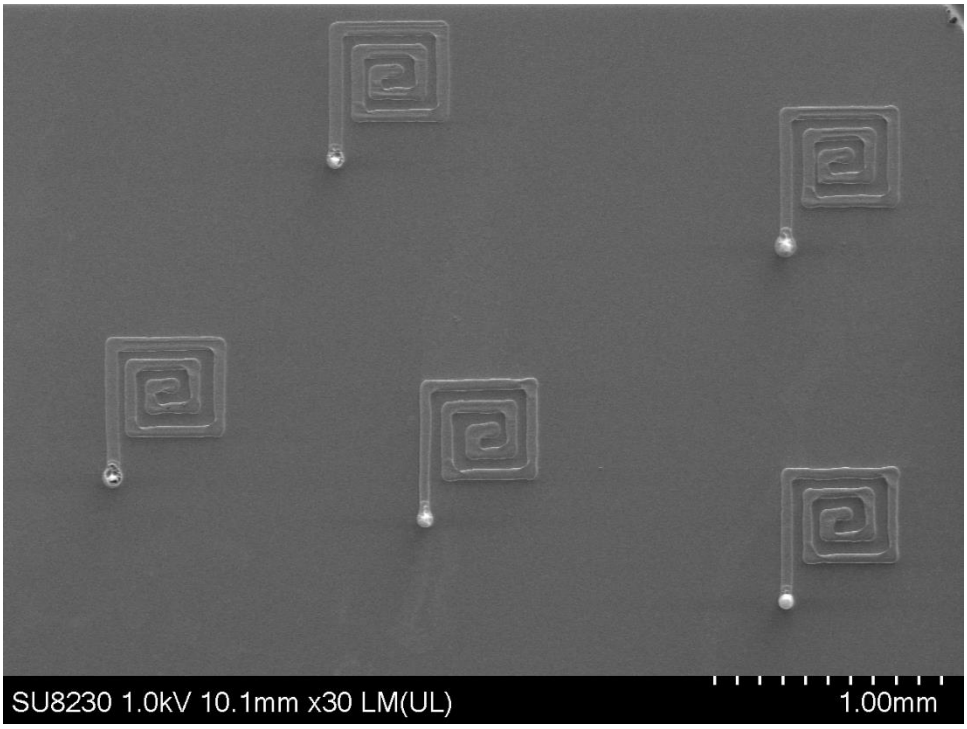

Figure 45 The surface pattern drawing by the molten glass method

There are some variations on the line width of the patterns. It should be caused by the temperature variation of the substrate. When substrate temperature has variations, the solidification time of the laid glass would be different. When the glass is solidified, its shape is fixed. This caused the variation of the line width. Figure 45 demonstrates some patterns made by the methods with gap between nozzle opening and substrate to 15 μm. The right and up corner of the substrate is near the center of the heating element under

the substrate. Thus, the line width more uniform than the patterns on the right and down corner of the substate. This method can serve as surface machining technique when resolution can be coarse, and speed is the priority.

Stacking the surface pattern drawing together is the lay-by-layer structures. It is the same as layer-by-layer 3D printing process. The setup can convert to conventional 3D printing instrument without difficult. The linewidth in figure 46 is about 100 μm. The smaller side of the structures are about 100 μm in diameter and the larger side is about 1 mm in diameter.

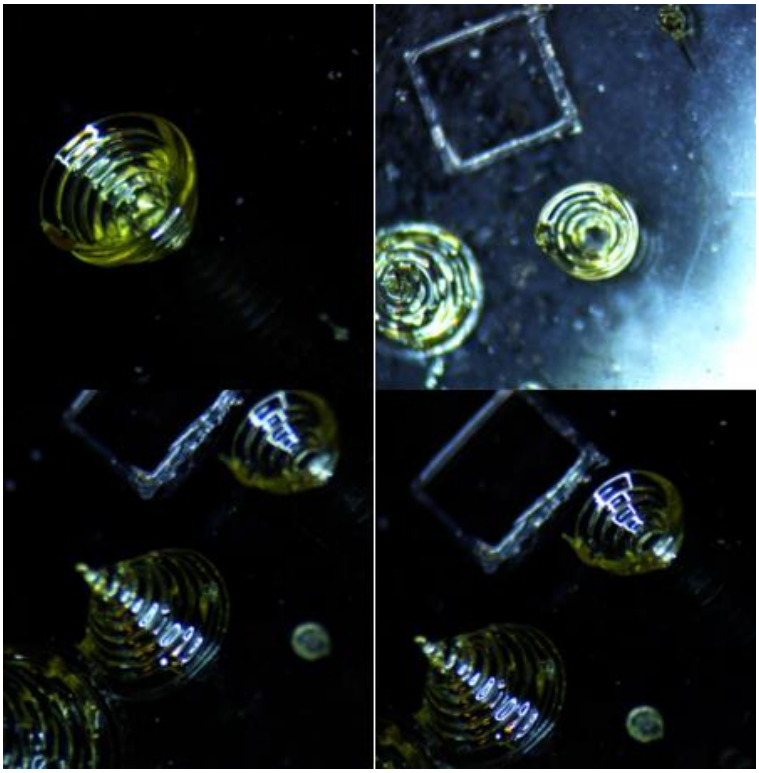

Figure 46 Layer by Layer Fabrication

Micro-lens arrays have a wide application in image systems such as 3D light field cameras, 3D image acquisition, fingerprint identification [81]. The fabrication methods for them include direct methods such as Thermal Reflow Method [82], Microplastic

Embossing Methods [83], Microdroplet Jetting Method [84], and indirect methods such as MEMS Based Methods [85] and Ultraprecision Machining Methods [86]. Among them, thermal reflow method first uses UV light to pattern on photoresist through mask, second develops the patterned photoresist and get cylindrical isolated-islands, and third heats the isolated-islands to turn them into spherical structures by the effect of surface. Like the last step of that method, our fabricated arrays can also turn into micro lens structures by the surface tension when they are heated. First, fabricate an array of wires/needles with same dimensions. Second, uniformly heat the fabricated array to make them into micro-lens. In our process, we don't need lithography process and simplify the process to two steps. Moreover, the glass lens can withstand higher temperature than those made by polymers. Figure 47 shows the micro lens array made by our setup.

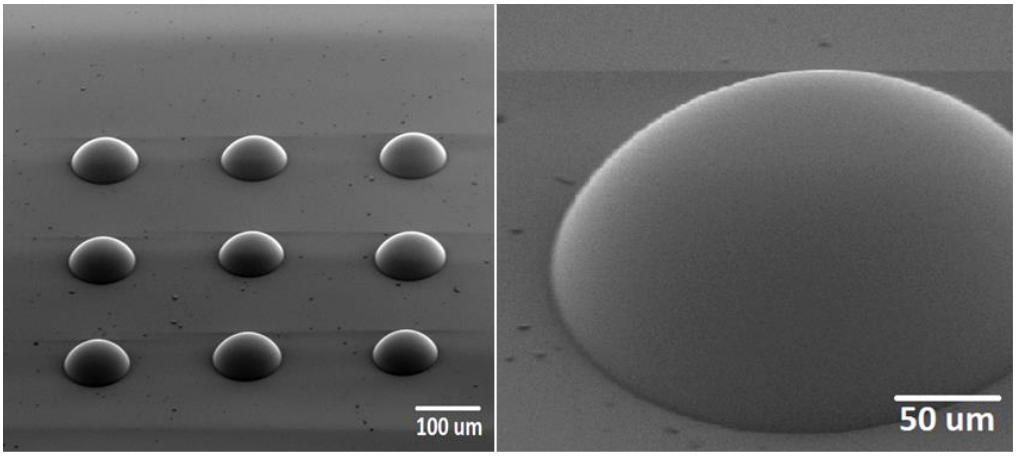

Figure 47 Micro Lens after B-Bi-Zn wire array heating at 550 ℃ for 20 minutes

4.6 Conclusion

Due to the unique properties of glass, more complicated structures are shown to be possible in this chapter. The high-aspect-ratio wires, modified base/top arrays and curved microstructures are demonstrated. The high-aspect ratio structures can have an aspect

ratio more than 10 which is difficult for other materials or method to achieve. Regarding buckling, these structures can be much longer than a polymer-based material with same diameter. By controlling the acceleration/deacceleration of motors or adding a re-melting process, the base and top of the micro-structures can be modified. It could have necked/uniform base as well sharp tip or ball on the top structures. By adjust the location of the heating source (the ceramic nozzle), directionality can be introduced in the fabrication process. Due to the fast-cooling process, the microstructures are self-supported. It provides a way to fabricate curved microstructures with easy steps. The method also has potential applications for rapid-prototyping on surface pattern drawing and layer-by-layer structures as well as fabrication of micro lens. Overall, the methods provide an efficient and high-quality way to fabricate microstructures that are difficult to fabricate by other methods.

Chapter 5 Fabrication of High Dense Microstructures Arrays

5.1 Introduction

Microstructure Array is the same microstructures formed in a periodic pattern. In the micro/nano fabrication, making structures in array form is critical important not only to prove the repeatability and stability of the process but also extend the application of the structures. For example, a single microwire may be too soft to serve as micro springs in certain scenario and an array of them can increase the overall spring constant to overcome this issue. A single microneedle may not have the volume to release enough medicine to cell and an array of them can release the required amount. A single microelectrode would not collect enough bio-signal and an array could collect enough signal to monitor human conditions and diagnose disease in early stage [87].

To fabricate practically useful microstructures that can be potentially used as precision mold or other devices, and surviving through the subsequent processes, two issues need to be considered, one is that the fabricated glass structure must be mechanically strong and the other is that the fabricated glass structure must bond on the dedicated substrate with sufficient bonding strength. The first issue can be solved by the strong mechanical properties of the glass itself and the second issue could be solved by heating the substrate to the temperature that can bond the molten glass well. Combining the viscous property of molten glass with the mechanical and bonding strength, we can fabricate a variety of novel structures which otherwise is very difficult to fabricate at high rate. Ultrahigh aspect ratio glass wire, high dense needle arrays with sharp tips and tapered/round micro wire arrays all can be fabricated at 50 um/s or even 100 um/s

Besides the geometry and properties of individual microstructures, the density also affects the functionality of the device made by these microstructures. During the 3D molten-glass based fabrication, the heat from the ceramic nozzle may melts the nearby high-aspect ratio microstructures when the spacing in the array is too small. A Multi-Step method is proposed and implement to fabricate dense array. The dense microstructure arrays have potential applications to use as micro springs or mold for microneedle array patch.

5.2 Array with Single Step Growth

Microstructures in array form is a nature result of combination of individual ones. By repeating the process of growing single microstructure at predefined locations on the substrate, various micro wire or needle arrays could be fabricated. After fabrication of the microstructures in one spot, the ceramic nozzle would be engaged with the next spot on the substrate and begin the fabrication of the next one until all the structures in the array finished. It is important to keep the temperature at different spots of the substrate constant. This is not only to ensure good bonding between the microstructures and substrate as explained in section 3.2.3 but also to make sure the uniformity in the array. The center of heated substrate has less interference from surroundings and our arrays are fabricated there to minimize the temperature variation on the substrate. The same base/tip modification method described in section 4.2 and 4.3 can also be used in the array.

Figure 48 shows part of array with 40 um and 120 um diameter wire. The height of the wires is 1 mm. (a) is an array with large base and (b) is an array with uniform base. The top of (a) is round and that of (b) has tapered end. The spacing between the wires in both array is 1 mm.

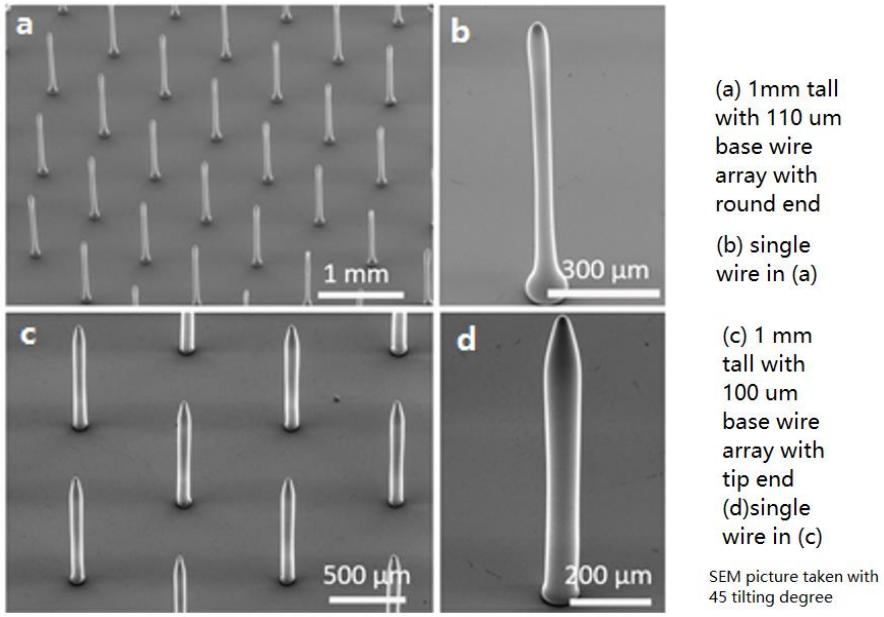

Figure 48 microwire array with base and tip modification

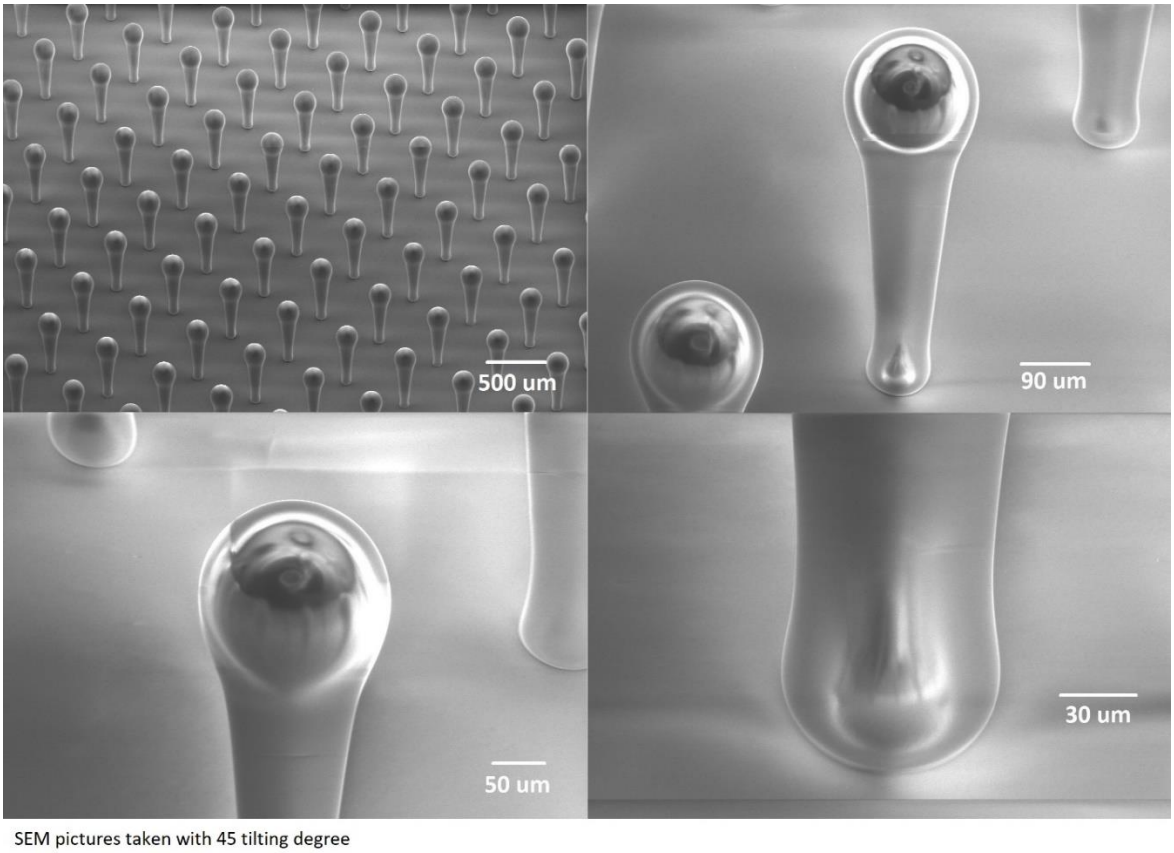

Figure 49 Array with ball on top microstructures

Figure 49 shows an array with wires ball on top. The ball is formed by remelting process at the end of each wire fabrications. Through a lager aera (more than 4 mm × 4 mm), the microstructures stay the same. Its height is around 1000 μm and the ball on top has 160 μm in diameter.

Similarly, the needle arrays could also be made with various shape by controlling parameters as explained in section 3.5. The tip sharpness of them could be a few micrometers down to hundred nanometers. The spacing are few hundred micrometers to maintain the tip sharpness.

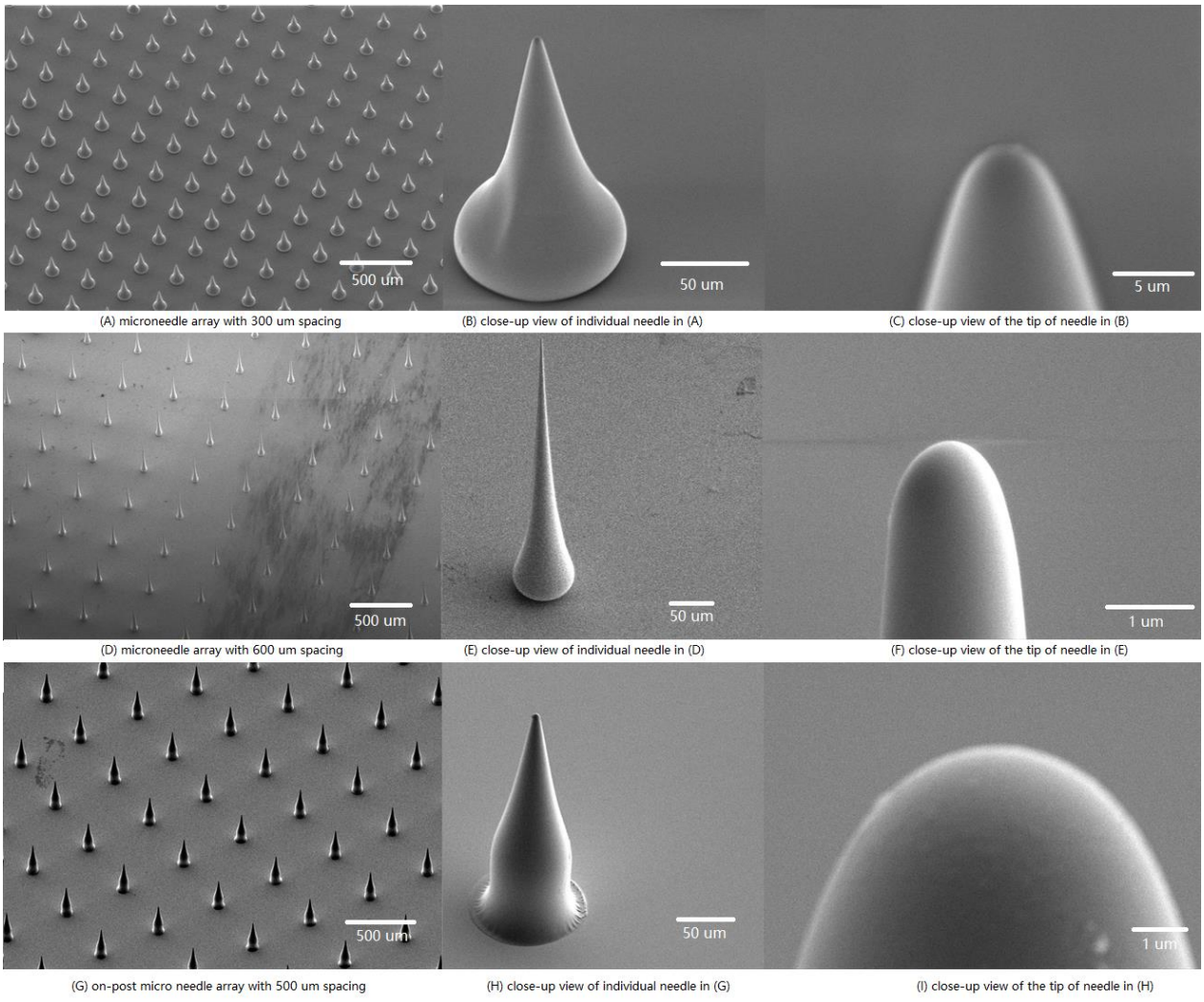

Figure 50 various microneedle arrys with different shape and spacing

However, the single step growth cannot make high dense arrays. By this method, the array spacing is limited by the geometry of the tapered micro nozzle used for the fabrication. The spacing is determined by the height of the wire/needle and the tapered angle of the nozzle to avoid the contact between the wire/needle and the side wall of the nozzle during fabrication of neighboring ones. It is also limited by the thermal dissipation from the heated nozzle. The spacing between two structures must be large enough to avoid re-melting the already grown neighboring glass wire/needle (s). By experiment, the ratio between the height of the wire/needle and the minimum array spacing is found to be 10:7 to avoid the remelt issue. For example, a spacing of 350 μm are needed for growing 500 um-tall glass wire arrays. Moreover, it is not possible to fabricate high dense curved structures array by the single step growth.

5.3 Multi-Step Method: Fabrication of Denser Array

Although various structures in array form have been fabricated, their density is limited by the geometry of the nozzle or the thermal dissipation in the fabrication process. The fabrication of nearby structures should not suffer due to the touching the sidewall of the nozzle or the heating from it during the fabrication of nearby one.

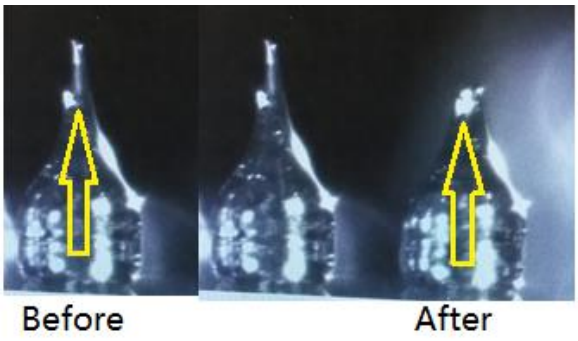

Figure 51 The Melting Effect of Nearby Structure

The figure shows above how the needle losses its sharp tip due to the thermal melting effect during the fabrication of a nearby one in the array.

However, in certain applications, we need dense structure arrays. The examples include a micro needle array, a spring array etc. The microneedle array has a wide application in drug delivery or signal collection. If the density of the micro needle is not high enough, the volume of drug delivered, or the signal collected would not be adequate. The spring array needs to reach certain density to distribute the load exerted on it.

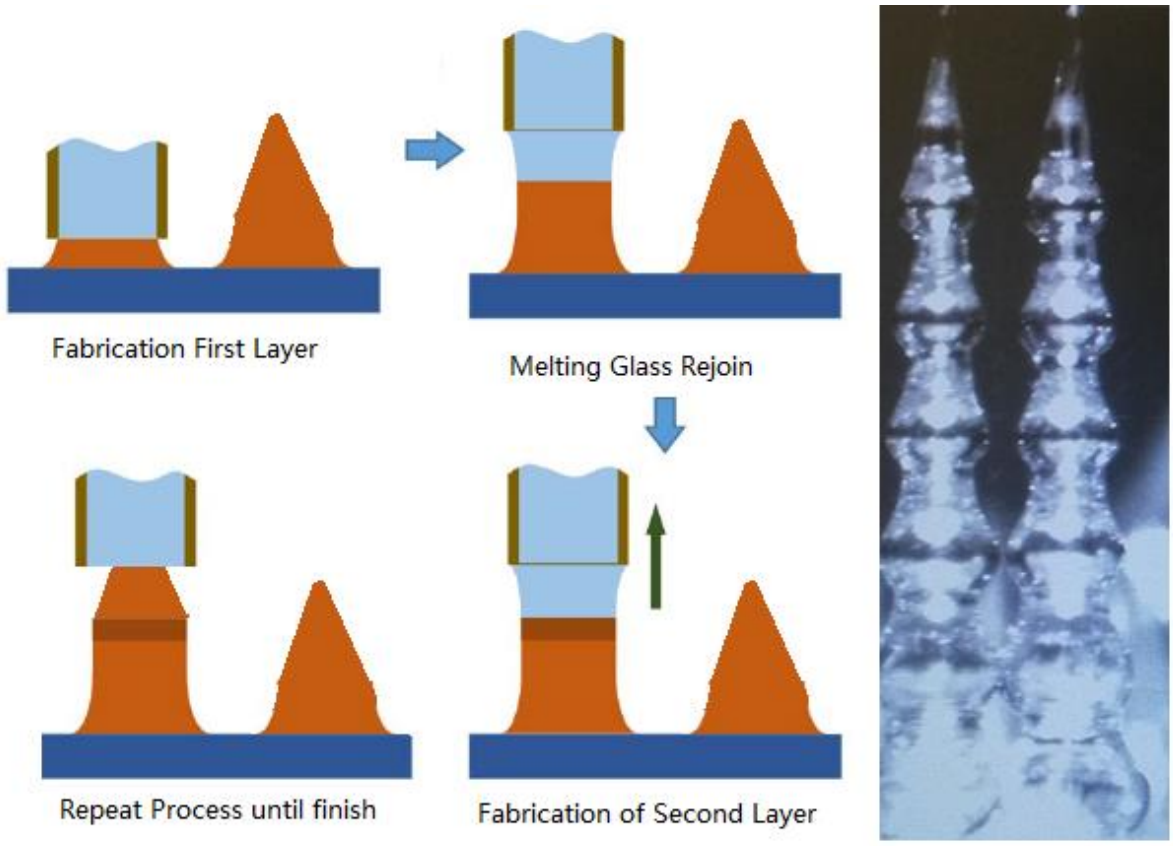

Figure 52 The process of Multi-Step Method

To overcome the geometry limit caused by these problems, a multi-layer method is developed. The general principle of the multi-layer method is schematically shown in Figure 52. The molten glass deposition is applied to deposit only a short segment of the

microstructures each time at every designated spot that can be highly closely spaced and is repeated on the same designated spots for growing the second short segments. The final structure array is fabricated by going through many of such repeated processes in an essentially “layer by layer” stacking fabrication process. In this digitized fabrication process, more complex-shaped and compact array microstructures can be fabricated. The microstructural and mechanical quality of the deposited glass is guaranteed by molten glass process in each layer. In this study, the diameter of each deposited segment depends on the diameter of the nozzle opening, and the height of each layer are around 100 μm to 500 μm. The height of each layer is controlled to make sure the sidewall of the nozzle would not cause melting or touching the nearby structures during the fabrication. The joint between layer is strong and smooth as part of the previous layer of glass would re-melt and merge with new layer of glass from the nozzle during the re-engagement process in the fabrication of new layer. Through this method, the heating zone formed by the nozzle would not melt the nearby structures and in principle the spacing in the array is only limited by the motor resolution.

The structures on the right of Figure 52 are an example of the structures made by the stacking methods. Compared to Figure 51, the nearby base-to-base distance is no longer limited. Its height can be built up with multiple layers of the stacking process.

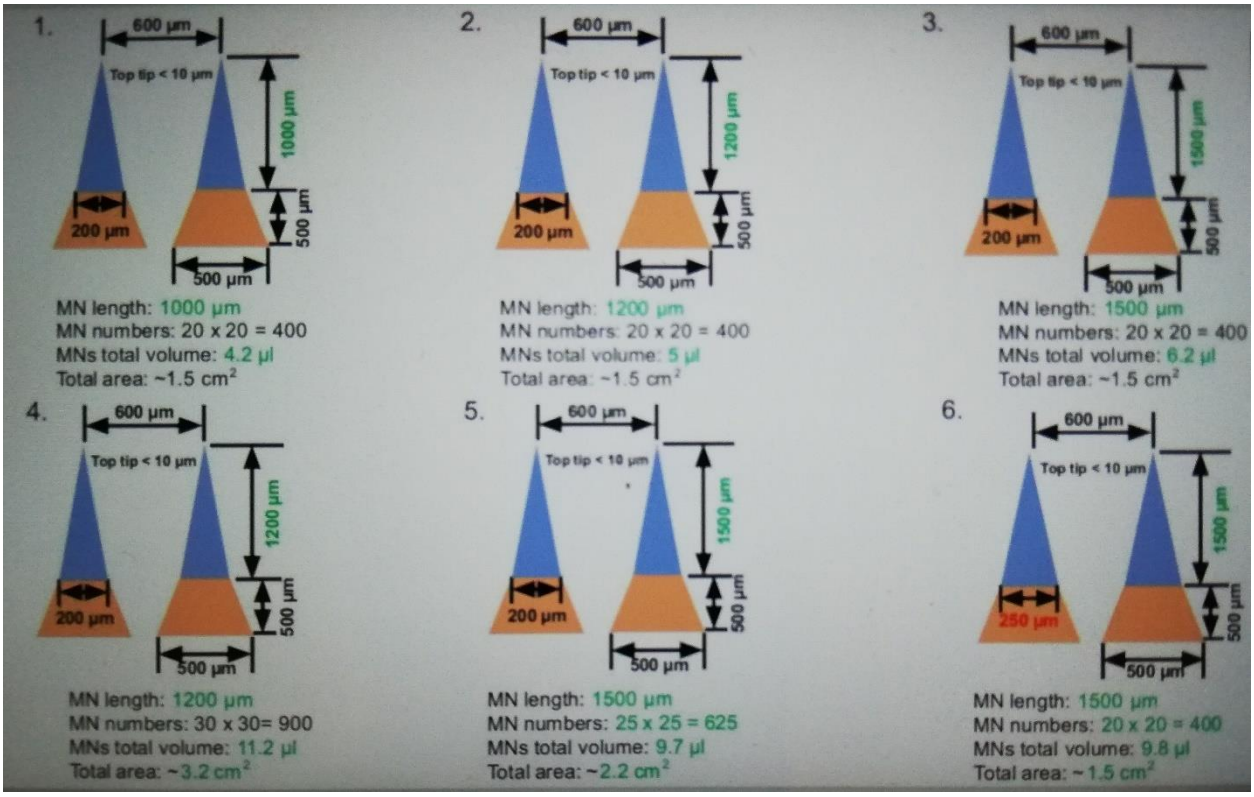

Figure 53 shows some examples of dimensions that drug delivery micro needle array required with their volume.

First application of this method is to make mold for large volume micro needle array. In figure 53 are typical dimensions of the drug delivery micro needle arrays. From the examples above, we can see the heights of the micro needle arrays needed to be more than 1 mm with base around 500 μm and their edge-to-edge distance of bases are 100 μm. With these dimension requirements, the volume of each needle can achieve values listed below each example. The volume is critical in many bio-applications as it determines the amounts of medicals or vaccines that can be delivered to the receivers [88]. With these requirements of the dimension and spacing, it is impossible to make them by single step method as shown in section 5.2. With the multi-step method, the needles can be discretized into three segments that are base, middle layer and needle tip.

Each layer is fabricated in on step and the spacing limit on the patterns of the same layer is eliminated.

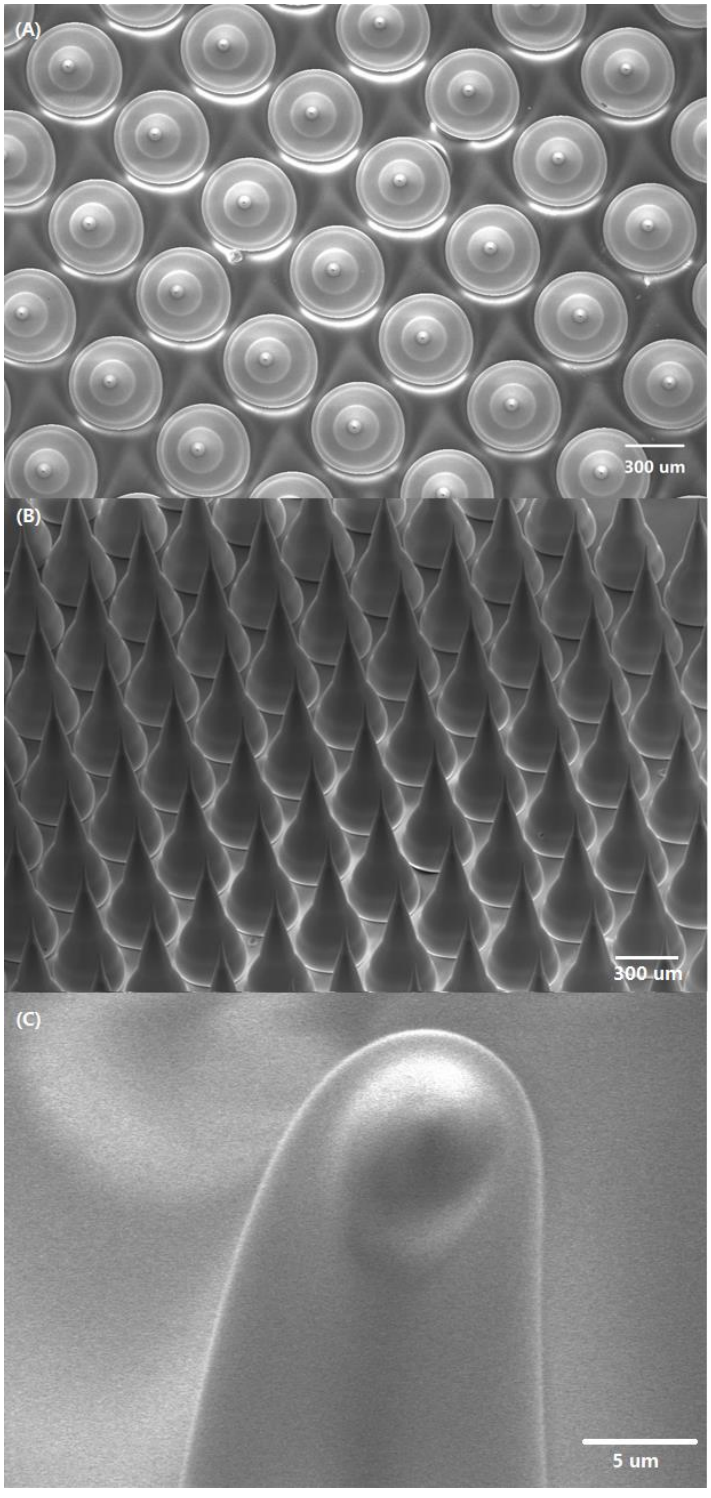

Figure 54 high-dense high-aspect-ratio Micro Needle Array by Multi-step method

This figure shown a micro needle array with edge-to-edge distance 100 μm. Its base is 500 μm with sharp tip. It is fabricated by 4-layer step methods. (A) is the top view of the array. From it, we can see 4 four rings cascade into each other. They are four layers during the fabrication process. The first 3 layers are used to overcome the spacing limit and built-up the required height and the last layer to make sharp tips on each of the needles. (B) is SEM the taken at 45 ° tilting. (C) shows the sharpness at the tip of the needles are maintained and the roundness caused by the re-melting is solved.

The multi-step method can also be extended to wire structures. By this method, more complex structures even with vertically overlapped features can be fabricated by taking advantages of the layer-by-layer stacking process. Different segment of the wires can merge smoothly by remelting process.

Figure 55 and Figure 56 demonstrate two zigzag microstructures by the multi-step method with high complexity. These two zigzag microstructures have different wire diameter which is determined by the growth condition of each segment. High density and high aspect-ratio glass microstructure arrays were readily fabricated, as shown in Figure 55. The height of the structures is more than 2 mm in height with 500 μm spacing that much more than 10:7 height-to-spacing ratio in the single step growth. The layer-by-layer nature of the zigzag structures is clearly seen in the structures. The limit on how close the neighboring structures can be fabricated next to each other only depends on precision of the motor control.

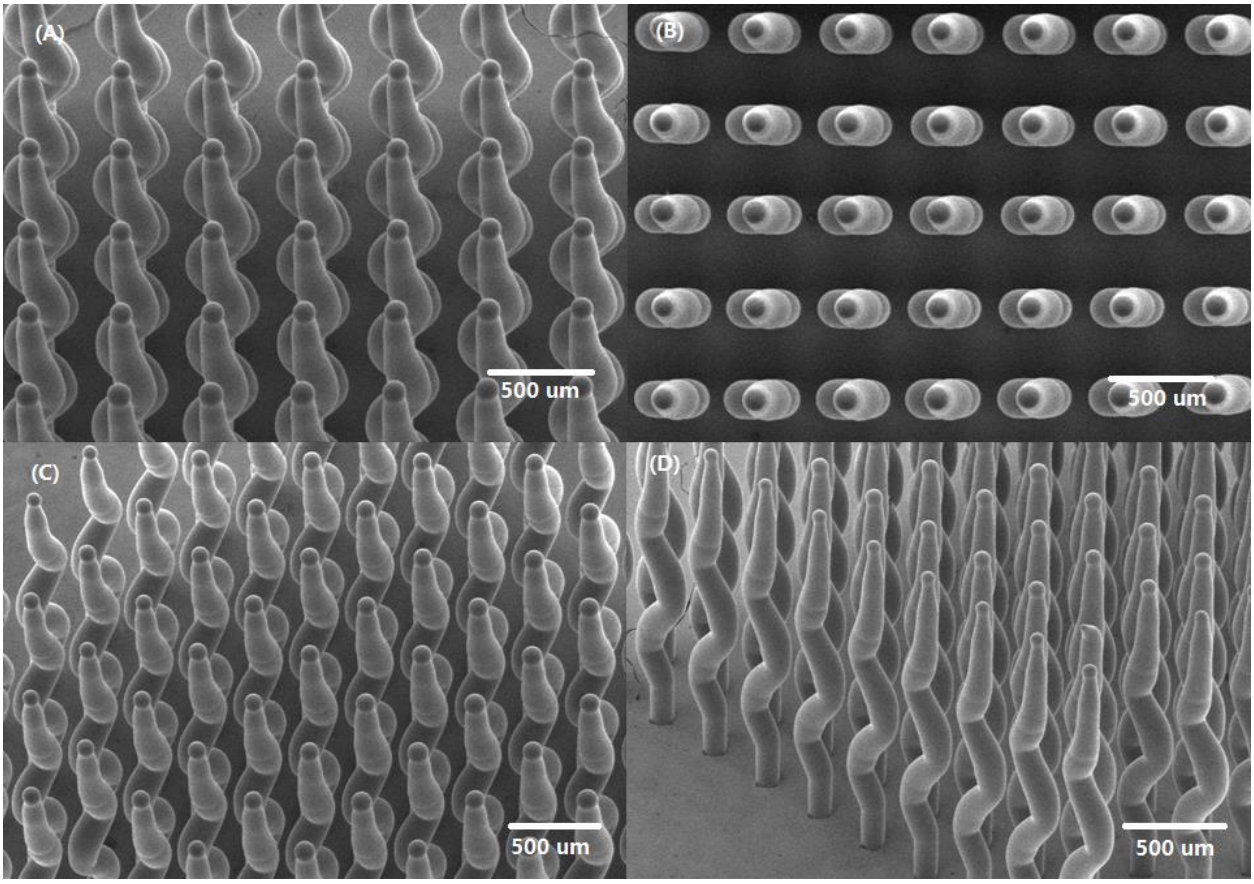

Figure 55 The Zigzag Structures by stacking methods

An array of this structures can be used as micro-mechanical springs. To avoid the melting of nearby zigzag structures during the fabrication, the array should be fabricated by multi-step method. First all the bases of the zigzag arrays are fabricated and then are the first segment, second segment and so on. The number of steps is determined by the melting effects during the growth of the segment in the same layer. The maximum height of each layer is the height the nearby structures would not be melted during the fabrication process. Different diameter could also be realized under different growth conditions. The top finish of the structures could also be modified by the way in section 4.3.

With the multi-step methods, the spacing limit is the array is breakthrough. Dense and complex structures arrays could be fabricated.

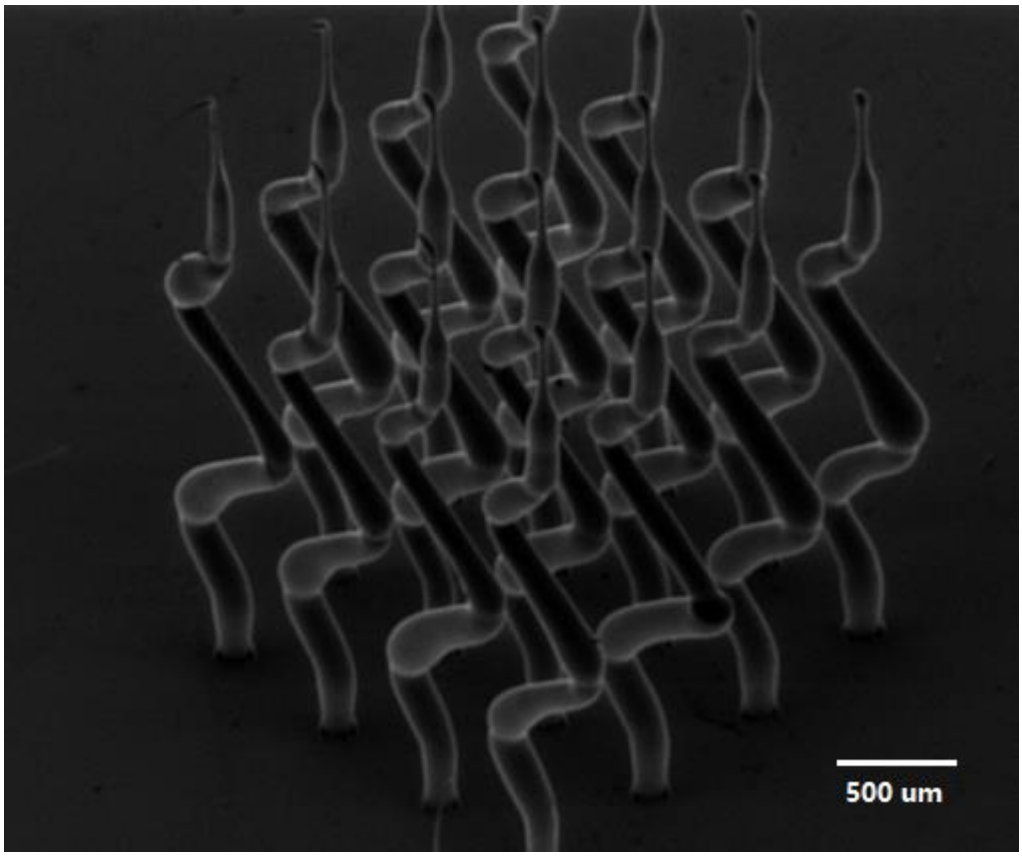

Figure 56 Zigzag Structures be multi-step method with thin wire

5.4 Conclusion

In this chapter, various structures in array form are demonstrated. Due to the heating from the nozzle during the fabrication of nearby structures, the structures may be melted in a single step method. It put a limit on the spacing of arrays and the shape of array structures. The multi-step method can solve the melting problem by finish the structures in multiple steps. Thus, the spacing limit is pushed further and only limited by the resolution of the motors. By multiple stacking, micro needle array with practical

clinical dimensions is fabricated. Moreover, the stacking method can also make more complex structures, such as zigzag arrays which can serve as micro springs.

Chapter 6 Molding of the Fabricated Micro Needle

Although the molten-glass based 3D direct-write method provides us the ability to fabricate these micro 3D structures, its usage in many applications is limited as it relies on properties of glass. One major application is in the biomedical field. However, glass is not a good biomedical material. Biocompatible materials are needed to replace the glass in the structures. Molding is a commonly used method to transfer 3D structures to different materials, especially for biomedical engineering [89] [90] . To make biocompatible replica, we use the microstructures arrays made by the molten-glass fabrication as mold. The process takes advantages of both the strong mechanical property and surface smoothness of the glass structures.

6.1 Introduction

Micro Needle Arrays (MNA) are especially usefully in biomedical applications [91]. Due to their size and shape, MNA can penetrate the skin barrier and do not reach the nerve cells under the skin for transdermal drug delivery to minimize the pain and reduce the anxiety of the patients [92], [93]. They also have proved to be more effective delivery of the vaccine than conventional intramuscular immunization by Koen van der Maaden et al [10]. During the fighting with COVID-19, the novel deliver of the vaccine without pain may let more people to be covered. Besides the drug and vaccine delivery, MNAs are also good methods to monitor human health [11]and in situ analysis [94]. They can also be utilized for glucose monitoring and insulin delivery [95], [96] which provides a promising method for diabetes therapy [97].

However, the fabrication process of the needles usually is time-consuming and needs an expansive lithography facility and cleanroom environment [98], [99]. Prausnitz M. R et al first used a MEMS method to fabricate the micro needle arrays [98]. They used microelectromechanical system fabrication techniques which involve mask making, photolithography, reactive ion etching and result in limited surface smoothness and flexibility of the fabrication process. TA Fofonoff et al use electrical discharge machining and chemical etching to fabricate needle arrays by cutting off unwanted material from the workpiece [100]. H. R. Nejad et al used laser ablation to curve out crossover lines on an acrylic sheet as the negative pattern and cast PDMS on to get positive arrays [101]. But their methods either need post steps to make the microneedle useable or the quality of the microneedles is far from satisfying. Thus, a fast and flexible methods to fabricate high quality microneedles arrays are needed to satisfy the increasing demanding for the MNA.

We have shown the melt glass based micro fabrication process can fabricated the micro needle array in a much easier way. However, glass is not an ideal material for MNA application. The material used in MNA usually are polymers, or drugs. Thus transfer the fabricated glass structure to other material is important.

6.2 Flowchart of the molding process

The following is the flowchart to get male master mold from the glass microneedle arrays to PDMS replica. The PDMS we use is SYLGARD™ 186 Silicone Elastomer Kit from Dow Corning®. It has two parts: Part A and base. The two parts need to be mixed at 10:1 right before the casting process. The mixed solvent will cure in 1.65 hours in room temperature or 15 minutes when heated to 125℃.

To make PDMS replica of the microneedle array, the glass mold is first served as the male mold. It is placed in a container and then a layer of mixed SYLGARD™ 186 Silicone solvent is casted. After the vacuum process to remove the bubbles and curing process at 125℃ for 15 minutes, the female mold of the microneedles is formed. When it cools to room temperature, it could be peeled off from the glass microstructures array.

The next steps are to use the female mold to get male PDMS replica. To prevent merge of polymers, a thin layer of Parylene C is deposited to act as a barrier layer. The coating process is done by SCS Parylene Coater in IEN of Georgia Tech. After a very thin (200 nm) Parylene C coating is deposited on the female mold, the mixed PDMS is casted on the female mold. After the vacuum and curing process, the replica of the original glass microneedle array is made. With the Parylene layer between them, the replica can be easily peeled off.

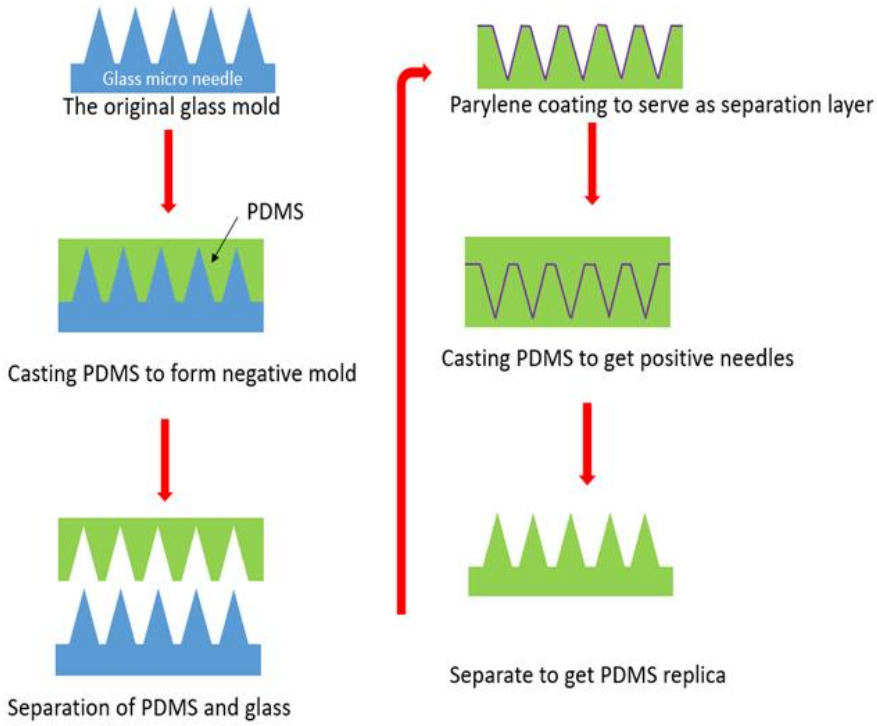

Figure 57 The process of Molding

Through these procedures, a PDMS replica of original glass microneedle arrays are made. The similar process would also be used to get other type of materials with some modifications. The two key issues are the strength of the mold and the replica quality. The strong mechanical strength and smooth surface of glass solve these problems well. The bonding strength are also strong enough throughout the process.

6.3 The Replica of the polymer Structures

The figures below show the replica of two needle arrays. The first array has a spacing of 150 μm and the second has 300 μm spacing. By comparing the needle tip of the glass mold and PDMS replica, the dimension of the tip maintains in the molding process. All the glass molds have been used to replicate more than 20 PDMS replicas without damage both on the structures and the bonding. The exactness of the replica shows the there is no distortion during the molding process and the glass mold is also intact. This provides an alternative way to make biochemical needle arrays in many other research.

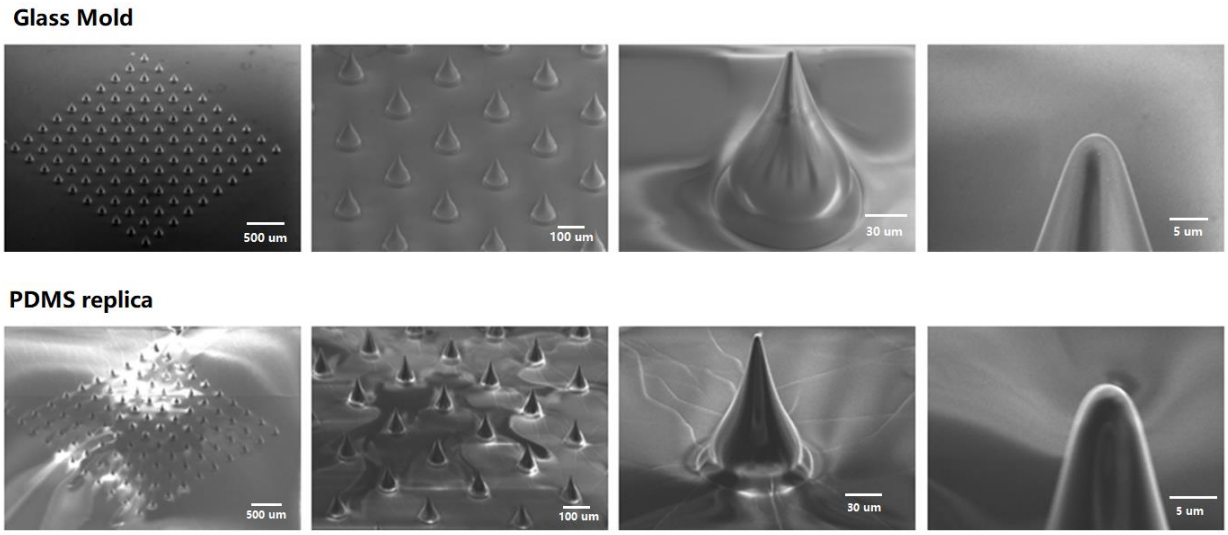

Figure 58 An 10 by 10 needle array of the Glass mold and PDMS replica with 150um spacing

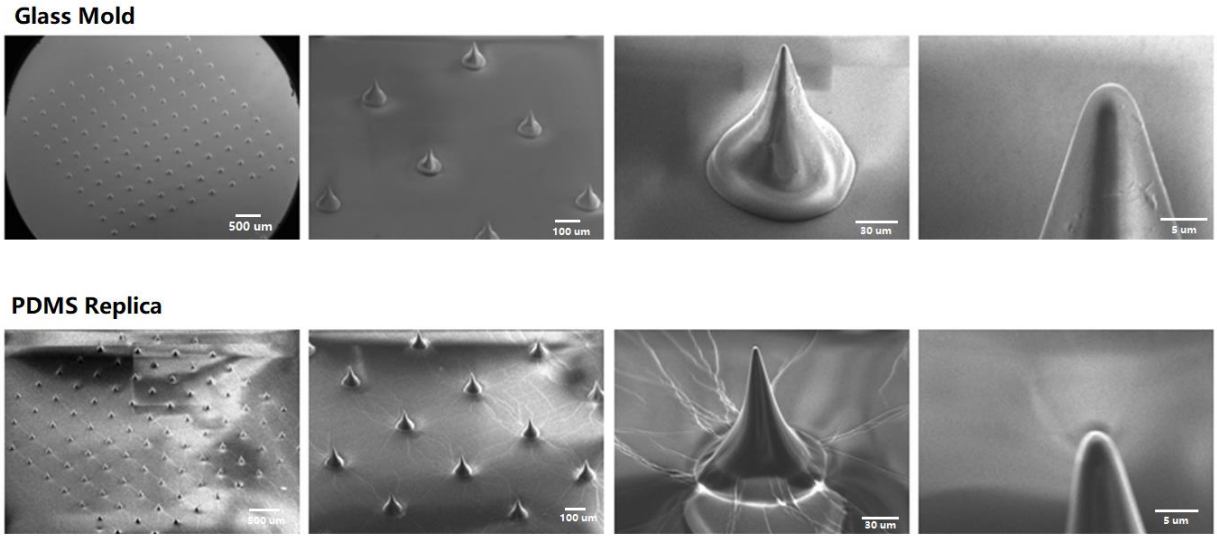

Figure 59 An 10 by 10 needle array of the Glass mold and PDMS replica with 300 um spacing

Figure 60 shows an optical image of the PDMS replica of the micro needle array.

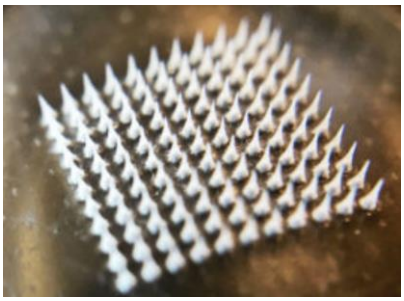

Figure 60 the PDMS replica of the micro needle array

6.4 Conclusion

To extend the application of molten-based 3-D Direct-write fabrication to biomedical field, polymer replica of the glass microstructures is needed. Molding is a common way to get them. In this chapter, flowchart of the procedures to get PDMS replica of the glass microneedle arrays is provided. The molding process takes advantages

of the strong mechanical property of the glass and its smooth surface. With Comparison of the original glass mold and PDMS replica, the shape and tip sharpness of the PDMS micro needle arrays are maintained. The mold remains intact after more than 20 times molding process. It provides alternative way to make micro needle arrays with low cost in further research.

Chapter 7 Conclusion

In this thesis, I demonstrate the molten-based 3D direct-write fabrication of micro/sub-micro structures. The hardware and software of the setup are developed in the lab. It needs 3-axis motor systems, temperature control system and pressure regulation systems. It provided an alternative method to fabricate high-aspect-ratio or complex micro 3D structures in a cost-effective way.

For the unique process of the fabrication, it involves many properties of the molten glass and analysis for them are provided. The exponential dependence of the viscosity and temperature is the key property in the process. Together with applied pressure and geometry of the exiting nozzle, it determines quality and rate of the fabrication. The fabrication process preserves the mechanical strength of the glass which provides the micro-structures an advantage over polymer-based or ink-based micro 3D process. The surface tension affects the stability of the wire growth. Evolution of the grow process from micro-wires to micro-needles are demonstrated. By tunning different parameters, micro wires/needle arrays with different size and shape are fabricated. The sharpness of the needles can be as small as 400 nm. An COMSOL model can qualitatively simulate the wire or needle forming process is built.

Ultra-high-aspect wires are also feasible due to the strong mechanical property of the glass. Both the base and top of the microstructures can be modified. Due to the fast cooling of the molten glass, curved and flexible structures are also feasible. The method can also extend to Surface Pattern drawing, Layer by Layer Structures and Micro Lens.

Arrays of various microstructures are fabricated to extend its application and show the repeatability of the process. To make more dense arrays, multi-step stacking methods are developed to solve the melting caused by fabrication of nearby structures. It can push the spacing limits of the arrays to the resolutions of the motor. With it, microneedle arrays with clinical dimension requirement and zigzag structures which can serve as micro springs are realized.

To extend the application to biomedical field, molding process to get polymer replica of the glass microneedle array is demonstrated. It utilizes the strong mechanical properties and smooth surface of glass structures. PDMS replica maintain the shape and sharpness of the original glass mold. The glass microneedle array remains intact after more than 20 times use. It can extend the potential applications in further research.

The method described in this dissertation is believed to be unique in the field of 3-D fabrication, and provides an efficient tool for fabricating micro/sub-micro structures with strong mechanical property, ultra-smooth surface, high aspect-ratio and spatial density that are either unfeasible or extremely costly by other traditional fabrication methods. Moreover, combine with other process such as molding or coating, replica of these microstructures could be made and further extended applications to new field. Fabricating more complicated 3-D structures beyond the simple glass material system based on the mechanisms and processes described in this thesis would also be feasible in an efficient way.

REFERENCES

[1] Y. Z. M.-F. Y. ,. Y.-P. Lin, "Parallel process 3D metal microprinting," *Adv. Mater. Technol.,* no. 4 Article 1800393, 2019.

[2] S. Xu et al, "Assembly of micro/nanomaterials into complex, three-dimensional architectures by compressive buckling.," *Science,* vol. 347, pp. 154-159, 2015.

[3] A. K. B. W. S. D. K. N. S. K. N. T. R. C. H. D. R. B. Kotz F, "Three-dimensional printing of transparent fused silica glass.," *Nature,* vol. 544, p. 337–339, 2017.

[4] T.G. Leong et al., "Tetherless thermobiochemically actuated microgrippers," *Proc. Natl. Acad. Sci. U.S.A,* vol. 106, pp. 703-708, 2009.

[5] B. Tian et al., "Macroporous nanowire nanoelectronic scaffolds for synthetic tissues," *Nat Mater. ,* vol. 11, pp. 986-94, 2012.

[6] D. P. F. B. C. e. a. Bishop, "Silicon Micro-Machines for Fun and Profit.," *J Low Temp Phys,* vol. 169, p. 386–399 , 2012.

[7] J. H. K. C. Y. S. J. P. J. S. J. M. M. S. O. &. T. E. L. Lee, "25th anniversary article: Ordered polymer structures for the engineering of photons and phonons," *Advanced Materials,* vol. 26, no. 4, pp. 532-569, 2014.

[8] H. Y. X. &. B. P. Zhang, " Three-dimensional bicontinuous ultrafast-charge and -discharge bulk battery electrodes.," *Nature Nanotech, ,* vol. 6, p. 277–281, 2011.

[9] K. Sun, T. Wei, B. Ahn, J. Seo, S. Dillon and J. Lewis, "3D printing of interdigitated Li-ionmicrobattery architectures.," *Adv. Mater. ,* vol. 25, p. 4539–4543, 2013.

[10] J. W. B. J. Van Der Maaden K, " Microneedle technologies for (trans)dermal drug and vaccine delivery.," *J Control Release,* vol. 161, p. 645–55., 2012.

[11] S. D. C. J. D. T. D. M. Rosemary L. Smith, "Silicon microneedle array for minimally invasive human health monitoring," *Proc. SPIE 10491, Microfluidics, BioMEMS, and Medical Microsystems XVI,,* p. 1049102, 19 February 2018.

[12] V. S. C.K. Malek, "Applications of LIGA technology to precision manufacturing of high-aspect-ratio micro-components and -systems: a review," *Microelectron J,,* vol. 35, pp. 131-143, 2004.

[13] M. J. Madou, "Fundamentals of microfabrication : the science of miniaturization," Boca Raton, FL, ed, CRC Press,. 2nd, 2002, p. 723.

[14] G. B. L. B. W. C. G. L. C. C. H. Lin, " A new fabrication process for ultra-thick microfluidic microstructures utilizing SU-8 photoresist," *J Micromech Microeng ,* vol. 12, pp. 590-597, 2002.

[15] P. M. J. K. H. G. S. Massoud-Ansari, "A multi-level, LIGA-like process for three dimensional actuators," *IEEE Proc. MEMS'96,* pp. 285-289, 1996.

[16] S. L. K.-C. Lee, "3D fabrication using deep X-ray mask with integrated micro-actuators," *IEEE Proc. MEMS'03 ,* pp. 558-561, 2003.

[17] e. a. D.Y. Oh, "A tetrahedral three-facet micro mirror with the inclined deep X-ray process," *Sens. Actuators,* vol. A93, pp. 157-161, 2001.

[18] e. a. O. Tabata, "3D fabrication by moving mask Deep X-ray Lithography (M2-DXL), with multiple stages," *IEEE Proc. MEMS'2002,* pp. 180-183, 2002.

[19] H. U. S. Sugimaya, "Novel shaped microstructures processed by deep x-ray lithography," *Transducers '01-Eurosensors XV 11th Int Cont on Solid-Stake Sensors and Actuators, Munich, Germany,* pp. 10-14, June (2001).

[20] I. W. H. J. D. Madden, "Three-dimensional microfabrication by localized electrochemical deposition.," *J Microelectromech S,* vol. 5, pp. 24-32, 1996.

[21] M. X. J. A. L. G. M. Gratson, "Microperiodic structures: Direct writing of three-dimensional webs.," *Nature ,* vol. 428, pp. 386-386, 2004.

[22] M. C. H. D. T. S. Z. Guo, "Properties of Polylactide Inks for Solvent-Cast Printing of Three-Dimensional Freeform Microstructures," *Langmuir,* vol. 30, pp. 1142-1150, 2014.

[23] E. B. D. M. J. M. X. G. S.-I. P. Y. X. J. Y. R. G. N. J. A. R. J. A. L. Bok Y. Ahn, "Omnidirectional Printing of Flexible, Stretchable, and Spanning Silver Microelectrodes," *Science,* vol. 323, no. 5921, pp. 1590-1593, 2009.

[24] F. G. N. G. A.-M. L. M.-C. H. D. T. S.-Z. Guo, "Solvent-cast three-dimensional printing of multifunctional microsystems," *Small,* vol. 9, pp. 4118-4122, 2013.

[25] D. L. P. Parandoush, "A review on additive manufacturing of polymer-fiber composites," *Compos Struct,* vol. 182, pp. 36-53, 2017.

[26] C. C. Z. D. Z. L. D. Z. L. L. S. S. C.Y. Yap, "Review of selective laser melting: materials and applications," *Appl Phys Rev,,* vol. 2, no. 4, p. Article 041101, 2015.

[27] B. Khoshnevis, "Automated construction by contour crafting - related robotics and information technologies," *Autom ConStruct,,* vol. 13, no. 1, pp. 5-19, 2004.

[28] J. F. D. G. F.P.W. Melchels, "A review on stereolithography and its applications in biomedical engineering," *Biomaterials,* vol. 31, no. 24, pp. 6121-6130, 2010.

[29] D. R. B. S. I. Gibson, "Directed energy deposition processes.," *Additive manufacturing technologies: 3D printing, rapid prototyping, and direct digital manufacturing Springer New York, New York, NY,* pp. 245-268, 2015.

[30] D. R. B. S. I. Gibson, "Sheet lamination processes," *Additive manufacturing technologies: 3D printing, rapid prototyping, and direct digital manufacturing Springer New York, New York, NY,* pp. 219-244, 2015.

[31] A. K. G. I. K. N. D. H. T.D. Ngo, "Additive manufacturing (3D printing): a review of materials, methods, applications and challenges," *Compos. B Eng.,* vol. 143, pp. 172-196, 2018.

[32] P. M. J. V. V. L. F. M. R. J.-P. Kruth, "Binding mechanisms in selective laser sintering and selective laser melting.," *Rapid Prototyping J,* vol. 11, pp. 26-36, 2005.

[33] H. S. a. S. Y. M. Vaezi, "A review on 3D micro-additive manufacturing technologies," *The International Journal of Advanced Manufacturing Technology,* vol. 67, no. no. 5–8, p. 1721–1754, Nov. 2012.

[34] X. Wang et al, "3D printing of polymer matrix composites: A review and prospective," *Composites Part B,* vol. 110, pp. 442-458, 2017.

[35] K. G. M. S. S.K. Malhotra, "Part One Introduction to Polymer Composites," *Polymer Composites (1st ed. Wiley-VCH,* vol. 1, 2012.

[36] L. L. D. D. E. H. W. &. R. V. M. Hench, "Glass and medicine.," *Int. J. Appl. Glass Sci. ,,* vol. 1, p. 104–117, 2010.

[37] A. F. T. &. S. K. Ikushima, "Silica glass: a material for photonics," *J. Appl. Phys.,* vol. 88, p. 1201–1213, 2000.

[38] N. P. &. D. R. H. Bansal, Handbook of Glass Properties 680, Elsevier, 2013.

[39] M. S. G. F. M. K. C. I. S. D. J. C. W. P. H. P. C. M. Y. a. N. O. J. Klein, "Additive Manufacturing of Optically Transparent Glass," *3D Printing and Additive Manufacturing,* vol. 2, no. 3, pp. 92-105, 2015.

[40] J. Lewis, "Direct Ink Writing of 3D Functional Materials," *Adv. Mater,* vol. 15, pp. 1639-1643, 2003.

[41] A. Fluegel, ""Glass Viscosity Calculation Based on a Global Statistical Modeling Approach"; (PDF, 3 MB),," *Glass Technol.: Europ. J. Glass Sci. Technol. A,,* vol. 48, no. 1, pp. p 13-30., 2007.

[42] V. M. N. C. S. S. D. T. C. B. W. T. E. L. Maruti Hegde, "3D Printing All-Aromatic Polyimides using Mask-Projection Stereolithography: Processing the Nonprocessable," *Adv. Mater,* vol. 29, no. 31, p. 1701240, 2017.

[43] I. Roppolo, A. Chiappone, A. Angelini, S. Stassi and F. Frascella, "3D Printable Light-Responsive," *Mater. Horiz,* vol. 4, no. 3, p. 396−401., 2017.

[44] E. B. E. O. P.J. Rae, "The mechanical properties of poly(ether-ether-ketone) (PEEK) with emphasis on the large compressive strain response," *Polymer,* vol. 48, pp. 598-615, 2007.

[45] D. M. J. P. V.F. Zackay, "Fundamentals of Glass-to-Metal Bonding," *Journal of the American Ceramic Society,* vol. 36, no. 3, p. 84–89., 1953.

[46] J. A. P. a. R. M. Fulrath, "Fundamentals of Glass-to-Metal Bonding: VIII, Nature of Wetting and Adherence," *J. Am. Ceram. Soc,* vol. 45, p. 592– 6, 1962.

[47] D. L. X. &. Q. J. Zhang, "3D printing of glass by additive manufacturing techniques: a review," *Front. Optoelectron.,* p. 1, 2020.

[48] W. B. Pietenpol, "Surface Tension of Molten Glass," *Physics,* vol. 7, no. 26, 1936.

[49] D.-S. K. S. H. H. K. S.-B. Shim, "Wetting and surface tension of bismate glass melt," *Thermochim. Acta,* vol. 496, no. 1–2, pp. 93-96, 2009.

[50] N. Parikh, "Effect of atmosphere on surface tension of glass," *J. Am. Ceram. Soc.,* vol. 14, pp. 18-22, 1958.

[51] K. J. V. M. L. A. P. F. Pereira L, "Experimental and numerical investigations of an oxygen single-bubble shrinkage in a borosilicate glass-forming liquid doped with cerium oxide," *J Am Ceram Soc.,* vol. 103, no. 12, p. 6736– 45, 2020.

[52] S. F. K. M. S. Toyoda, "Density, viscosity and surface tension of 50RO–50P2O5 (R: Mg, Ca, Sr, Ba, and Zn) glass melts," *Journal of Non-Crystalline Solids,* vol. 321, no. 3, pp. 169-174, 2003.

[53] R. Z. MG Velarde, Interfacial phenomena and the Marangoni effect, New York: 2002, 2002.

[54] S. D. D. R. B. P. Schena M, "Quantitative monitoring of gene expression patterns with a complementary DNA microarray," *Science,* vol. 270, pp. 467-470, 1995.

[55] M. C. Pirrung, " How to Make a DNA Chip," *Angew. Chem., Int. Ed,* vol. 41, p. 1276–1289, 2002.

[56] H. S. H. F. T. S. Takeo Kawase, "Inkjet Printed Via-Hole Interconnections andResistors for All-Polymer Transistor Circuits," *Advanced Materials,* vol. 13, no. 21, pp. 1601-1605, 2001.

[57] E. G. A. L. M. R. H. L. E. S. D. J. Norris, "Opaline photonic crystals: How does self-assembly work?," *Adv. Mater.,* vol. 16, p. 1393–1399, 2004.

[58] S. F. a. K. M. S. Toyoda, "Density, Viscosity and Surface Tension of 50RO–50P2O5 (R: Mg, Ca, Sr, Ba, and Zn) Glass Melts," *J. Non-Cryst. Solids,* vol. 321, no. 3, p. 169–174, 2003.

[59] R. M. F. JOSEPH A. PASK, "Fundamentals of Glass-to-Metal Bonding: VIII, Nature of Wetting and Adherence," *J. Am. Ceram. Soc,* vol. 45, no. 12, pp. 592-596, 1962.

[60] Q. B. a. Y. B. G. Tao Li, "High precision batch mode micro-electro-discharge machining of metal alloys using DRIE silicon as a cutting tool," *J. Micromech. Microeng.,* vol. 23, no. 095026, 2013.

[61] M. Datta, "Fabrication of an Array of Precision Nozzles by Through-Mask Electrochemical Machining," *Journal of Electrochemical Society,* vol. 142, pp. 3801-3806, 1995.

[62] P. P. R. C. V. M. P. R. Petitjean C, "Electrochemical behavior of glass melts: application to corrosion processes," *Procedia Materials Science,* vol. 7, p. 101–10, 2014.

[63] S. Stookey, "Coloration of glass by gold, silver, and copper.," *J. Am. Ceram. Soc. ,* vol. 32, p. 246–249, 1949.

[64] M. S. S. A. e. a. H. Izumi, "Realistic imitation of mosquito's proboscis: electrochemically etched sharp and jagged needles and their cooperative inserting motion," *Sensors Actuators A Phys,* vol. 165, pp. 115-123, 2011.

[65] G. J. R. P. H. M. C. A. H. A. Held J, "Design of experiment characterization of microneedle fabrication processes based on dry silicon etching," *J. Micromech. Microeng,* vol. 20, no. 2, p. 025024, 2010.

[66] B. M. M. M. M. T. L. V. E. D. F. F. Perennes, "Sharp beveled tip hollow microneedle arrays fabricated by LIGA and 3D soft lithography with polyvinyl alcohol," *J. Micromech. Microeng,* vol. 16, p. 473–479, 2006.

[67] M. H. K. F. S. S. S. Khumpuang, "Geometrical strengthening and tip-sharpening of a microneedle array fabricated by X-ray lithography," *Microsyst. Technol.,* vol. 13, p. 209–214, 2007.

[68] D. R. E. B. a. F. S. P. Tathireddy, "Fabrication of 3-dimensional silicon microelectrode arrays using micro electro discharge machining for neural applications," *IEEE TRANSDUCERS Conf. Tech. Dig,* pp. 1206-1209, 2009.

[69] J. P. a. M. Matovich, "Spinning a molten threadline-Stability," *Ind. Eng.Chem. Fundam.,* vol. 8, p. 605–609, 1969.

[70] Y. S. a. J. Pearson, "On the stability of nonisothermal fiber spinning," *Ind. Eng. Chem. Fundam. ,* vol. 11, p. 145–149, 1972.

[71] Y. S. a. J. Pearson, "On the stability of nonisothermal fiber spinning-general case.," *Ind. Eng. Chem. Fundam,* vol. 11, p. 150–153, 1972.

[72] D. Gelder, "The stability of the fiber drawing processes," *Ind. Eng. Chem. Fund,* vol. 10, p. 534–535, 1971.

[73] M. D. R. Fisher, "A theory of isothermal melt spinning and draw resonance," *AIChE,* vol. 22, no. 2, pp. 236-246, 1976.

[74] G. S. W. A. E. e. a. Gupta, "Nonisothermal model of glass fiber drawing stability," *Rheola Acta ,* vol. 35, p. 584–596, 1996.

[75] Y. Y. a. R. Pitchumani, "Numerical study on the dopant concentration and refractive index profile evaluation in an optical fiber manufacturing process," *Int. J. Heat Mass Transf.,,* vol. 49, no. no. 13/14,, p. 2097–2112, 2006.

[76] A. M. a. R. Pitchumani, "Optical fiber drawing process model using an analytical neck-down profile," *IEEE Photon. Technol. Lett.,* vol. 2, p. 620–629, 2010.

[77] Y. L. M. M. T. a. J. P. B. Pan, "Surface micromachining polymer-core-conductor approach for high-performance millimeter-wave air-cavity filters integration," *IEEE Trans. Microw. Theory Tech.,* vol. 59, no. 4, pp. 959-970, 2008.

[78] B. C. J. P. Schmitz GJ, "Manufacture of high-aspect-ratio micro-hair sensor arrays," *J Micromech Microeng ,* vol. 15, p. 1904–1910, 2005.

[79] B. C. H. M. B. H. Chagnaud B, "Measuring Flow Velocity and Flow Direction by Spatial and Temporal Analysis of Flow Fluctuations," *The Journal of Neuroscience,* vol. 28, no. 17, p. 4479–4487, 2008.

[80] M. S. J. L. W. C. &. C. J. R. Jorfi, "Progress towards biocompatible intracortical microelectrodes for neural interfacing applications," *J. Neural Eng,* vol. 12, p. 011001, 2015.

[81] L. L. H. L. W. B. e. a. Yuan W, " Fabrication of microlens array and its application: A review," *Chin J Mech Eng,* vol. 31, no. 16, 2018.

[82] C. K. C. M. K. W. e. a. H Yang, "High fll-factor microlens array mold insert fabrication using a thermal refow process," *Journal of Micromechanics and Microengineering,* vol. 14, no. 8, p. 1197, 2004.

[83] J. G. D. L. e. a. S Moore, "Experimental study of polymer microlens fabrication using partial-flling hot embossing technique," *Microelectronic Engineering,* vol. 162, pp. 57-62, 2016.

[84] L. W. Y. D. e. a. Y Luo, "Direct fabrication of microlens arrays with high numerical aperture by ink-jetting on nanotextured surface.," *Applied Surface Science,* vol. 279, pp. 36-40, 2013.

[85] L. N. C. G. e. a. J Albero, "Fabrication of spherical microlenses by a combination of isotropic wet etching of silicon and molding techniques," *Optics Express,* vol. 17, no. 8, pp. 6283-6292, 2009.

[86] Z. Z. T. K. e. a. J Yan, "Fabricating micro-structured surface by using single-crystalline diamond endmill," *The International Journal of Advanced Manufacturing Technology,* vol. 51, no. 9, pp. 957-964, 2010.

[87] L. M. S. G. B. L. Ventrelli, "Microneedles for Transdermal Biosensing: Current Picture and Future Direction," *Adv. Healthc. Mater. 4 (17) ,* vol. 4, no. 17, pp. 2606-2640, 2015.

[88] S. C. M. P. L.Y. Chu, " Fabrication of dissolving polymer micro-needles for controlled drug encapsulation and delivery: bubble and pedestalmicroneedle designs," *J. Pharm. Sci,* vol. 99, p. 4228–4238, 2010.

[89] S. Yang, Y. Feng, L. Zhang, N. Chen, W. Yuan and T. Jin, "A Scalable Fabrication Process of Polymer Microneedles.," *Inter. J. Nanomed,* vol. 7, 2012.

[90] K. Krieger, N. Bertollo, M. Dangol, J. Sheridan, M. Lowery and E. O'Cearbhaill, "Simple and customizable method for fabrication of high-aspect ratio microneedle molds using low-cost 3D printing," *Microsyst. Nanoeng,* vol. 5, p. 1–14, 2019.

[91] R. Jamaledin, C. Di Natale, V. Onesto, Z. B. Taraghdari and Zare, "Progress in microneedle-mediated protein delivery," *J. Clin. Med.,* vol. 9, no. 2, p. 542., 2020.

[92] R. S. T. W. A. Donnelly RF, "Microneedle-based drug delivery systems: Microfabrication, drug delivery, and safety," *Drug delivery,* vol. 17, no. 4 doi:10.3109/10717541003667798, pp. 187-207, 2010.

[93] e. a. M. Cormier, "Transdermal delivery of desmopressin using a coated microneedle array patch system," *J. Contr. Release,* vol. 97, no. 3, pp. 503-511, 2004.

[94] S. C. R. I. R. S. E. Mukerjee, "Microneedle array for transdermal biological fluid extraction and in situ analysis," *Sensors and Actuators a-Physical,* vol. 114, pp. 267-275, 2004.

[95] D. F. B. S. A. W. F. a. D. L. S. Zimmermann, "A microneedle-based glucose monitor: fabricated on a wafer-level using in-device enzyme immobilization," *TRANSDUCERS '03. 12th International Conference on Solid-State Sensors, Actuators and Microsystems. Digest of Technical Papers (Cat. No.03TH8664), Boston, MA, USA, ,* vol. 1, pp. 99-102, 2003.

[96] Z. Y. Y. Y. e. a. Yu J, "Microneedle-array patches loaded with hypoxia-sensitive vesicles provide fast glucose-responsive insulin delivery," *Proc Natl Acad Sci U S A,* vol. 112 pmid:26100900, p. 8260–8265, 2015.

[97] R. T. C. X. B. Y. G. W. Y. L. Q. N. F. Z. Z. Z. J. W. G. N. Y. M. L. X. Chen, "Microneedle-array patches loaded with dual mineralized protein/peptide particles for type 2 diabetes therapy," *Nat. Commun,* vol. 8, no. 1, pp. 1-11, 2017.

[98] M. D. V. A. M. G. P. M. R. Henry S., "Microfabricated Microneedles: A Novel Approach to Transdermal Drug Delivery," *J. Pharm. Sci,* vol. 87, no. 8, p. 922–925, 1998.

[99] P. D. L. H. C. W. K. K. L. J.-B. A. C. Kim K, " A tapered hollow metallic microneedle array using backside exposure of su-8," *J. Micromech. Microeng,* vol. 14, p. 597–603, 2004.

[100] M. S. H. N. D. J. H. I. Fofonoff TA, "Microelectrode array fabrication by electrical discharge machining and chemical etching," *IEEE Trans Biomed Eng,* vol. 51, p. 890–895, 2004.

[101] A. S. G. K. S. S. H. R. Nejad, "Lowcost and cleanroom-free fabrication of microneedles," *Microsyst. Nanoeng,* vol. 4, p. 17073, 2018.

VITA

Yining Chen was born in Hangzhou, China. He received the B.S. degree in electrical and computer engineering from Shanghai Jiao Tong University, Shanghai, China in 2011, and M.S degree in aerospace engineering from Georgia Institute of Technology, Atlanta, USA in 2020. His research interest is on microscale and nanoscale fabrication/characterization, precision 3-D manufacturing and instrument development. In this research, he developed a molten-glass-based 3D direct-write fabrication method for making high density and complex microstructures.